

UNIVERSITY OF NAPLES FEDERICO II



# **Dynamics and Structures of Nanoparticles in Polymer Melts**

Martina Salzano de Luna

**PhD in *Materials and Structures Engineering* (XXVII Cycle)**

Department of Chemical, Materials and Industrial Production Engineering

---

PhD Supervisor: Dr. Giovanni Filippone  
PhD Coordinator: Prof. Giuseppe Mensitieri

April 2015





# *Abstract*

## **Dynamics and Structure of Nanoparticles in Polymer Melts**

Martina Salzano de Luna

The possibility of combining the physical properties of different components to obtain materials with new structural or functional features is what really makes polymer nanocomposites attractive. Actually, to fully exploit the potential of such a class of materials, the morphological and structural implications stemming from the nanometric sizes of the filler have to be taken into account. In the present dissertation, the physical mechanisms governing the nanoparticle dynamics and connectivity in polymer melts are investigated from a fundamental point of view. For such a purpose, the linear viscoelastic response of polymer nanocomposites has been deeply studied and morphological analyses have been used as support.

As thermodynamically out-of-equilibrium materials, if provided by sufficient energy, polymer nanocomposites evolve to achieve equilibrium. In this process, the nanoparticles rearrange themselves in the melt and typically aggregate, dictating the ultimate microstructure of the material from which its macroscopic performances depend. In the first part of the study, the key role of the mobility of nanoparticles on their dynamics of assembly has been highlighted. The investigation then focuses on the rheological implications of the superstructures formed by the nanoparticles when they are free to rearrange in the host polymer medium. A simple two-phase model, recently proposed in the literature, has been used for such a purpose. First, the ability of the model in recognizing the elasticity of filler networks too weak to be identified by conventional viscoelastic analyses has been demonstrated. More importantly, the generalization of the model has been proposed and validated, proving that it is able to describe the linear viscoelasticity of polymer nanocomposites differing among them both in the nature of the nanoparticles and in the affinity between the polymer and filler phases. A further test of the robustness of the approach is given by verifying the possibility of satisfactorily describing the viscoelastic response of other complex fluids, such as nanocomposites based on biphasic polymer matrices. In the end, the gained fundamental knowledge has been exploited for practical purposes. The study is targeted to the investigation of the effect of material- and process-related factors on the filler state of dispersion in the final polymer nanocomposite.





# Contents

<b>1 Introduction</b>	<b>1</b>
1.1 Motivation	1
1.2 Thesis organization	2

## **PART I**

### **Nanoparticle dynamics in polymer melts**

<b>2 Particle assembly in complex liquids – Literature review</b>	<b>7</b>
2.1 From Brownian motion to glassy dynamics in soft matter	7
2.2 Nanoparticle flocculation in polymer melts	9
<b>3 Effect of the presence of a preferred liquid-liquid interface on the mobility of nanoparticles in polymer melts</b>	<b>15</b>
3.1 Prefatory notes	15
3.2 Morphology of the biphasic polymer system	17
3.3 Filler localization	19
3.4 Dynamics of assembly of the nanoparticles	23

## **PART II**

### **Nanoparticle networks in polymer melts**

<b>4 Linear viscoelasticity of polymer nanocomposites – A brief survey</b>	<b>35</b>
4.1 General considerations	35
4.2 Scaling of the viscoelasticity: a two-phase model	37
<b>5 Elasticity of weak filler networks: predictive feature of the two-phase model</b>	<b>41</b>
5.1 Prefatory notes	41
5.2 Filler structure and nanocomposite morphology	42

5.3	Linear viscoelasticity and detection of the liquid to solid transition	45
5.4	Predictive feature of the two-phase model	52
5.5	Estimation of the percolation threshold	58
<b>6</b>	<b>Generalization of the two-phase model: a unifying approach for the linear viscoelasticity of polymer nanocomposites</b>	<b>61</b>
6.1	Prefatory notes	61
6.2	Generalizing the two-phase model: nanoparticles nature	63
6.3	Generalizing the two-phase model: polymer nature and polymer-particle interactions	70
6.4	Network elasticity and stress-bearing mechanisms	73
<b>7</b>	<b>Robustness of the two-phase model: extension to nanocomposites based on a biphasic polymer matrix</b>	<b>77</b>
7.1	Prefatory notes	77
7.2	Linear viscoelasticity of the neat biphasic polymer system	78
7.3	Linear viscoelasticity of the nanocomposites	83
7.4	Filler network in the mono- and biphasic matrices	85
7.5	Elasticity and structure of the filler networks	92

### **PART III**

#### **Structure-property relationships in polymer nanocomposites through rheological analyses**

<b>8</b>	<b>Current issues in the research on polymer nanocomposites</b>	<b>103</b>
8.1	Applications and future perspectives for polymer nanocomposites	103
8.2	Main challenges in the preparation of polymer nanocomposites	104
8.3	Filler state of dispersion through rheological analyses	106
<b>9</b>	<b>Role of the morphology of primary aggregates of carbon nanotubes on their dispersibility in polymer melts</b>	<b>111</b>
9.1	Prefatory notes	111
9.2	Morphology and structure of the primary aggregates	112
9.3	State of dispersion of the carbon nanotubes	114
9.4	Macroscopic performances of the nanocomposites	122
<b>10</b>	<b>Dispersing hydrophilic nanoparticles in hydrophobic polymers: nanocomposites by a novel template-based approach</b>	<b>125</b>
10.1	Prefatory notes	125

10.2 Melt mixing route	127
10.3 Template-based approach	131
10.4 State of dispersion of the nanoparticles	134
<b>Conclusions</b>	<b>139</b>
<b>Methods</b>	<b>143</b>
Raw materials	143
Nanocomposite preparation	145
Characterizing techniques	146
<b>Appendices</b>	<b>149</b>
Appendix to Chapter 6	149
Appendix to Chapter 7	152
Appendix to Chapter 9	156
<b>References</b>	<b>159</b>



# 1

## Introduction

*In this chapter the motivation and organization of the dissertation are outlined. First a short and general primer on the scientific key-concepts is given, setting the stage for the presentation of the rationale and the main objectives of the performed research activity (§ 1.1). Then, the structure of the thesis is briefly illustrated (§ 1.2).*

### 1.1 Motivation

Polymeric materials are widely used due to their unique attributes: ease of production, light weight and ductile nature. However, for most current applications of plastics, performance requirements, as well as cost and processing considerations, necessitate the introduction of additives and fillers into the polymer matrices. As a matter of fact, the possibility of combining the physical properties of different components to obtain materials with new structural or functional features is what really makes composites attractive. The use of nanoscale fillers pushed this strategy to the next level by exploiting the advantages that nanometer-size particulates offer compared with macro- or microscopic fillers. In principle, on the nanometer scale the common additive rules are simply passed: one plus one can make three, or even more. New physical properties and novel behaviors that are absent in the unfilled matrix can be provided by the use of nanoparticles. In addition, unanticipated improvements and huge dividends are expected in the structural and functional performances if the process could prescribe precise spatial arrangement of nanoparticles. It is a general idea that the new generation of nanocomposites should be represented by spatially “engineered, designed and tailored” materials. As suggested by the title of a *News & Views* article on *Nature Materials*, nanocomposites can be “stiffer by design” [Manias (2007)]. Realistically, however, most of the research efforts and almost all of the commercial examples of polymer-based nanocomposites to date have revolved around introducing nanoscale fillers into polymers and simply capitalizing on the filler properties to enhance performance of the composites. This produces a class of polymer/inorganic materials that is perhaps better described by the term “nano-filled polymers” [Vaia and Maguire (2007)]. It turns out that the full exploitation of the exceptional properties arising from the spatial arrangement and ordering of the constituents of polymer nanocomposites is hampered by an inadequate systematic control of the nanoparticles dispersion and material morphology.

Actually, despite the huge volume of literature published on the relationships between the nano-scale structural variables and macro-scale physical and mechanical properties of polymer nanocomposites, the understanding of the basic physical origin of the property changes remains in its infancy. This is partly due to the complexity of polymer nanocomposites, which require the re-considering of the meaning of some basic polymer physics terms and principles.

Polymer nanocomposites are usually thermodynamically out-of-equilibrium materials. Owing to their natural instinct to achieve equilibrium, if provided by sufficient energy, their structure evolves. This could happen while testing their properties above the melting or glass transition temperature of the polymer matrix, during the processing steps or even at the compounding stage of the primary components. Technically, what commonly happens is that the nanoparticles spontaneously aggregate, negating to the ultimate product any benefit associated with their nanoscopic dimension. One should thus ask how it is possible to aspire to polymer nanocomposites having never-before-realized property suites if the basic physics and principles and the governing underlying mechanisms are still poor understood. It thus clearly emerges that the morphological and structural implications stemming from the nanometric sizes of the filler have to be taken into account. Therefore, together with a detailed knowledge of the molecular structure of the polymer matrix, it is also required the fundamental understanding of the nanoparticle dispersion process, the (self-)assembly phenomena, the particle-chain interactions and nanocomposite preparation processes [Jancar et al. (2010)]. In this sense, ascertaining and quantifying the contributions of nanoparticle dynamics and connectivity in polymer melts becomes a task of primary importance.

## 1.2 Thesis organization

The present dissertation is divided into three main parts, which reflect the tracks on which the research activity has been carried out. Part I and Part II enclose the two souls of the work which also emerge from the title: *dynamics* and *structure* of nano-sized particles dispersed in polymer melts, respectively. Part III, instead, represents the application of the fundamental knowledge gained during the first part of the research activity, being it devoted to the use of linear viscoelastic analysis as a tool for the assessment of the filler state of dispersion in polymer nanocomposites. Each section is basically self-consistent: at the beginning, a preliminary introduction to the central topic of the section is provided together with a brief overview of the state-of-the-art, then the results of the investigations are presented and discussed.

Part I is focused on the study of the dynamics and kinetics by which the nanoparticles aggregate within polymer melts, under the driving force of Brownian motion and van der Waals interactions. *Chapter 2* provides the background of the

phenomenon of the filler restructuring in soft glassy materials: the principal features of the process are examined by reporting the main findings of the leading studies in the field. In this frame, *Chapter 3* is dedicated to the fundamental study of the role of nanoparticles mobility on their dynamics of assembly in polymer melts. For such a purpose, a biphasic polymer system filled with nanoparticles, whose mobility is limited by their tendency to locate at the polymer-polymer interface, has been used.

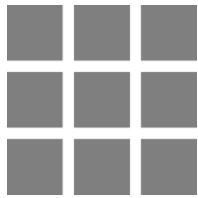
The linear viscoelasticity of polymer nanocomposites is the subject matter of Part II. In detail, the study is focused on the analysis of systems in which the nanoparticles form a three-dimensional network inside the polymeric phase. A brief overview of the general understanding of the linear rheology of nanoparticle filled polymer is provided in *Chapter 4*. In the following chapters, the main results of the research activity are then described. Throughout the section, a rheological two-phase model, recently proposed in the literature to describe the linear viscoelasticity of polymer nanocomposites, is invoked. First, in *Chapter 5* the possibility of using the aforementioned model to deduce the elasticity of networks of nanoparticles too weak to be recognized by conventional viscoelastic analyses is demonstrated. Then, *Chapter 6* proposes and validates the generalization of the model by successfully describing the viscoelastic response of nanocomposite polymer systems differing among them both in the nature of the nanoparticles and in the affinity between the polymer and filler phases. A further test of the robustness of the approach is given in *Chapter 7*, by verifying the ability of the model to satisfactorily describe the linear viscoelasticity of other complex fluids, in which a superposition of the elasticity of the components is possible, such as nanocomposites based on biphasic polymer matrices.

Part III rests on the competences gained and established through the research activity described in Part I and Part II. The work essentially concerns the use of linear viscoelastic measurements for the analysis of the state of dispersion of the nanoparticles in polymer matrices, looking at its consequent impact on the macroscopic performances. The current issues in the preparation of polymer nanocomposites having targeted performances are briefly examined in *Chapter 8*. Then, two case-studies are presented. The effect of the morphology and structure of the primary aggregates of carbon nanotubes on their ease of dispersion in polymer melts is investigated in *Chapter 9*. The effectiveness of a novel compounding technique in overcoming the difficulties related to the dispersion of hydrophilic nanoparticles in hydrophobic polymer matrices is verified in *Chapter 10*.

Finally, the *Conclusions* section is dedicated to a brief summing-up of the activities, aiming to highlight the main findings of the performed research.

All the experimental details have been collected in the *Methods* section at the end of the dissertation to preserve the fluency and the clarity when presenting and discussing the main results of the work. For the same purposes, additional data and plots supporting the presented results are provided separately in the *Appendices*.



 PART  
**I**

# **Nanoparticle dynamics in polymer melts**



# 2

## Particle assembly in complex liquids – Literature review

*In this chapter a brief survey of the internal dynamics in soft matter materials is presented. Starting from the first appearance of the idea of Brownian motion, the concept of “aging” in soft glassy materials is generally discussed (§ 2.1). Then the focus moves on polymer nanocomposites (§ 2.2). The rheological implications of their time-dependent behavior are first discussed. Then, the factors which are believed to influence the spatial rearrangement of nanoparticle in polymer melts and the proposed underlying mechanisms for it are illustrated.*

### 2.1 From Brownian motion to glassy dynamics in soft matter

At the beginning of the XIX Century, dancing pollen granules and other small particles were first described systematically by the Scottish botanist Robert Brown [Brown (1928)] and independently by his French colleague Adolphe Brongniart [Brongniart (1827)]. Based on the intuitive association between motion and life, the observable jiggling motions of micron-sized objects might be attributed to the particles being “alive”. It was not until the 1905 that Einstein’s calculations pointed that they were in fact the consequence of thermal fluctuations of “dead” matter [Einstein (1905)]. In his paper, Einstein explained the hitherto mysterious observations claiming that “according to the molecular-kinetic theory of heat, bodies of a microscopically visible size suspended in liquids must, as a result of thermal molecular motions, perform motions of such magnitudes that they can be easily observed with a microscope”. The facets of this vision, together with its related works [Smoluchowski (1906), Langevin (1908)], have continuously multiplied, providing ample evidence for a real scientific revolution. Brownian motion remains a leading paradigm in a development towards the understanding of the principles underlying the emergence of collective properties in many-particle assemblies, for which P.W. Anderson has coined the mantra “more is different” [Anderson (1972)], meaning that “at each new level of complexity, entirely new properties appear, and the understanding of these behaviors requires research which I think is as fundamental in its nature as any other”.

Soft matter and biological physics indeed are both fields governed by meso-scale structures for which thermal fluctuations are important, the relevant dynamics

often bridging the gap between the microscopically fast and the macroscopically slow. Actually, thermal motion is not the only driving force when dealing with colloidal size entities. From a physical point of view, colloidal particles in a suspending fluid are submitted to particle-particle forces, particle-fluid interactions, viscous forces under flow and finally Brownian forces [Russel et al. (1992)]. Dispersion forces, arising from London-van der Waals attraction, would make the particles flocculate while electrostatic repulsion would not [Israelachvili (2011)]. Doublets and more complicated structures formed during flocculation have long lifetimes, since Brownian motion is too weak to overcome the strong attractive force between particles near contact. The complex phase behavior of soft matter systems stems from the different forces that act among the particles, determining their spatial distribution and governing their dynamics. As a result, thus, the physics of suspensions and even more its extension to molten filled polymers is extremely complicated as the simplest case of inert and rigid spheres at low concentration, often taken as reference starting system, is generally far from real life [Joshi (2014)].

Glassy dynamics are a natural consequence of two properties shared by a wide variety of soft materials: structural disorder and metastability [Sollich et al. (1997)]. In such systems, thermal motion alone is not enough to achieve complete structural relaxation. The system has to cross energy barriers that are very large compared to typical thermal energies. Therefore the system adopts a disordered, metastable configuration even when the state of least free energy would be ordered. The obvious consequence of such peculiarities is the natural instinct of soft glassy materials to achieve equilibrium, in a process of physical aging during which, if provided with sufficient energy from an external field, their structure evolves into state characterized by lower internal energy. Aging has been intensively studied in the context of spin glasses [Cugliandolo and Kurchan (1995), Bouchaud et al. (1997)], on the other hand some of the earliest experimental investigations of it involved rheological studies of glassy polymers [Struik (1977)]. Although various kinds of aging effects are often observable experimentally in soft materials, they have rarely been studied in detail. Fielding et al. (2000) pointed out that aging effects in soft materials are seldom reported and instead viewed as artifacts obfuscating the “true” behavior of the material. But this may be illusory: aging, when present, can form an integral part of a sample’s rheological response.

In the last decade, the interest in “decoding” the motion of particulate matter in a variety of soft materials has been fueled by the promise of deciphering the rules of the (self-)assembly of particles, an endeavor which, if realized, could enable large-scale engineering of complex structures with broad societal impact. As a matter of fact, a genuine line of investigation is dedicated to the dynamic and structural features of colloidal particles in fluid media [Kaushal and Joshi (2014), Christopoulou et al. (2009), Bandyopadhyay et al. (2006), Cloitre et al. (2000)]. Nonetheless, despite the huge volume of work in the field, to date the full

understanding of the underlying mechanism is still controversial and subject of heated debates [Frey and Kroy (2005)].

## **2.2 Nanoparticle flocculation in polymer melts**

Polymer nanocomposites are the natural extension of colloidal suspensions: they are nothing more than suspensions of particles and particle agglomerates dispersed in a fluid medium. Two further specifications are yet necessary. First, the suspending medium is not a simple Newtonian liquid but a complex, viscoelastic melt, having some internal structure which exhibits its own long-range spatial and temporal correlations. In addition, despite the high viscosity of the fluid phase, the dispersed solid particles still experience appreciable Brownian motions due to their nanometric dimension. The result is that polymer nanocomposite, unlike their micro-filled counterparts, can be depicted as “living systems”, in which the particles are free to move and rearrange in the melt, both in flow and even at rest, towards more favorable thermodynamic states. However, given the multiplicity of involved forces and interested factors, it is not a priori obvious what mechanism will control the clustering of the nanoparticles, and how the clustering will be affected by tuning various control parameters. As a result, since the basic studies of Sollich and co-workers [Sollich et al. 1997, Sollich et al. 1998], the fundamental understanding of time-dependent rheological behavior of soft condensed matter in general, and more specifically in the case of polymer nanocomposites, has received the attention of the whole scientific community. In the following, a brief survey on the restructuring and assembly processes of nanoparticle in polymer melts is provided. Far from being exhaustive, it just serves to give an hint about the huge volume of available scientific literature, which testifies the profound interest in the fundamental understanding of such phenomena.

As a matter of fact, due to its relevance both from a fundamental and technological perspective, the mechanism by which nanoparticles rearrange and assemble in the polymer melt and the structures resulting therefrom have been the central subject of numerous studies of physicists, chemists and material engineers. From a technical point of view, there are many different ways to monitor the evolution of the microstructure, and hence the flocculation process, in polymer nanocomposites. For such a purpose, both linear and non-linear rheological measurements indeed have been widely employed. Concerning first category, many authors focused on the time evolution of the viscoelastic moduli at low frequency, either soon after the loading of the sample in the rheometer or after having presheared the sample to erase its flow history, or even in both cases [Treece M and Oberhauser (2007a)]. Actually, in the low frequency region, roughly  $\omega \leq 0.1 \text{ rad s}^{-1}$ , the length-scale corresponding to the meso-structures formed by the flocculation of the nanoparticles is probed. In addition, Ren et al.

(2003) demonstrated that the trends are unchanged for different frequencies at which the process is monitored, at least up to  $\omega \sim 1 \text{ rad s}^{-1}$ . However, single frequency tests lack the information for a complete scaling analysis. More accurately, other authors preferred to carry out a sequence of frequency sweeps in the whole accessible frequency window. In such a way, the evolution of the rheological response can be observed at any frequency and not only in the low frequency range [Wang et al. (2010), Zouari et al. (2012), Huang et al. (2012)]. Such a procedure, yet originally developed to study gelation, is ideally suited for an experimental study of out-of-equilibrium materials with time-dependent connectivity. The standard output of this class of measurements consists in a time-dependent increase of the linear viscoelastic moduli, the effect being much more pronounced on the elastic modulus,  $G'$ , at low frequency. Moreover, most of the authors found that such a dependence follows a logarithmic trend [Ren et al. (2003), Treece and Oberhauser (2007b), Kim and Macosko (2009), Domenech et al. (2014), Cao et al. (2010a), Joshi (2014)]. Alternatively, the process by which the nanoparticles rearrange and assemble within the host polymer melt can be studied by means of steady shear flow experiments. Again, in the scientific literature such measurements have been performed both on as-processed and presheared samples. The characteristic fingerprint of an evolving microstructure is represented by an overshoot of the transient viscosity, or equivalently of the shear stress [Eslami et al. (2009), Ackora et al. (2010), Tang et al. (2011)].

Whatever the selected probing protocol, two main lines of investigation have essentially been pursued: revealing the factors which affect and govern the filler flocculation process and assessing the driving force of the phenomenon. Intriguingly, some rheological signatures have been found to be largely universal, whereas other aspects are still highly controversial.

As an example, the role of the interfacial tension between polymer and filler phases has been widely acknowledged. Typically, the surface free energy of nanoparticles, from inorganics solids to carbonaceous materials, is pretty different from that of polymers, and such a difference is recognized to play a crucial role in driving the flocculation process of the filler. By modeling the aggregation of carbon black particles, indeed, Song et al. (2012) found that the aggregation rate constant scales almost linearly with increasing the interfacial tension between the filler and the polymer melt. Actually, they highlight that, for the formation of clusters of nanoparticles and, ultimately, the building of a three-dimensional filler network, the interstitial fluid has to be squeezed out, and this is an interfacial tension-derived process. Analogously, the effect of the presence of a compatibilizer has been also investigated [Cao et al. (2010b), Nazockdast et al. (2008)]. In this regard, Bailly et al. (2010) found that, upon specific functionalization of the filler which enable the formation of covalent bonds with some chemical functionality of the matrix, the capacity of the particles to associate with each other and form aggregates is limited, leading to a steady rheological response

Differently, the role of the temperature on the particle flocculation process has not been unambiguously ascertained. Increasing the temperature indeed leads to a reduction in the viscosity of the polymer medium and, more importantly, to the enhancement of the thermal activated Brownian fluctuations of the nanoparticles. As a result, one can expect that the kinetics of filler rearrangement should be sensibly accelerated at higher temperatures. Such an intuitive conjecture has been confirmed for a wide range of polymer nanocomposites filled with particles of different size and shape. Some representative examples are the results of Wang et al. (2010) on organoclay-based nanocomposites, of Huang et al. (2012) on carbon black-filled samples and those of Cipriano et al. (2008) on carbon nanotube and nanofiber-based nanocomposites. On the other hand, Treece and Oberhauser (2007a) found that the temperature dependence of the transient viscosity overshoots is rather complex: at early times, temperature appears to play a role, suggesting a thermally driven relaxation process. However, the rate at which the peak viscosity increases appears to be largely insensitive to temperature at longer annealing times. In addition, for presheared samples the rate at which the peak viscosity increases shows minimal effect of temperature. Moreover, Ren et al. (2003) only found a slight increase in the kinetics at elevated temperatures, which they suggest to be indicative of just a small coupling to the matrix viscosity. In this context, the work done by Cao et al. (2010a) is particularly interesting. The authors indeed proved that the investigated nanocomposite systems approach the equilibrium state more quickly at higher temperatures, but modeling the kinetics of aggregation of the particles they found that some parameter are temperature independent. They concluded that increasing the annealing temperature can improve the mobility of both polymer chains and nanoparticles aggregates. However, the formation of filler meso-structures, and ultimately the buildup of a filler network, restrain the movement of polymer chains. The two contradictory aspects may account for the complex temperature dependence of the flocculation process. More in general, given the multiplicity of the involved parameters, most of which exhibit an inherent complex dependence on temperature, defining a universal rule for the effect of the temperature on the particle flocculation and aggregation processes is not so immediate.

It is worth noting that also the effect of the filler volume fraction on the time evolution of the rheological response of polymer nanocomposites is doubtful. In a recent review on the linear viscoelasticity and dynamics of suspensions and molten polymers filled with nanoparticles of different aspect ratios, Cassagnau (2013) observed that the time evolution of the viscoelastic moduli in polymer nanocomposites generally consists of a recovery process, during which the buildup of the filler network takes place. He stresses that the nanoparticles are submitted to strong orientation under flow resulting in the break-up of the filler network. The resulting filler structure upon cessation of the flow is not stable and most of the time such a nanostructure is observed to evolve with time. As a start, it truly seems

reasonable to assume that the changes over time of the viscoelastic moduli, especially the elastic connotation, have to be ascribed to the gradual formation/restoration of a space spanning three-dimensional network of nanoparticles which markedly contribute to the overall elasticity of the sample. Indeed, the rheological evolution over time has been often observed only for samples having a relatively high filler volume fraction, that is when the content of nanoparticles is high enough to allow the formation of a percolated superstructure. This has been expressly stressed by a number of authors for different polymer-nanoparticle pairs [Li et al. (2012), Ke et al. (2012), Song et al. (2012)]. On the other hand, appreciable variations of the rheological functions over time have been also reported for nanocomposite systems considerably far from the percolation threshold. In a beautifully complete study on the soft glassy dynamics in polymer nanocomposites, Treece and Oberhauser (2007b) proved that the storage modulus of the sample at the lowest investigated filler content also shows a clear time-dependence despite the fact that its linear viscoelastic behavior was distinctly polymer-like. Moreover, almost ten years before Bonn et al. (1999) raised a doubt relevant to the question. Specifically, in a colloidal dispersion of Laponite particles they observed a large increase in viscosity during time, yet without the formation of a network as testified by static light scattering measurements. A possible explanation for such an evidence is that the effective volume occupied by the particles is much larger than the nominal one: the fact that the particles can rotate clearly implies an increase in the effective volume, thus explaining the observed enhanced viscosity. Also in this case, the phenomenon cannot be ascribed to a particular kind of filler. Just to give an example, Filippone and co-workers reported an appreciable growth over time of the elastic modulus for nanocomposite below the percolation threshold both for spherical particles [Filippone et al. (2010)] and for plate-like ones [Filippone et al. (2014)]. In conclusion, a more comprehensive and authentic description of the effect of the filler content on the time-dependent rheological response of polymer nanocomposites has been given by Kim and Macosko (2009), and it can be summarized as follows. At very dilute concentration, spatial rearrangement of the filler phase take place, but it does not result in particle contact since the spheres of rotation do not intersect, explaining the observed weak, yet still present, increase in the elastic modulus of polymer melts with low filler content. When the concentration increases, the particles (or particle aggregates) can interact after the rotary relaxation via direct contacts or bridging by polymer chains, and build a sample spanning filler network, which gives rise to a marked elastic response to small amplitude shearing. Finally, in the concentrated regime, isotropic orientation cannot be achieved due to excluded volume interactions between particles. Due to this confinement, the rise of the elastic modulus is significantly slower than that of more diluted samples. Although such a picture has been originally conceived by the authors for disk-like nanoparticles, it can be truly extended to any kinds of filler. Unless using targeted

processing expedients, the presence of single primary nanoparticles in “real” polymer nanocomposites is actually a chimera, even more so if flocculation and aggregation processes takes place. What really happens thus is that the polymer matrix is filled by irregularly shaped clusters of nanoparticles [Filippone and Salzano de Luna (2012)], which are able to rotate within the matrix affecting the relaxation behavior of portions of the polymer melt even at very low filler content.

The picture of particles or particle clusters able to rotate has been also exploited to explain the often observed obedience of the modulus evolution to a two-step process [Treece and Oberhauser (2007a), Treece and Oberhauser (2007b), Huang et al. (2011), Li et al. (2012)]. Zouari et al. (2012) indeed concluded that the first kinetic can be associated with the disorientation of nanofillers by Brownian motion and the second one to the aggregation of clusters into a network. However, discerning a real transition between this two regimes is more of an artifact than an effective scientific evidence. Actually, the identification of the most relevant driving force of the flocculation process likely represents the most debated issue in the field [Cassagnau (2013)]. Generally speaking, the driving forces invoked to explain the propensity of the nanoparticles to rearrange and assemble into polymer melts are fundamentally two: diffusion processes related to the Brownian motion of the filler and interparticle attractive interactions. Nonetheless, conflicting arguments can be found in the scientific literature on this topic. For example, Ren et al. (2003) concluded that independence of the disorientation kinetics with nanoparticle size and polymer matrix indicates that the disorientation process is not governed by Brownian motion. Similarly, Solomon et al. (2001) determined that Brownian motion cannot be the driving force for the filler flocculation and network reconstitution because the processes could not occur sufficiently fast to account for the observed changes in the rheological experiments. They rather believe that attraction forces among the particles govern the phenomenon. Nazockdast et al. (2008), Mobuchon et al. (2009) and Li et al. (2012) are of the same opinion. On the contrary, Huang et al. (2006) supposed that each particle aggregate undergoes Brownian diffusion movement until it meets another one. The collided aggregates stick permanently, generating a new larger aggregate which again has a Brownian motion. Studying the time-dependent rheological response of different polymer-nanoparticle pairs, Cao et al. (2010a) and Guimont et al. (2011) also came to the same conclusions.

A non-trivial consequence of particle restructuring and assembly during thermal treatments is the violation of the well-known time-temperature superposition (TTS) principle. Most of the studies dedicated to the investigation of the linear viscoelastic properties of nanocomposites indeed assume that the sample structure does not change during small amplitude oscillatory shear experiments. This stability generally comes from chemical or thermal treatments of the samples [Krishnamoorti and Giannelis (1997), Nazockdast et al. (2008)]. Under these conditions, no remarkable structural changes occur within the material, at least in

the experiment time scale, for different temperatures. Studies dealing with time evolutive nanostructured materials did not mention any time-temperature equivalence and the authors investigated rheological features associated with the sample at a fixed temperature with well-defined protocols [Reichert et al. (2001), Ren et al. (2003), Mobuchon et al. (2007)]. Thereby some investigations showed that the TTS principle applies and a master curve could be obtained to describe the rheological behavior of the nanostructured material on a broader frequency range than that allowed by the rheometer [Solomon et al. (2001)]. On the other hand, numerous authors found some failures by applying TTS principle, especially in the low frequency range [Zhao et al. (2005); Treece and Oberhauser (2007a, 2007b)]. Reichert et al. (2001), Wagener and Reisinger (2003), and Drosdov et al. (2010) highlight that the structure changes within the nanocomposite are responsible for the observed violation of the TTS principle. Actually, if the evolution of the microstructure is allowed to be fully completed, the resulting sample exhibits a well-developed internal morphology which is now stable in time. As a result, the TTS principle can be successfully applied to the investigated materials. This concept have been clearly pointed out by Reichert et al. (2001), who have checked the validity of the TTS principle for nanocomposite samples with an unstable morphology and concluded that the it does not hold unless a thermal treatment (aging) is applied to the samples at the highest tested temperature to ensure that they reach a thermodynamically stable state. More recently, Zouari et al. (2012) systematically faced the problem in a dedicated paper. They studied nanocomposite systems characterized by a time-dependent rheological response due to the disorientation of the filler phase and, eventually, to the build-up of a space-spanning network. Although such evolution of the structure theoretically brings about a violation of the TTS principle, they proved that the time-temperature equivalence exists if the samples were previously annealed for different times, depending on temperature, in order to obtain similar nanostructures, quantified by the same melt yield stress.

# 3

## Effect of the presence of a preferred liquid-liquid interface on the mobility of nanoparticles in polymer melts\*

*In this chapter the effect of a reduced or even frustrated mobility of the nanoparticles on their dynamics of assembly in polymer melts is investigated. The importance of the filler mobility on the space rearrangements of nanoparticles in polymeric media is first highlighted (§ 3.1). To pursue the targeted research, the study is focused on a biphasic polymer system filled with plate-like nanoparticles which preferentially adsorb at the liquid-liquid interface. The morphology of the neat polymeric systems is first analyzed (§ 3.2). Then, the thermodynamic criteria used to predict the localization of the filler phase are reported together with electron microscopy images which confirm the predictions (§ 3.3). Finally, the dynamics of assembly of the nanoparticles in the biphasic matrix are studied in comparison to a systems based on a single phase matrix through a combination of rheological and morphological analyses (§ 3.4).*

### 3.1 Prefatory notes

Polymer nanocomposites can be described as suspensions of particles and particle agglomerates dispersed in a polymeric medium. However, when dealing with nanoparticles, the morphological and structural implications stemming from the nanometric sizes of the filler have to be taken into account. Specifically, the presence of a nano-sized filler implies an extremely high numerical density of particles, or alternatively very small interparticle distances. As an example, for randomly distributed monodisperse spherical particles, the wall-to-wall distance between contiguous particles,  $h$ , can be approximated to  $h \approx (V/N)^{1/3}$ , where  $V$  represents the volume of the sample and  $N$  the number of particle. By expressing the filler volume fraction,  $\Phi$ , as  $\Phi = N \cdot u / V$ , where  $u = (4 \cdot \pi / 3) \cdot r^3$  represents the volume of the single particle, the distance between the centers of two particles can be written as:

---

\* Part of the results has been published in «Filippone G, Causa A, Salzano de Luna M, Sanguigno L, Acierno D, “Assembly of plate-like nanoparticles in immiscible polymer blends - Effect of the presence of a preferred liquid-liquid interface”, *Soft Matter* 10, 3183-3191 (2014)».

$$h = \left[ \left( \frac{4\pi}{3\Phi} \right)^{1/3} - 2 \right] r \quad (3.1)$$

For diluted systems ( $\Phi < 0.1$ ), such those we are interested in, Equation 3.1 gives  $h \sim 2r$ . This means that, if the filler particles are well dispersed within the host polymer, nanometric inter-particles distances are expected for nanocomposites. Consequently, above the melting or glass transition temperature of the polymer matrix, both Brownian motion and interparticle interactions become of major importance and radically affect the dynamics of the filler phase, making the nanoparticles typically to aggregate.

The flocculation process by which the particles reassemble into bigger structures can be monitored during time by measuring the linear viscoelastic moduli at frequency low enough to consider negligible the elastic contribution of the surrounding polymeric matrix. Most polymer nanocomposites share the same qualitative behavior, also common to the whole class of soft glassy materials which are usually out of equilibrium and thus have a structure which evolves to lower the free energy [Joshi (2014)]. Specifically, the elastic modulus,  $G'$ , increases during the earlier stage, then it reaches a steady state value; a similar trend is noticed for the viscous modulus,  $G''$ , but the changes are much less pronounced. Such variations are usually ascribed to the space rearrangements of the particles or particle clusters in the host polymer melt. Actually, nanoparticles are characterized by a very high specific surface area, typically of order of  $10^2 \text{ m}^2 \text{ g}^{-1}$ , and the matrix properties are significantly affected in the vicinity of the particles, varying continuously from the interface towards the bulk polymer. Accordingly, even subtle changes in the spatial configuration of the filler phase sensibly alter the viscoelastic response of the material.

The timescale of the flocculation process is essentially dictated by the Smoluchowski time for two clusters of nanoparticles to come in contact [Russel et al. (1989)]:

$$\tau_c = \frac{\pi\eta R^3}{\Phi^* k_B T} \quad (3.2)$$

where  $R$  is the radius of the particle cluster,  $\eta$  corresponds to the viscosity of the suspending medium,  $T$  is the temperature,  $k_B$  represents the Boltzmann's constant and  $\Phi^*$  stands for the actual filler volume fraction, that is the volume of the particles in a cluster plus the free volume enclosed between them.

Decreasing the temperature and increasing the particle size have been proved to reduce the filler mobility, eventually arresting any evolution of the viscoelastic moduli over time [Romeo et al. (2009)], independently of the nanosized nature of

the filler phase. It seems thus that the flocculation phenomenon is not a direct consequence of the nano-metric size of the particles, but it rather depends on the mobility of the nanoparticles, which consequently represents a key-parameter for the filler rearrangements to happen. In the light of the previous considerations, the aim of the present work is to investigate the effect of a reduced or even frustrated mobility of the particles on the their dynamics of assembly in polymer melts. For such a purpose, the study focuses on a nanocomposite system based on a biphasic polymer matrix, in which the nanoparticles preferentially adsorb at the liquid-liquid interface. Using nanocomposites based on a homogeneous polymer matrix as reference systems, it allows to study the differences in the assembly dynamics between a system in which the particles are free to rearrange in the host polymer medium and a system in which the particles are not able to move inside the polymer phases because of their trapping at the polymer-polymer interface.

The Chapter is organized as follows. Since the fine tuning of the morphological features of the investigated nanocomposite system represents a key-step to accomplish the targeted research activity, the microstructure of the neat biphasic polymer system is first characterized. Then, the thermodynamic considerations invoked to foresee the localization of the selected filler at the polymer-polymer interface are illustrated and the resulting conclusions are supported via direct morphological analyses. Finally, the study focuses on the investigation of the assembly dynamics in the presence of a dispersed polymer phase, at whose interface the nanoparticles gather.

### **3.2 Morphology of the biphasic polymer system**

The system which is the focus of the present study consists of a biphasic polymer matrix made of polystyrene (PS) and poly(methyl methacrylate) (PMMA) at a composition PS/PMMA of 85/15 by weight. The blend exhibits a drop-matrix morphology, in which the PS represents the continuous phase and the drops are made of PMMA.

The morphology of the biphasic PS/PMMA system has been characterized by estimating the characteristic size of the dispersed PMMA phase. The average size of the drops has been evaluated from the analysis of the SEM micrographs of the PS/PMMA blends. A representative SEM micrograph and the corresponding binary image obtained after manually detecting the inclusions of PMMA are shown in Figure 3.1. Note that the cryo-fractured surface of the observed samples has been previously etched with formic acid to selectively remove the PMMA phase in order to make the two polymeric phases easily distinguishable. The so-obtained binary images have then been analyzed by means of a public domain Java image processing program (ImageJ 1.42q). The radius of the  $i$ -th inclusion,  $R_i$ , has been evaluated as:

$$R_i = \sqrt{\frac{A_i}{\pi}} \quad (3.3)$$

where  $A_i$  corresponds to the measured area of the inclusion amplified by a factor of  $4/\pi$  in order to account for the systematic underestimation of the dimensions of an object from its print on a flat surface [Wu (1985)].

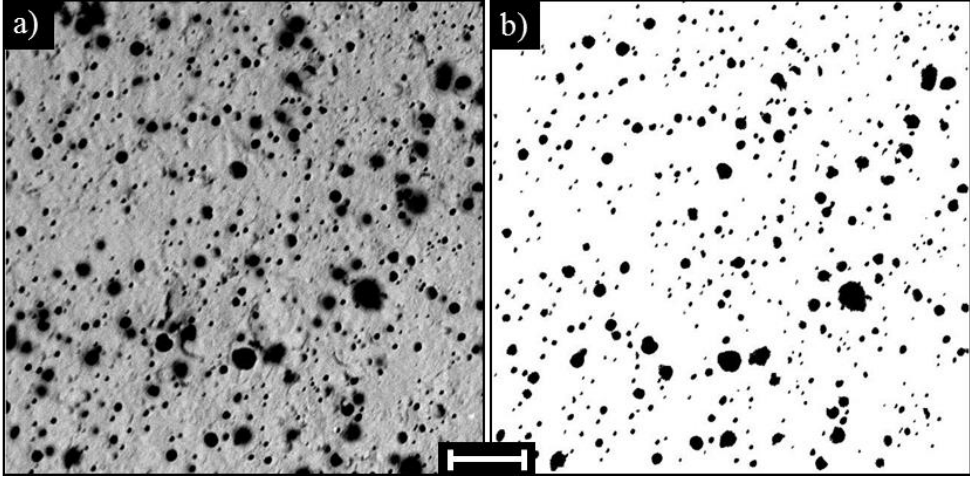


**Figure 3.1** (a) Original SEM micrograph of a PS/PMMA sample (85/15 by weight) and (b) corresponding binary image. The scale bar corresponds to 10  $\mu\text{m}$ .

The number-average drop radius,  $R_n$ , and the volume-average drop radius,  $R_v$ , have been then estimated as:

$$R_n = \sum_{i=1}^n \frac{n_i}{n_{\text{tot}}} R_i \quad (3.4)$$

$$R_v = \sum_{i=1}^n \frac{V_i}{V_{\text{tot}}} R_i \quad (3.5)$$

where  $n_i/n_{\text{tot}}$  and  $V_i/V_{\text{tot}}$  are the numerical and volumetric fractions of drops with radius  $R_i$ , respectively. The analysis of the SEM images leads to  $R_n = 0.461 \mu\text{m}$  and  $R_v = 0.895 \mu\text{m}$ .

### 3.3 Filler localization

Keeping in mind the ultimate goal of the present work, the filler to be added to the PS/PMMA system has to fulfil two requisites. First of all, it has to preferentially locate at the polymer-polymer interface to allow the investigation of the role of nanoparticles mobility on their dynamics of assembly. Secondly, the elastic rheological response associated to the presence of the nanoparticles has to be clearly discernible via conventional linear viscoelastic analysis. In the light of the previous considerations, plate-like nanoparticles have been chosen because, with respect to spherical fillers, they better adapt to the polymer-polymer interface. Among all the lamellar fillers, an organo-modified montmorillonite (Cloisite® 15A, O-Clay) has been selected, since thermodynamic considerations suggest its preferential positioning at the interface in the PS/PMMA system.

In detail, the positioning of the filler at equilibrium has been predicted through the comparison among the interfacial tensions,  $\gamma_{ij}$ , between the constituents of the nanocomposites based on the biphasic matrix. The wettability parameter,  $\omega_{12}$ , which represents the ability of the filler phase “*F*” to be wetted by liquids “*I*” and “*2*”, is defined as:

$$\omega_{12} = \frac{(\gamma_{F2} - \gamma_{F1})}{\gamma_{12}} \quad (3.6)$$

where  $\gamma_{F2}$  and  $\gamma_{F1}$  correspond to the interfacial tensions between the filler and the polymers “*I*” and “*2*”, respectively, and  $\gamma_{12}$  is the interfacial tension between the two polymeric constituents. In an equilibrium configuration, if  $\omega_{12} > 1$  the filler enriches the phase “*I*”, whereas if  $\omega_{12} < -1$  it enriches the phase “*2*”. On the other hand, an intermediate value of the wettability parameter, that is  $|\omega_{12}| < 1$ , means that the nanoparticles are inclined to accumulate at the interface between the two polymeric constituents.

Moreover, to support the expectations suggested by the wettability parameter, the spreading coefficient,  $\lambda_{ij}$ , can be calculated as well:

$$\lambda_{ik} = \gamma_{jk} - \gamma_{ij} - \gamma_{ik} \quad (3.7)$$

Such parameter was originally defined to evaluate the tendency of a polymer “*i*” to encapsulate dispersed domains of a second polymer “*k*” in a matrix of a third polymer “*j*”. Nonetheless, as suggested by Steinmann et al. (2002), it can be applied to filled blends by replacing the polymer “*k*” with the filler “*F*”. As a result, if  $\lambda_{iF} > 0$ , the polymer “*i*” is expected to encapsulate the filler phase, and its tendency to do so is proportional to the value of  $\lambda_{iF}$ . Conversely, if  $\lambda_{iF} < 0$ , encapsulation does not take place.

The estimation of the wettability parameter and spreading coefficients presumes the knowledge of the  $\gamma_{ij}$  values, which can be easily calculated starting from the polar and dispersive components of the surface tension by exploiting theoretical models. Specifically, for material pairs with comparable surface tensions the harmonic mean equation can be used:

$$\gamma_{ij} = \gamma_i + \gamma_j - 4 \left( \frac{\gamma_i^d \gamma_j^d}{\gamma_i^d + \gamma_j^d} - \frac{\gamma_i^p \gamma_j^p}{\gamma_i^p + \gamma_j^p} \right) \quad (3.8)$$

where  $\gamma_i$  and  $\gamma_j$  corresponds to the surface tension of the constituents “*i*” and “*j*”, respectively,  $\gamma_i^p$  and  $\gamma_j^p$  are the corresponding polar components of such surface tensions and  $\gamma_i^d$  and  $\gamma_j^d$  are the dispersive counterparts.

On the other hand, the geometric mean equation is recommended in the case of material pairs with very different surface tensions:

$$\gamma_{ij} = \gamma_i + \gamma_j - 2 \left( \sqrt{\gamma_i^d \gamma_j^d} - \sqrt{\gamma_i^p \gamma_j^p} \right) \quad (3.9)$$

Before estimating the  $\gamma_{ij}$  values, a further specification is necessary: the wetting parameter and spreading coefficient have to be estimated at the temperature at which the material of interest has been effectively prepared, i.e. at  $T = 190^\circ\text{C}$  (see Methods section for details). Consequently, to use either Equation 3.8 or 3.9, the surface tensions at  $T = 190^\circ\text{C}$  of all the constituents of the PS/PMMA/O-Clay system are needed. Assuming a linear dependence of the surface tension on the temperature, literature data of the surface tensions at room temperature and the corresponding coefficients of variation with temperature,  $\partial\gamma_i/\partial T$ , have been used for such a purpose. Then, the surface tension at  $T = 190^\circ\text{C}$  has been split in its polar and dispersive parts keeping the same ratio between the two as that at room temperature.

The values of surface tension at room temperature and the corresponding coefficient of variation with temperature for the neat PS and PMMA are widely reported in the literature. On the contrary, a lack of literature data exists for the surface tensions of the organo-modified montmorillonite. Nonetheless, many organo-modified layered silicates share comparable values of  $\gamma_i^d$ , whereas  $\gamma_i^p$  exhibits a greater sensitiveness to the nature of the organo-modifier [Picard et al. (2007)]. As a first approximation, here the same values reported for Cloisite® 10A by Kamal et al. (2009) have been used for Cloisite® 15A.

The values of the surface tensions and the corresponding polar and dispersive components at room temperature are summarized in Table 3.1, together with the related temperature coefficients and the extrapolated values at  $T = 190^\circ\text{C}$  for the neat PS and PMMA phases and for the selected O-Clay.

**Table 3.1** Dispersive and polar components of the surface tensions at room temperature and at  $T = 190^\circ\text{C}$  as obtained by using the temperature coefficients.

[units]	$T = 20^\circ\text{C}$			$\partial\gamma_i/\partial T$ [mN m <sup>-1</sup> °C <sup>-1</sup> ]	$T = 190^\circ\text{C}$		
	$\gamma_i$	$\gamma_i^d$	$\gamma_i^p$		$\gamma_i$	$\gamma_i^d$	$\gamma_i^p$
PS	40.7	34.5	6.1	-0.072	28.5	24.2	4.3
PMMA	41.1	29.6	11.5	-0.076	28.2	20.3	7.9
O-Clay	45.3 <sup>a</sup>	33.4 <sup>a</sup>	11.8 <sup>a</sup>	-0.136 <sup>b</sup>	22.9	16.9	6.0

<sup>a</sup> Values at  $25^\circ\text{C}$ .

According to the values reported in Table 3.1, the interfacial tension  $\gamma_{12}$  between PS (polymer “1”) and PMMA (polymer “2”) at  $T = 190^\circ\text{C}$  has been estimated via Equation 3.8, whereas Equation 3.9 has been used for the interfacial tensions  $\gamma_{F1}$  and  $\gamma_{F2}$  between the filler and the two polymers. The resulting values of  $\gamma_{ij}$  are summarized in Table 3.2. Finally, the values of the wettability parameter and spreading coefficients have been obtained by simply substituting the computed interfacial tensions into Equations 3.6 and 3.7, respectively. The results of the calculations are reported in Table 3.3.

**Table 3.2** Interfacial tensions at  $T = 190^\circ\text{C}$ .

Material pair	$\gamma_{ij}$ [mN m <sup>-1</sup> ]
PS/PMMA	1.48
PS/O-Clay	0.91
PMMA/O-Clay	0.34

**Table 3.3** Wettability parameter and spreading coefficients for the PS/PMMA biphasic system filled with O-Clay.

Parameter	Value [units]
Wettability parameter, $\omega_{12}$	0.39 [-]
Spreading coefficient, $\lambda_{1F}$	- 2.05 [mN m <sup>-1</sup> ]
Spreading coefficient, $\lambda_{2F}$	- 0.91 [mN m <sup>-1</sup> ]

The thermodynamic arguments invoked to foresee the positioning of the filler at equilibrium clearly indicates the propensity of the O-Clay to locate at the interface between the PS and PMMA phases. Indeed, the wettability parameter indicates that the filler phase tends to accumulate at the interface between the two polymeric media. Accordingly, the spreading coefficients suggest that neither the PS phase nor the PMMA one should encapsulate the O-Clay, and thus the filler should be located at the interface between the two.

The positioning of the filler at the PS/PMMA interface has been also verified by transmission electron microscopy (TEM) analyses. The morphology of a representative nanocomposite based on the biphasic polymer matrix is shown in the TEM micrographs of Figure 3.2. Note that for the sake of clarity a diluted sample has been selected.

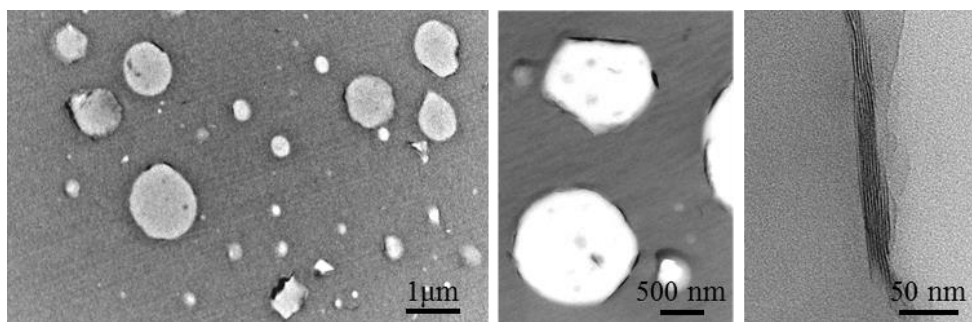


**Figure 3.2** TEM micrographs at different magnification of a PS/PMMA/O-Clay sample at  $\Phi = 0.0032$ .

Micrometric PMMA drops are suspended in the PS matrix. The clay mostly lies on the surface of the droplets. It is worth noting that the tactoids, which at this composition do not saturate the available polymer-polymer interface, do not bend to trace out the contours of the drops, being instead the latter which adapt to the clay. In other words, the bending stiffness of the particles prevails over the interfacial tension. Such a finding reflect the fact that the filler has been selected in order to be clearly discernible via conventional linear viscoelastic analysis. At higher magnification, the O-Clay appears in the form of stacks of several silicate layers. Wide angle X-ray diffractometry (WAXD) analyses have been performed on the pristine particles and on three as-extruded polymer/O-Clay samples to investigate the lamellar structure of the O-Clay (Figure 3.3). Note that, again, diluted samples have been selected for the sake of clarity. A moderate expansion of the basal spacing with respect to the pristine particles emerges from the spectra of the polymer/O-Clay samples. To estimate the interlayer spacing between the

silicate layers,  $d_{001}$ , the Bragg's condition is applied to the low-angle peak ( $2^\circ < 2\theta < 4^\circ$ ) of the scattering intensity, which corresponds to the  $\{001\}$  basal reflection of the montmorillonite. Although the PMMA seems having somewhat better interaction with the O-Clay, the diffraction peaks of the three polymer nanocomposites are too wide and too close to draw unambiguous conclusions about which of the polymers preferentially intercalates the filler.

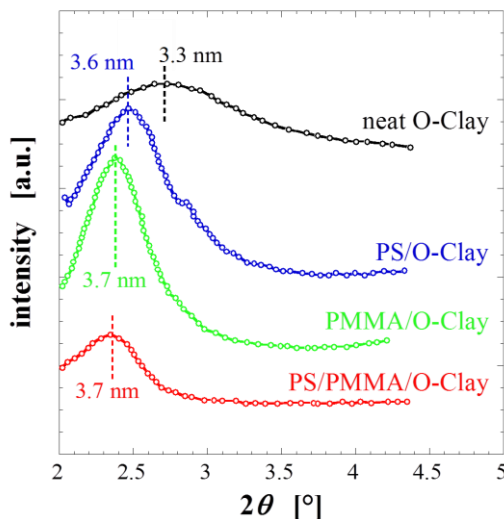


**Figure 3.3** WAXD patterns for pristine O-clay, PS/O-Clay, PMMA/O-Clay and PS/PMMA/O-Clay samples at  $\Phi \sim 0.009$ . The interlayer spacing is reported as well.

The most reasonable deduction is that both PS- and PMMA-intercalated tactoids exist. In addition, as sometimes proposed to explain the presumed compatibilizing action of organo-clays, the presence of interfacially-located stacks simultaneously intercalated by both polymers is also possible [Fang et al. (2007)]. Such conclusions exactly reflect the criterion adopted to select the materials: since the rationale is promoting the positioning of the filler at the polymer-polymer interface, a filler that does not exhibit preferential interactions with none of the polymers of the system has been selected.

### 3.4 Dynamics of assembly of the nanoparticles

Nano-sized particles are inclined to rearrange towards more stable configurations once the temperature is raised up above the melting/softening point of the host polymer matrix. The key-parameter in such a process is represented by

the inherent mobility of the nanoparticles. To investigate the effect of the reduced/frustrated mobility of the particles anchored to the PMMA drops in the biphasic PS/PMMA system, the time evolution of the linear viscoelastic moduli has been monitored. The elastic modulus, which is more sensitive to the presence of the filler than its viscous counterpart, is shown in Figure 3.4 as a function of time,  $t$ , for PS/PMMA/O-Clay samples at different filler content. The same analysis has been performed on nanocomposites based on a homogeneous PS matrix for comparison. Note that the evolution dynamics of the elastic modulus are reported in terms of time-normalized elastic modulus to highlight the differences. In detail, the  $G'(t)$  curve of each sample has been divided by the initial value,  $G'(t = 0)$ .

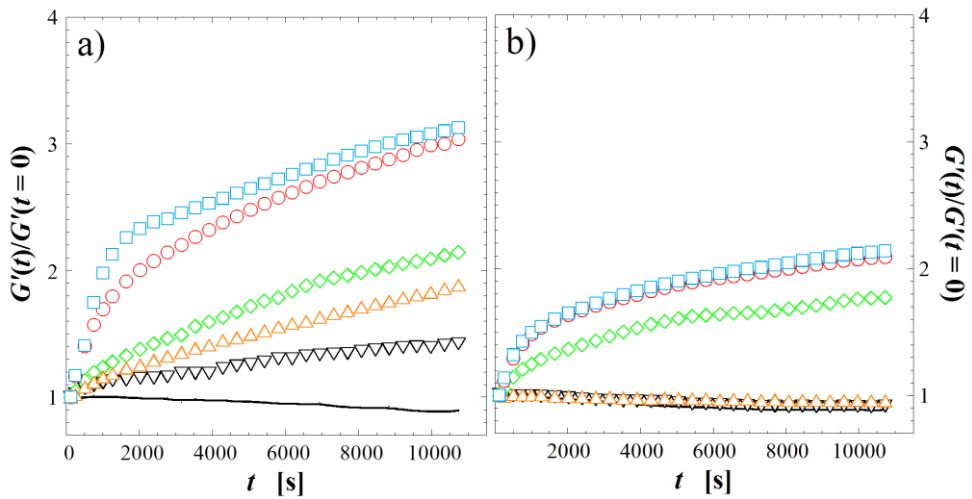


**Figure 3.4** Time evolution of  $G'$  at  $\omega = 0.1 \text{ rad s}^{-1}$  normalized over the initial value for (a) PS/O-Clay and (b) PS/PMMA/O-Clay samples at different filler content. From bottom to top: (a)  $\Phi = 0.0007, 0.0044, 0.0060, 0.0132$  and  $0.0163$ ; (b)  $\Phi = 0.0032, 0.0075, 0.0093, 0.0132$  and  $0.0205$ . Solid line represent the modulus of (a) PS and (b) PS/PMMA matrices.

The elasticity of the PS/O-Clay samples grows during time at any  $\Phi$ . The growth rate is faster in the earlier stages, then the elasticity approaches a time-independent value,  $G'(t \rightarrow \infty)$ . Differently, the behavior of the PS/PMMA/O-Clay samples at  $\Phi < 0.0093$  exactly retraces that of the neat biphasic PS/PMMA matrix. Only above this threshold the elasticity starts to increase over time. The growth of elasticity at rest is a rheological fingerprint of nanofilled polymers. Such a phenomenon is ascribed to the well-known particle flocculation process, which causes polymer confinement and more intensive hydrodynamic effects. Moreover, above the percolation threshold,  $\Phi_c$ , a space-spanning filler network eventually

forms/restores, further increasing the overall elasticity. In the PS/O-Clay system,  $G'$  increases even at very low  $\Phi$ , that is when the number of particles is not enough to make inter-particle interactions possible. In the specific case of plane fillers, the growth of  $G'$  at very low  $\Phi$  reflects the increasing effective volume of the particles, which rotate losing the alignment imposed by the squeezing flow during sample loading [Kim and Macosko (2009), Treece and Oberhauser (2007b)]. In such a dilute regime, indeed, the nanoparticles are able to freely rotate about their center of mass, without any interference interaction with neighboring ones. The particle diffusivity is controlled by the Brownian forces in the suspending liquid which exerts the Stokes friction on the particle [Cassagnau (2013)]. The characteristic timescale for the structural rearrangements of plate-like particles can be thus roughly estimated as the inverse of the rotary diffusivity of rigid disks,  $D_{r0}$ :

$$D_{r0} = \frac{3k_B T}{4\eta d_F^3} \quad (3.10)$$

where  $d_F$  represent the diameter of the disk-like particle [Larson (1999)].

Actually, the diameter of the particles is rather difficult to evaluate accurately, since it depends on the conditions of the production process of the filler and of the nanocomposite samples. Setting  $\eta \approx 3000$  Pa s, which is the zero-shear rate viscosity of neat PS at  $T=190^\circ\text{C}$ , the rotational relaxation time  $D_{r0}^{-1}$  is reported in Figure 3.5 as a function of the diameter of the particles.

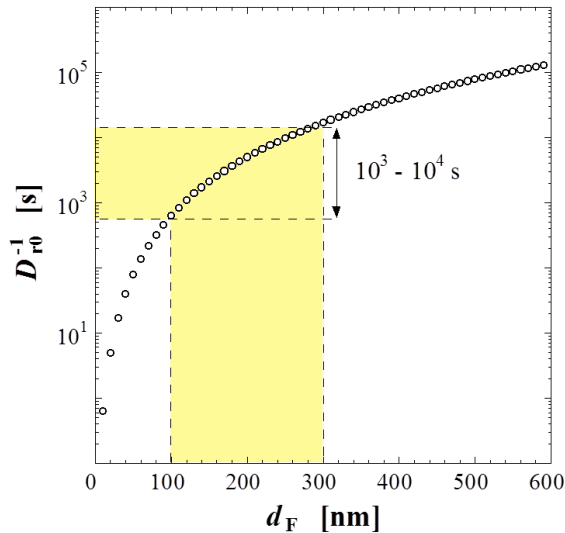


**Figure 3.5** Rotational relaxation time as a function of the characteristic lateral dimension of the disk-like particles.

The rotational relaxation time is a strong function of the particle diameter. Consequently, at least a rough estimation of such a parameter is strictly necessary to have an idea of the timescale of the nanoparticle disorientation process. The single silicate layers on which commercial O-Clays are based are intrinsically variable in characteristic lateral dimension [Ploehn and Liu (2006)]. In addition, the platelets may be skewed relative to one another within the tactoids, which results in further variability in the distribution length [Chavarria and Paul (2004)]. Nonetheless, the lateral dimension of O-Clays has been found to typically range between 100 nm and 300 nm, with occasional big tactoids more than 1  $\mu\text{m}$  long in case of bad dispersion of the pristine clay aggregates. For such dimensions, Equation 3.10 returns values of  $D_{r0}^{-1}$  in the range  $10^3 \div 10^4$  s for the PS/O-Clay system, which is compatible with the timescale for the growth of  $G'$  shown in Figure 3.4a. On the other hand, for the PS/PMMA/O-Clay samples Equation 3.10 cannot be used, the particles being mostly trapped at the polymer-polymer interface. Indeed, filler rearrangements able to affect the macroscopic viscoelastic response would imply energetically costly processes, such as a detachment of the particles from the interface or the dragging/deformation of the drops on which they are adsorbed. As a result, the particle mobility is frustrated and the viscoelastic moduli remain stable during time (Figure 3.4b). Although the anchoring of the particles on the PMMA drop surface inhibits any motion of the filler, once the available PS/PMMA interface is saturated, the exceeding particles are free to rearrange in the host medium irrespective of its biphasic nature. This can be clearly appreciated looking at the normalized equilibrium modulus,  $G'(t \rightarrow \infty)/G'(t = 0)$ , shown for the two families of nanocomposites in Figure 3.6 as a function of  $\Phi$ .

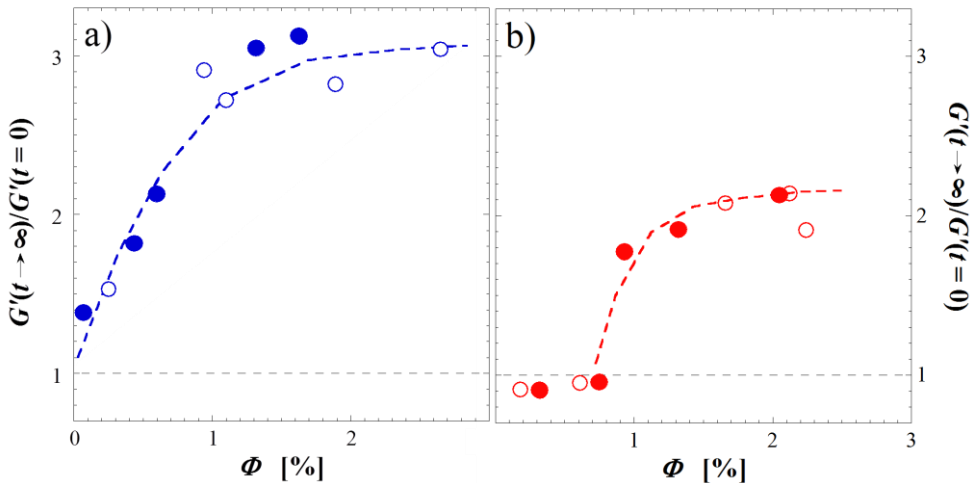


**Figure 3.6** Normalized equilibrium modulus as a function of filler content for (a) PS/O-Clay and (b) PS/PMMA/O-Clay samples. Full symbols are the same samples of Figure 3.4.

In the PS/O-Clay system, the normalized equilibrium modulus gradually scales with  $\Phi$  at low filler contents, reflecting the inherent mobility of the particle. After a certain  $\Phi$  a kind of saturation is achieved, because in the concentrated regime the filler motion is highly restricted by excluded volume interactions among particles. On the other hand, in the PS/PMMA/O-Clay system, an abrupt transition in the  $\Phi$ -dependence of  $G'(t \rightarrow \infty)/G'(t = 0)$  can be noticed. The jump of the normalized equilibrium modulus at  $\Phi \sim 0.01$  reflects the “off-to-on” switch of the particle mobility once the filler saturates nearly completely the PS/PMMA interface. The sudden change in the normalized equilibrium modulus of Figure 3.6b suggests that such a saturation occurs at a filler fraction in the range  $0.0075 < \Phi < 0.0093$ . Further support to such a result can be gained by theoretically estimating the filler volume fraction at saturation,  $\Phi_S$ . By definition,  $\Phi_S$  represents the nanoparticle content at which the surface area of the filler phase,  $S_F$ , equals the available PS/PMMA interface,  $S_I$ :

$$S_F = S_I \quad \text{at } \Phi = \Phi_S \quad (3.11)$$

As a first approximation, the PMMA drops can be considered as monodisperse spheres and the O-Clay particles as disks. Consequently, the available PS/PMMA interface is given by the total surface of the PMMA droplets, which can be expressed as:

$$S_I = n_D S_D \quad (3.12)$$

where  $n_D$  is the total number of inclusions and  $S_D$  is the surface of a single PMMA drop given by:

$$S_D = 4\pi R_D^2 \quad (3.13)$$

where  $R_D$  is the mean radius of the PMMA drops in the system.

Analogously to the estimation of the surface of the PMMA droplets, the surface area associated to the filler phase is given by:

$$S_F = n_p S_p \quad (3.14)$$

where  $n_p$  is the total number of particles and  $S_p$  is the surface of a single lamella.

Actually, a specification is required before giving an analytical expression to  $S_p$ . Indeed, the external surface of the disk-like particle does not contribute in its totality to the coverage of the PMMA drops. In the oversimplified picture considered here, the involved surface in fact corresponds to the extent of only one “face” of the disk, that is:

$$S_p = \frac{\pi D_p^2}{4} \quad (3.15)$$

where  $D_p$  represents the mean diameter of the nanoparticles.

The total number of drops and the total number of particles can be expressed in terms of volume fraction of drops,  $\Phi_D$ , and volume fraction of filler, respectively, as:

$$n_D = \Phi_D \frac{V_{tot}}{V_D} \quad (3.16)$$

$$n_p = \Phi \frac{V_{tot}}{V_p} \quad (3.17)$$

where  $V_{tot}$  is the volume of the sample and  $V_D$  and  $V_p$  correspond to the volume of a single drop and that of a single particle, respectively, and according to the assumed geometric approximations are given by:

$$V_D = \frac{4}{3} \pi R_D^3 \quad (3.18)$$

$$V_p = \frac{\pi D_p^2}{4} s \quad (3.19)$$

where  $s$  corresponds to the thickness of the particle disk.

Substituting the expressions of  $n_D$  and  $S_D$  into Equation 3.12 and the expressions of  $n_p$  and  $S_p$  into Equation 3.14, the condition for saturation to occur becomes:

$$\Phi_S = 3s \frac{\Phi_D}{R_D} \quad (3.20)$$

The estimation of the filler volume fraction at saturation through Equation 3.20 requires the knowledge of three parameters: the volume fraction of drops, their mean radius and the thickness of the particle disks.

The volume fraction of PMMA drops can be calculated starting from the weight composition of the blend. The values of density at room temperature,  $\rho_i$ , and the corresponding coefficients of variation with temperature,  $\partial\rho_i/\partial T$ , used to calculate the volume fractions of the constituents of the biphasic PS/PMMA system are reported in Table 3.4.

**Table 3.4** Values of the density and of the coefficient of variation of density with temperature for the PS and PMMA. Values taken from [Mark (2009)].

Material	$\rho$ [g/cm <sup>3</sup> ] at 25°C	$\partial\rho_i/\partial T$ [g/(cm <sup>3</sup> K)]
PS	1.040 ÷ 1.065	$-2.65 \times 10^{-4}$ ( $T < T_g$ ) $-6.05 \times 10^{-4}$ ( $T > T_g$ )
PMMA	1.170 ÷ 1.200	Not available

Concerning the PMMA, literature values for  $\partial\rho_{\text{PMMA}}/\partial T$  are not available, so data of Pressure-Volume-Temperature measurements are used [Chandra et al. (2010)]. With respect to the room temperature, the specific volume change of PMMA,  $dV_{\text{PMMA}}$ , is about 0.044 cm<sup>3</sup>/g at 190°C (at a pressure of ~ 0 MPa). Consequently, the density of PS and PMMA at 190°C can be estimated as:

$$\rho_{\text{PS}} = \rho_{\text{PS}}|_{25^\circ\text{C}} + \left. \frac{\partial\rho_{\text{PS}}}{\partial T} \right|_{T < T_g} (T_g - 25) + \left. \frac{\partial\rho_{\text{PS}}}{\partial T} \right|_{T > T_g} (190 - T_g) \quad (3.21)$$

$$\rho_{\text{PMMA}} = \rho_{\text{PMMA}}|_{25^\circ\text{C}} / (1 + dV_{\text{PMMA}}) \quad (3.22)$$

The calculations lead to  $\rho_{\text{PS}} = 0.978$  g/cm<sup>3</sup> and  $\rho_{\text{PMMA}} = 1.135$  g/cm<sup>3</sup>, from which  $\Phi_{\text{D}} = \Phi_{\text{PMMA}}$  in the PS/PMMA system at a composition of 85/15 by weight can be evaluated as:

$$\Phi_{\text{PMMA}} = \frac{(m_{\text{PMMA}}/\rho_{\text{PMMA}})}{(m_{\text{PMMA}}/\rho_{\text{PMMA}} + m_{\text{PS}}/\rho_{\text{PS}})} \quad (3.23)$$

where  $m_{\text{PMMA}}$  and  $m_{\text{PS}}$  represent the weight fractions of PMMA and PS, respectively, in the biphasic system. Combining the previous equations, a value of  $\Phi_{\text{PMMA}} = 0.132$  is obtained for the PS/PMMA blend 85/15 by weight.

The estimation of the mean radius is more challenging. Actually, Filippone and Acierno (2012) demonstrated that the addition of plate-like particles to a polymer blend with drop-matrix morphology has a twofold effect. It promotes a refinement of the morphology during the intense flows which occur during compounding and it induces coarsening in the course of prolonged slow flows experienced during the rheological analysis. Nonetheless,  $R_{\text{D}}$  can be considered of the same magnitude of the value of  $R_{\text{v}}$  estimated for the neat PS/PMMA system (see § 3.2 for details), and thus it can be approximated to 1  $\mu\text{m}$ .

According to Equation 3.20, the filler volume fraction at saturation is reported as function of the thickness of the particles in Figure 3.7.

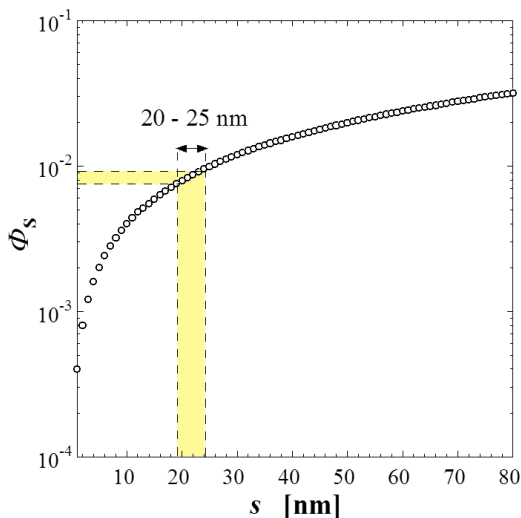


**Figure 3.7** Filler volume fraction at saturation as function of the thickness of the particle disk setting  $R_D = R_v \sim 1 \mu\text{m}$  and to  $\Phi_{\text{PMMA}} = 0.132$  the volume fraction of the drops. The highlighted area corresponds to the values of  $\Phi_s$  deduced from time scans in Figure 3.6.

As evidenced in Figure 3.7, the range for  $\Phi_s$ , experimentally identified by linear viscoelastic analyses, should correspond to nanoparticles of about  $20 \div 25 \text{ nm}$  in thickness. Despite the simplifications considered to get Equation 3.20 and the approximations in the estimate of the variables therein, morphological analyses indicate a good agreement between the estimated and the real value of  $s$ , supporting the conclusions drawn from viscoelastic data. High-magnification TEM images of a representative sample at  $\Phi = 0.0075$  are shown in Figure 3.8.

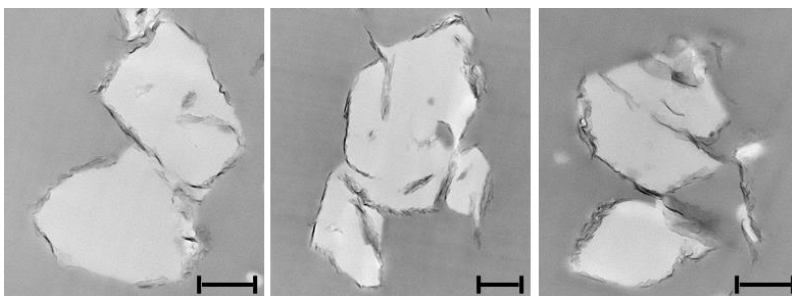


**Figure 3.8** TEM images of a PS/PMMA/O-Clay sample. Scale bars correspond to 250 nm.

In addition, morphological analyses have been performed on two nanocomposites samples around the threshold of  $\Phi_s \sim 0.01$  to definitely confirm the obtained results (Figure 3.9).

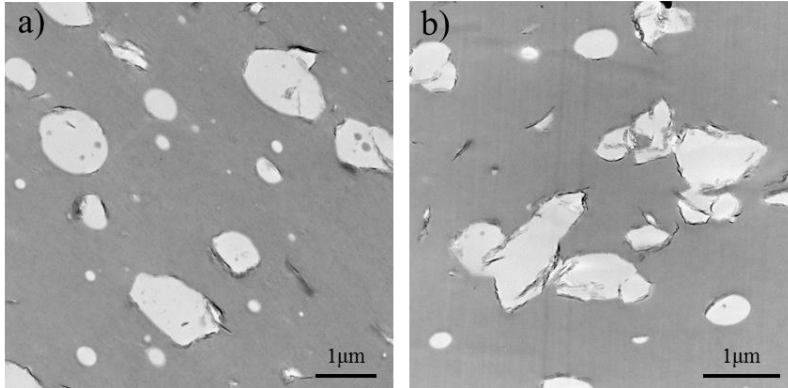
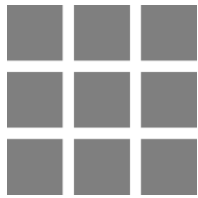


**Figure 3.9** TEM micrographs of the PS/PMMA/O-Clay samples at (a)  $\Phi = 0.0075$  and (b)  $0.0132$ .

The TEM images eventually confirm the detected saturation content of nanoparticles. Bare or partially covered PMMA droplets, indeed, can be noticed at  $\Phi = 0.0075$ , the covering is instead nearly complete in the sample at  $\Phi = 0.0132$ , whose drops appear more distorted because of the bending stiffness of the lamellae. As expected, once most of the interface is saturated, unconstrained tactoids suspended in the continuous PS phase can be noticed.





**PART**  
**II**

# **Nanoparticle networks in polymer melts**



# 4

## Linear viscoelasticity of polymer nanocomposites – A brief survey

*In this chapter the general understanding on the linear viscoelasticity of polymer nanocomposites is discussed. First, its universal appearing and underlying mechanism are presented (§ 4.1). Then, the origin and phenomenology of a two-phase model able to interpret the viscoelasticity above the filler percolation threshold are briefly illustrated (§ 4.2).*

### 4.1 General considerations

Real materials, and especially soft materials, are neither ideal solids nor ideal liquids. Consider the classic toy: silly-putty. When squeezed slowly, it deforms and flows like a liquid; however, when thrown against a wall, it bounces like a rigid elastic solid. Real soft materials analogously exhibit both elastic and viscous responses and are therefore called viscoelastic. In general, the internal structures of soft solids and complex fluids composed of colloidal particles, filamentous and flexible polymers, or other supra-molecular arrangements lead to complicated mechanical responses. As a result, the relations between stress and strain are not simply defined by elastic and viscous constants, rather, these relations can be functions of time, direction, and extent of deformation. In this context, the goal of rheological experiments is to relate the viscoelastic properties to the meso- and macro- structure of the material.

Focusing on polymer nanocomposites, as they represent the essence of the present dissertation, their linear viscoelastic behavior is an old and challenging topic. Although a wide range of literature exists dealing with the linear viscoelastic response of polymer-based nanocomposites, general physical models able to describe the frequency-dependent behavior of the viscoelastic moduli as function of filler volume fraction are still scarce. This is not surprising, since continuum rheological models, successfully capturing the main features of polymers filled with micrometer-sized particles, generally fail when applied to nanostructured systems [Jancar et al. (2011)]. When the characteristic size of the filler is on the nanometers scale, indeed, the linear viscoelastic properties of polymer melts are generally profoundly affected by the addition of even small amount of nanoparticles. Broadly speaking, the main effects are usually the monotonic

increase of the viscoelastic moduli with the filler loading and the broadening of the relaxation dynamics of the polymer. Actually, a lot of papers and reviews, such as those of Chatterjee and Krishnamoorti (2013), Cassagnau (2008), Litchfield and Baird (2006) and Krishnamoorti and Yurekli (2001), have addressed the rheology of nanocomposites. Many authors have discussed the connection that can be made between the filler nature and the melt viscoelastic properties of polymeric materials. However, the multitude of involved factors stemming from the variety of nanoparticle shape, size and chemical nature, as well as from the diversity of polymeric materials, makes the rheological behavior of polymer nanocomposites a non-trivial topic, which deserve dedicated studies to be fully understood. As an example, although many papers have been devoted to the mechanisms of polymer reinforcement, it is still an open debate in the literature, and only the last work of Jouault et al. (2012) on model nanocomposites seems to have proved the relevant mechanisms. Thus we do not strive here for a comprehensive description of the observed phenomena and underlying mechanisms of the rheological behavior of polymer nanocomposites, since they represent a too wide subject of research to be satisfactorily addressed in a thesis chapter. Rather, the aim is to provide a general picture of the linear viscoelasticity of nanofilled polymer melts, which only serves as foundation for the experimental result which will be discussed later. Despite the inherent complexity, indeed, some general patterns in the linear viscoelastic properties emerge when adding a small volume fraction of particles to polymeric media.

For non-interacting particles, an increase of the linear viscoelastic moduli is typically observed over the whole range of frequencies [Carreau et al. (1996, Aral and Kalyon (1997), Le Meins et al. (2002)]. One effect is the enhanced local deformation rates caused by the mere presence of solid particles. Because the particles are solid, the global straining motion is concentrated in the interstitial fluid. The corresponding increase in the shear stresses is determined by the volume of particles present and can be expressed as an increased effective deformation. This also leads to a decreased linear viscoelastic region [Ohl and Gleissle (1993), Kim and White (1999), Schaink et al. (2000)]. On the other hand, an attractive potential among the nanoparticles often exists, and such an aspect is rendered even more prominent due to their high available surface area. As a result, the particles show pronounced colloidal interactions, which make them typically to flocculate (see Chapter 2 for details). This causes an additional increase in the low frequency moduli, which gradually scales with the amount of filler phase. At a certain value of filler volume fraction,  $\Phi$ , however, an abrupt increase in the viscoelastic moduli, especially in the elastic one, is usually observed. The enhancement of the moduli is coupled with a drastic change in the terminal behavior, indeed the moduli gradually lose the dependency on frequency which is typical of the polymer melt. The critical value of  $\Phi$  is system-specific, since it strictly depends on the filler type, polymer nature and processing conditions. Nonetheless, the underlying mechanism for the

sudden changes in the elastic and viscous moduli and in the flattening of the relaxation spectra is generally the same, that is the formation of a space-filling network, which may result from either direct interaction between particles [Ren et al. (2000), Inoubli et al. (2006)] or from inter-particle polymer-bridging mechanisms [Zhang and Archer (2002), Saint-Michel et al. (2003)]. The rheological evidence of such superstructures formed by the nanoparticles is twofold, since two different kinds of network can be distinguished. In the presence of a permanent filler network, a low-frequency plateau in the elastic modulus is expected to develop, indicating the complete arrest of the relaxation dynamics. Alternatively, the particles can arrange in a transient three-dimensional structure, which slowly and continuously relaxes with a broad spectrum of relaxation times [Romeo et al. (2008), Prasad et al. (2003), Wolthers et al. (1997)]. The wide diversity of microstructures and possible dynamics, which arise from the multiple particle-particle and polymer-particle interactions which set up in the nanocomposite, makes the linear viscoelastic behavior of nanofilled polymer melts extremely variegated. Nonetheless, the rheological fingerprint common to most of the polymer nanocomposites enabled some authors to propose a simple, yet general, model for the description of the linear viscoelasticity. Among others, Song and Zheng (2011) and Filippone et al. (2012) independently introduced two different models, which describe the viscoelasticity of polymer nanocomposites in terms of only two phases. In the next paragraph, a brief description of the underlying physics of the model proposed by Filippone and co-workers is provided, since it is largely exploited in the following chapters when the obtained experimental results are discussed.

## **4.2 Scaling of the viscoelasticity: a two-phase model**

The linear viscoelastic behavior of polymer nanocomposites is extremely complex due to both inherent viscoelastic nature of the suspending medium and the wide variety of microstructures and possible dynamics, which arise from the multiple particle-particle [Solomon et al. (2001)] and polymer-particle interactions [Zhang and Archer (2002)]. Because of this high complexity, a general description of how the frequency dependent elastic and viscous moduli vary with the filler volume fraction is effectively difficult to attain.

Despite some fundamental differences, polymer nanocomposites exhibit numerous analogies to colloidal dispersions, which in fact represent their simpler counterparts. First, they both possess a wide spectrum of rheological properties, ranging from simply viscous fluids to highly elastic pastes depending on the amount of particles and the sign and magnitude of inter-particles interactions. Moreover, the nanometric size of the particles brings about a relevant filler mobility. Indeed, nanoparticles can experience significant Brownian motions even

in highly viscous mediums such as polymer melts. The result is that polymer nanocomposites continuously evolve toward more favorable states in relatively short time scales. They are in all the aspects reminiscent of colloidal suspensions, which can be thus taken as a starting point to which new complexities can be added step by step.

Actually, this exactly represents the foundation on which is based a model recently proposed by Filippone and co-workers to describe the linear viscoelasticity of polymer nanocomposites above the filler percolation threshold. The authors first verified the presumed parallelism between the linear viscoelastic behavior of polymer nanocomposites and colloidal suspensions. Specifically, they considered a two-component model proposed to describe the behavior of aggregating Newtonian suspensions [Trappe and Weitz (2000), Prasad et al. (2003)] and they successfully extended it to nanofilled polymer melts with negligible polymer-particle interactions [Romeo et al. (2008)]. The underlying physics of the model lies in the independent rheological responses of the polymer and the particle network. For times longer than the polymer relaxation time, the only contribution to the elastic modulus comes from the filler network. Such an elastic contribution increases with the particle volume fraction and its crossing with the viscous modulus of the nanocomposite allows for the scaling of the frequency-dependent moduli of samples at different filler contents on a single pair of master curves. Although the scaling worked well, there were still unresolved issues regarding the interpretation and correctness of the values used to scale the curves. In addition, hydrodynamic effects have not been taken into account. Filippone and co-workers further addressed such questions in an another paper [Filippone et al. (2012)]. They again focused on a nanocomposite system characterized by negligible polymer-particle interactions, thus ascribing any alterations in its linear viscoelastic behavior to the structuring of the pristine nanoparticle aggregates. Their work introduced two great novelties to the approach conceived by Trappe and Weitz (2000).

First, they accounted for the mere hydrodynamic effect of the filler, which is only responsible for a vertical shift of the viscoelastic moduli at high frequency. To do so, they referred to the work done by Gleissle and Hochstein (2003) on non-Newtonian liquids filled with micrometer-sized, who introduced the concept of shear stress equivalent deformation: the rigid particles reduce the effective gap distance available for the suspending medium by an amount proportional to the filler content. Filippone and co-workers argued that a similar hydrodynamic approach holds true for the nanocomposite systems in the high frequency range, that is when the polymer governs the rheological response. As a result, they introduced an amplification factor to account for such an effect, which was found to follow the same trend of an empirical relationship describing the increase of the relative zero-shear rate viscosity of a Newtonian suspension of hard spheres due to hydrodynamic interactions. Such agreement is quite surprising, since the nanocomposite samples at the highest  $\Phi$  are characterized by the presence of a

space-spanning filler network. The interpretation given by the author is that, at least in the frequency region where the response is dominated by the suspending medium, the hydrodynamic disturbance depends more on the effective volume fraction than on the way in which the nanoparticle clusters are arranged in the melt.

Second, they redefined the shift factors which are necessary to build up the master curve of the viscoelastic moduli in order to better reflect the physical meaning of the model. In detail, the underlying physics of the two-phase model is that the viscoelasticity of polymer nanocomposites above the percolation threshold arises from the combination of the response of the space-spanning filler network and that of the polymer matrix. However, it can be assumed that the entire elasticity derives from the filler and scales with its content, whereas the viscous connotation is totally encompassed in the unfilled matrix. Consequently, to respect such a physical picture they believe that the horizontal and vertical shift factors to build the master curve have to be identified by the coordinates of the point in which the network elasticity equals the viscous feature of the matrix, properly “corrected” to erase the mere hydrodynamic effects. The result is surprisingly interesting: the scaled elastic moduli of samples at different filler volume fraction lie on top of each other over more than five decades of scaled frequencies. Moreover, the authors tested the accuracy of the proposed approach by comparing the obtained master curve with those obtained by using shift factors differently defined, i.e. without considering hydrodynamic effects and referring to the viscous modulus of the nanocomposites samples rather than that of the neat matrix. The output clearly confirm the importance of their observations in order to emphasize the fundamental physics underlying the two-phase model. In such a way, the scaling parameters have thus a precise physical meaning that clearly emerges once their inter-relationships are analyzed. Briefly, the vertical shift factor simply corresponds to the elasticity of the filler superstructure, whereas the horizontal one distinguishes the frequency range in which the network contribution prevails from that in which instead the polymer matrix response dominates. An evident consequence of such a reinterpretation of the scaling factors is that, in contrast to Trappe and Weitz (2000), the viscous modulus of the nanocomposite samples does not play any role. Consequently, trying to obtain a master curve of the viscous modulus results in a scaling of scarce quality, especially in the non-hydrodynamic regime. The authors indeed stressed that in such a region, the viscous modulus of the filled samples represents the dissipation of the filler network, and thus a targeted modeling of this phenomenon would be required in order to identify another couple of possible scaling factors.



# 5

## Elasticity of weak filler networks: predictive feature of the two-phase model\*

*In this chapter the rheological two-phase model presented in § 4.2. is demonstrated to be able to easily recognize the elasticity of even very weak networks of nanoparticles, which build up in polymer nanocomposites above a certain filler content. First, a preliminary description of the nanoparticles used in this study and of their relevance as a filler for polymer nanocomposites is provided (§ 5.1). Then, the morphology of the pristine nanoparticles and that of nanocomposite samples is illustrated (§ 5.2). After, the linear viscoelastic behavior of the nanocomposites at different filler content is deeply investigated (§ 5.3). Conventional rheological methods are proved to be inadequate to identify the liquid-to-solid transition in the investigated nanocomposite systems. The two-phase model instead can be profitably exploited to infer the elasticity of the networks forming at low filler content, which are too tenuous to be detected through conventional dynamic-mechanical spectroscopy (§ 5.4). Eventually, this allows to easily estimate the percolation threshold with a high accuracy (§ 5.5).*

### 5.1 Prefatory notes

Among all the potential fillers for polymer nanocomposite, those based on layered silicates have been most broadly investigated, probably because of the wide availability of starting clay materials and the consolidated know-how about their intercalation chemistry [Theng (1974), Lan et al. (1995)]. This kind of nanoparticles generally exhibits low electrical and thermal conductivity, which impedes their use in a number of technologically relevant applications where metal parts could in principle be replaced with lighter materials [Kuilla et al. (2010)]. Such shortcomings can be overcome through the use of conductive fillers such as graphite, carbon black, carbon fibers, ceramic or metal particles. Carbon-based fillers appear to be the most promising ones, since they couple high conductivity and lightness [Han and Fina (2011)]. Furthermore, the recent discovery of one-atom-thick graphene nanoparticles has renewed the interest in a series of graphite-

---

\* Part of the results has been published in «Filippone G, Salzano de Luna M, Acierno D, Russo P, “Elasticity and structure of weak graphite nanoplatelet (GNP) networks in polymer matrices through viscoelastic analyses”, *Polymer* 53, 2699-2704 (2012)».

based particles. In this context, Chen and coworkers proved that ultrasound sonication of the thermally-expanded form of graphite intercalated compounds (GICs), conventionally named expanded graphite (EG), effectively results into few-nm-thick stacks of graphene planes spaced by nanogalleries in which polymer chains can intercalate (graphite nanoplatelets, GNPs) [Chen et al. (2003), Chen et al. (2004)]. The low cost and ease of processing make GICs particularly attractive as filler for conductive polymer nanocomposites.

The performances of nanofilled polymers are strictly related to the degree of nanoparticle dispersion. Usually, the better is the quality of dispersion, the higher is the interfacial area and the better are the macroscopic properties. Linear viscoelastic measurements are often employed to characterize the state of dispersion of the nanoparticles and the internal structures that form upon mixing the polymer and filler phases. Typically, an abrupt rheological transition takes place around the filler percolation threshold,  $\Phi_c$ , which can be consequently detected with good accuracy. As a rule of thumb, the lower is the percolation threshold, the better is the quality of the filler dispersion. However, the extremely wide planar extension of GNPs brings about a low bending stiffness of the particles, which makes the estimation of  $\Phi_c$  through mechanical techniques a challenging task. The aim of the present study is to demonstrate that the rheological two-phase model proposed by Filippone et al. (2010) can be profitably used to univocally infer the elasticity of networks which are too tenuous to be detected through usual viscoelastic analyses. Moreover, it is demonstrated that the physical constraints of the model allow to identify the samples whose filler content is below the percolation threshold, which can be thus more accurately estimated.

The Chapter is organized as follows. The structure of the investigated nanoparticles is illustrated first, together with the morphology of the resulting polymer nanocomposites. Then, several rheological criteria, commonly used to detect the liquid to solid transition, are presented. Contextually, they are also shown to be inadequate when trying to apply them to the rheological data of the investigated system. Finally, the predictive feature of the two-phase model proposed by Filippone et al. (2010) is unveiled, allowing an accurate detection of the filler percolation threshold whose value is also confirmed by electrical conductivity measurements.

## 5.2 Filler structure and nanocomposite morphology

The hierarchical structure of the graphitic particles is elucidated in Figure 5.1, where the wide angle X-ray powder diffraction patterns of the untreated graphite intercalated compounds, the expanded graphite obtained through thermal expansion of GICs and the graphite nanoplatelets obtained after ultrasound sonication of EG in N,N-dimethylformamide (DMF) are shown.

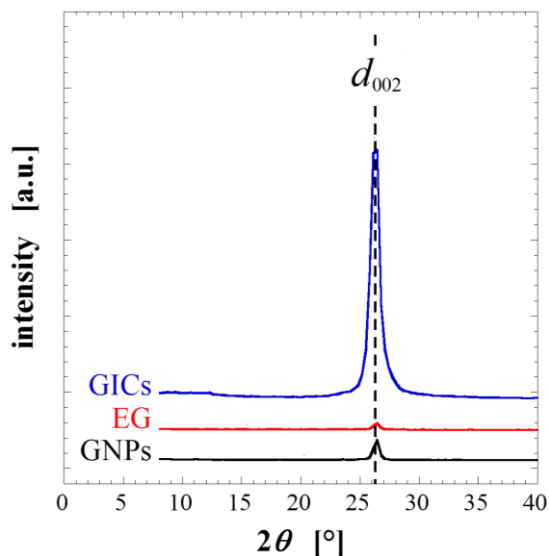


**Figure 5.1** X-ray powder diffraction patterns of untreated GICs, EG and GNPs.

The thermal expansion step of the GIC flakes is the key-step to destroy the most part of the ordered lamellar structures formerly present. Specifically, the intensity of the diffraction peak of GICs at  $2\theta \approx 26.4^\circ$ , approximately corresponding to the  $c$ -axis spacing  $d_{002} = 0.335$  nm of crystalline graphite, remarkably reduces upon thermal shock irrespective of the additional ultrasonication step. The latter, however, is crucial to obtain lamellar particles having nano-sized thickness, as evidenced by scanning electron microscopy (SEM) images of the powders presented in Figure 5.2.

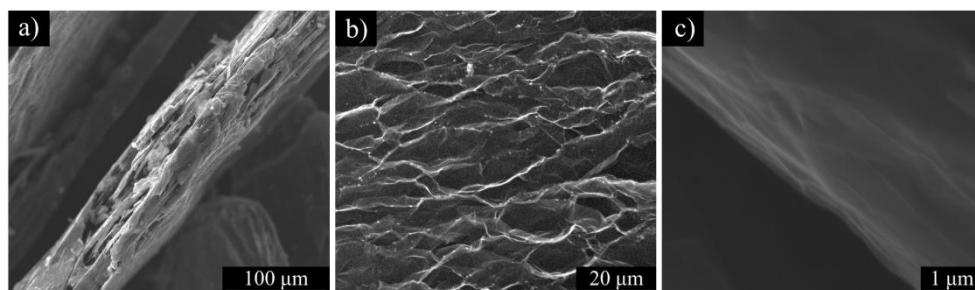


**Figure 5.2** SEM micrographs of (a) an untreated GIC flake, (b) the surface of an EG particle soon after thermal expansion and (c) a single stack of GNPs resulting after ultrasound sonication of EG in DMF.

Untreated GICs appear as compact micron-sized planar flakes (Figure 5.2a). Thermal expansion results in a characteristic flattened honeycomb structure constituted by stacks of graphite sheets with thickness of few hundreds of nanometers (Figure 5.2b). The subsequent processing steps of dispersion in (DMF) and ultrasonication break the weak bonds between such stacks, producing graphitic lamellae with nano-sized thickness. A magnification of one of such layered structures is given in Figure 5.2c.

Nanocomposite samples have been prepared by mixing polystyrene (PS) with different contents of GNP nanoparticles. The microstructure of the polymer nanocomposites is shown Figure 5.3. Representative samples at relatively low filler volume fraction,  $\Phi$ , have been selected for the morphological analyses to allow an easy visual inspection of the space distribution of the nanoparticles. In overcrowded samples at higher filler content, indeed, it would be extremely challenging to appreciate.

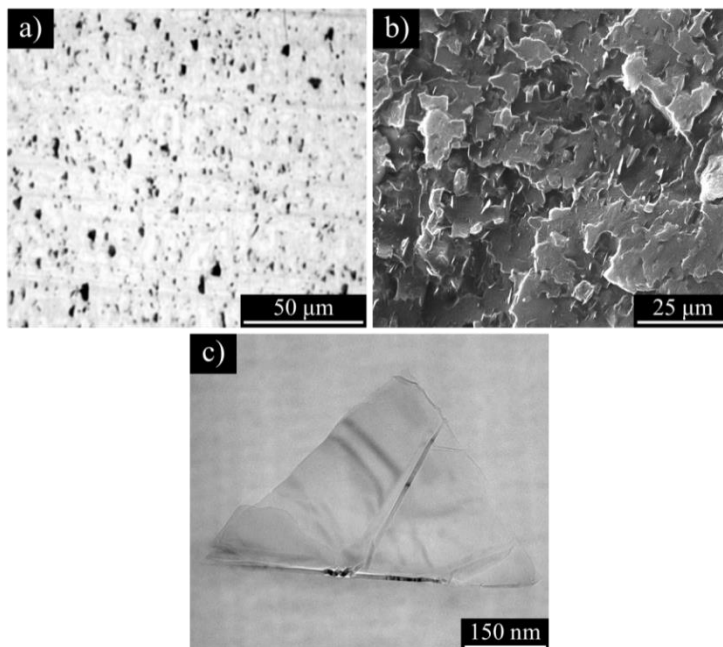


**Figure 5.3** (a) Optical, (b) scanning electron and (c) transmission electron micrographs of GNP-based nanocomposites at (a, c)  $\Phi = 0.005$  and (b)  $\Phi = 0.014$ .

As illustrated in the optical micrograph of Figure 5.3a, the filler phase is uniformly and homogeneously distributed inside the polymer matrix on the micro-scale. Isolated graphite sheets embedded in the host polymer can be recognized in

the SEM micrograph of Figure 5.3b. In addition, many few tens-thick GNPs, not easily detectable through X-ray diffractometric techniques, have been noticed through TEM analysis. One of such isolated GNPs is shown in Figure 5.3c. The estimated thickness of such a platelet is  $\sim 15$  nm, roughly corresponding to about 60 graphene layers. As suggested by the numerous folds and ripples, the very high width-to-thickness ratio of GNPs brings about a low bending stiffness of the nanoparticles. As a consequence, their contribution to the mechanical strength of the nanocomposite is expected to be less important than that of other kinds of stiffer layered nanoparticles such as clays.

### 5.3 Linear viscoelasticity and detection of the liquid to solid transition

The elastic,  $G'$ , and viscous,  $G''$ , shear moduli in the linear viscoelastic regime are shown as a function of frequency,  $\omega$ , in Figure 5.4 for the neat polymer and the PS/GNPs nanocomposites at different filler content.

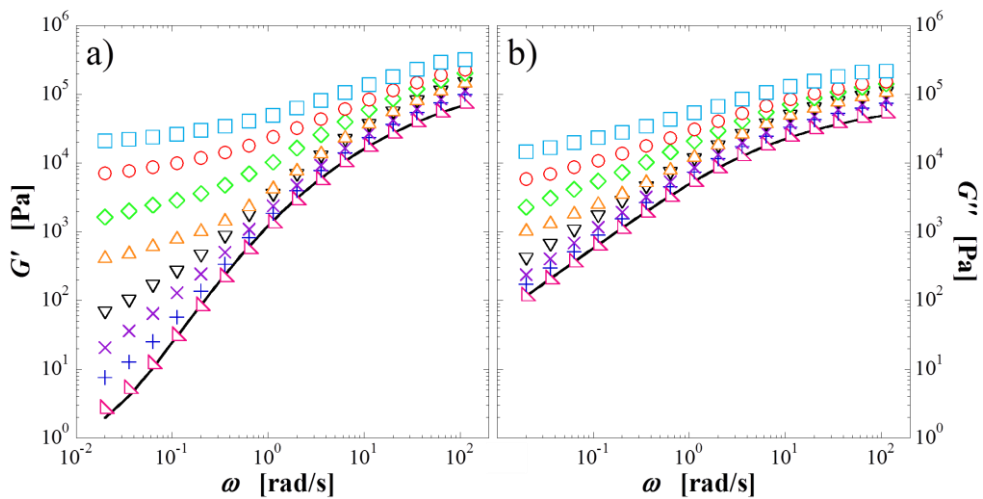


**Figure 5.4** Frequency-dependent (a) elastic and (b) viscous moduli of the neat PS (solid lines) and the PS/GNPs nanocomposites at different composition. From bottom to top:  $\Phi = 0.009, 0.014, 0.018, 0.024, 0.029, 0.036, 0.037, 0.049$ .

The PS matrix is predominantly viscous in the investigated frequency range, exhibiting terminal Maxwellian behavior ( $G' \sim \omega^2$ ,  $G'' \sim \omega^1$ ) at low frequency. The filler strongly affects the melt state relaxation spectra of the nanocomposites: both

$G'$  and  $G''$  monotonically increase with GNP content in the whole range of frequency, the effect being much more pronounced on  $G'$  at low  $\omega$ . The high-frequency dynamics of the nanocomposites remind those of the neat matrix irrespective of the sample composition, the nanoparticles being responsible for only a vertical shift of both moduli by an amount which is proportional to  $\Phi$ . Actually, the presence of the filler merely causes a local increase of the deformation rate experienced by the matrix in the gaps between the particles. Over such short timescales, indeed, the nanoparticles are unable to affect the relaxation modes of small segments of the polymer chain and, consequently, the rheological response is governed by the behavior of the neat matrix. On the other hand, over longer timescales non-continuum effects start to emerge and the filler slows down the relaxation dynamics, eventually resulting in the arrest of the long timescales relaxation processes at the highest filler content. The appearance of a low-frequency plateau of  $G'$  is rather common in nanofilled polymers, being often ascribed to the formation of a three-dimensional filler network that spans the whole sample.

An evident rheological transition from liquid- to solid-like behavior usually takes place at the percolation threshold, which allows for the estimate of  $\Phi_c$ . In Figure 5.4, however, the slowing down of the relaxation dynamics appears rather gradual, making the identification of the liquid to solid transition not straightforward. This can be clearly appreciated in Figure 5.5, where the low-frequency moduli and their slopes,  $\alpha^i = \partial(\log G^i)/\partial(\log \omega)$ , are reported as a function of  $\Phi$  after normalization over the corresponding values of the neat matrix.

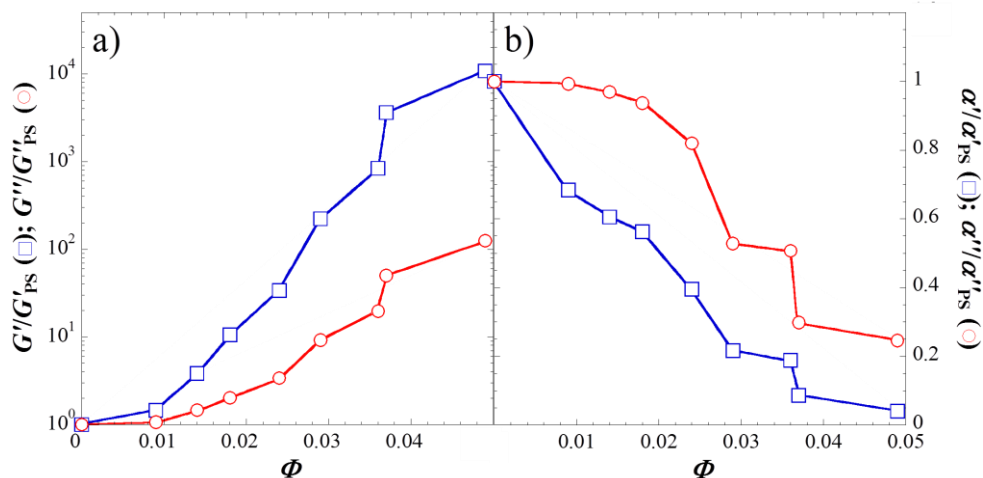


**Figure 5.5** (a) Low-frequency moduli and (b) their slopes, both normalized over the values of the neat PS, as a function of filler content.

Although linear viscoelastic measurements have been widely used in the literature to identify the liquid to solid transition in polymer nanocomposites, none of the parameters shown in Figure 5.5 exhibits sharp changes from which the value of  $\Phi_c$  can be unambiguously inferred. Actually, in the present study graphite nanoplatelets have been expressly selected as a filler because their low bending stiffness is coupled with an inherent high electrical conductivity. As a result, the  $\Phi$  at which a space-spanning filler network develops, whilst not easily distinguishable through mechanical techniques, can be simply detected by monitoring the electrical conductivity,  $\sigma$ , of the nanocomposites as a function of filler content (Figure 5.6).

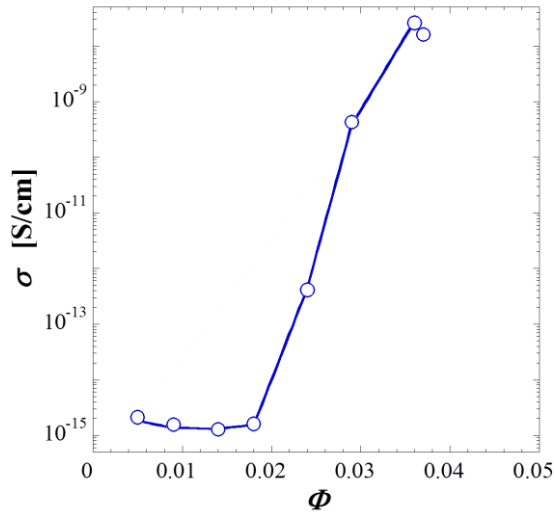


**Figure 5.6** Electrical conductivity of PS/GNPs nanocomposites as a function of filler content.

The conductivity of the PS/GNPs samples suddenly increases at some  $\Phi$  between 0.018 and 0.024, meaning that a continuous path of nanoparticles starts to build up across the sample in this composition range. In spite of slight differences between mechanical and electrical percolation due to the different underlying mechanisms, such a result unequivocally sets the lower and upper bounds of  $\Phi_c$ , respectively. Song and Zheng (2015) recently reviewed the linear rheology of nanofilled polymers, gathering four rheological methods frequently used to show clear-cut evidences of the liquid to solid transition. Such criteria are now applied to the rheological data of the PS/GNPs nanocomposites, looking for an estimation of  $\Phi_c$  in line with the results of electrical conductivity experiments.

The first criterion is represented by the plot of the complex viscosity,  $\eta^*$ , versus  $G^*$  [Enikolopyan et al. (1990), Mitchell and Krishnamoorti (2007)], which is analogous to the plot of the steady viscosity versus shear under steady shear proposed by Vermant et al. (2007). The  $\eta^*$ - $G^*$  plot of the neat PS matrix and the GNP-based nanocomposites at different composition is show in Figure 5.7.

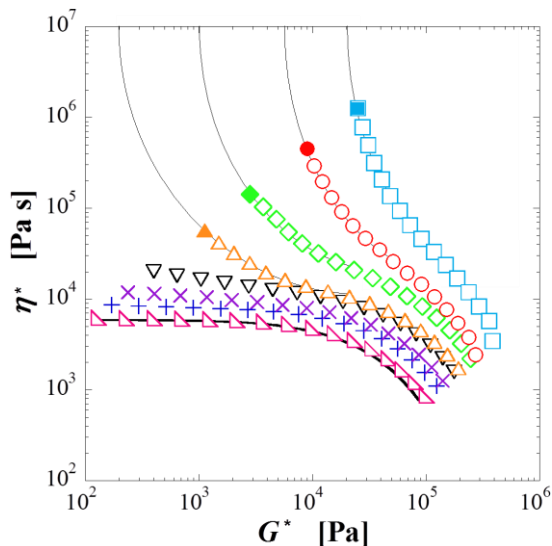


**Figure 5.7** Complex viscosity as a function of complex modulus for the neat PS (solid line) and PS/GNPs nanocomposites at different composition. From bottom to top:  $\Phi = 0.009, 0.014, 0.018, 0.024, 0.029, 0.036, 0.037, 0.049$ . Thin solid lines are guides for the eye.

The neat matrix and the filled samples below the percolation threshold typically exhibit a plateau of  $\eta^*$ . Instead, the formation of a percolated structure at  $\Phi \geq \Phi_c$  is associated with the development of a finite yield stress, which manifests as a divergence of the complex viscosity at a finite value of the complex modulus,  $G^*_{|\eta^* \rightarrow \infty}$ . In the PS/GNPs nanocomposites, a transition between these two behaviors happens at some  $\Phi$  between 0.024 and 0.029. Moreover, Mitchell and Krishnamoorti (2007) found that the yielding complex modulus scales linearly with  $\Phi$  in a lin-lin plot and thus suggested that a more accurate value of the percolation threshold can be obtained by linear extrapolation of the  $G^*_{|\eta^* \rightarrow \infty}$  to zero. However, the definite estimation of the value of the complex modulus at which the complex viscosity diverges is not trivial. Therefore, two different approaches have been followed: assuming  $G^*_{|\eta^* \rightarrow \infty}$  (i) equal to the last value of  $G^*$  in the right hand side (full symbols) and (ii) equal to a rough estimation of the vertical asymptote of the

curves. The  $\Phi$ -dependence of the values of  $G^*|_{\eta \rightarrow \infty}$  is shown in Figure 5.8 for the samples at  $\Phi \geq 0.029$ .

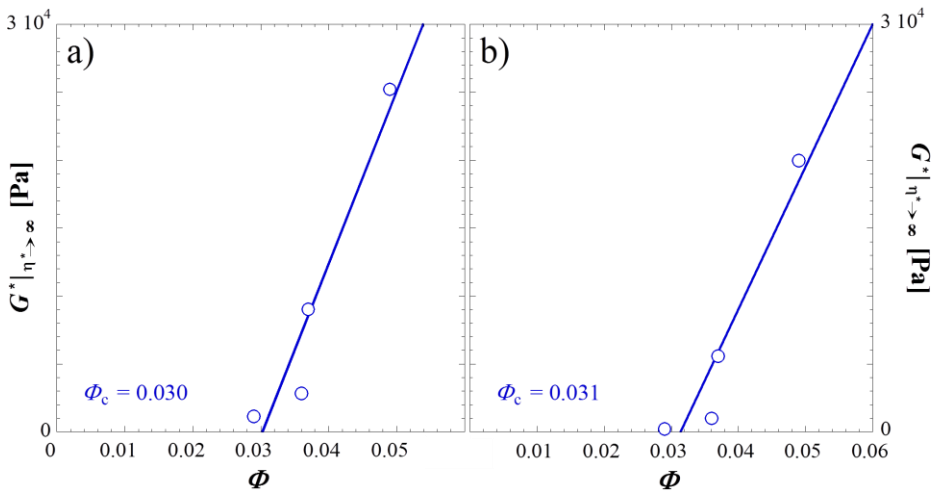


**Figure 5.8** Complex modulus at which the complex viscosity diverges as a function of filler content for samples at  $\Phi \geq 0.029$ . The values of the complex modulus have been taken (a) as the last values of  $G^*$  and (b) as the vertical asymptote.

Remarkable discrepancies between the moduli obtained following the two different procedures can be noticed, the differences being much more pronounced for the samples at lower filler content. In any case, the yielding modulus does not cleanly scale as a linear function of the filler content. As a result, whatever the approach to identify  $G^*|_{\eta \rightarrow \infty}$  is, the extrapolating procedure returns a value of  $\Phi_c$  (reported in Figure 5.8) which is even higher than the upper limit recognized by simple visual inspection of Figure 5.7, that is  $\Phi = 0.029$ .

The second criterion is the Han plot of  $G'$  versus  $G''$  [Han and Kim (1993)], which is reported in Figure 5.9 for the neat polymer and the GNP-based nanocomposites at different composition. The curves of samples at low filler content largely overlap onto that of the neat matrix. On the other hand, further increasing  $\Phi$  causes a decrease in the slope of the curve in the terminal region (left hand side of the plot), eventually resulting in a plateau. The shift and the change in slope of the curves are generally ascribed to significant changes in the microstructure of the samples due to the formation of a percolated network [Wu et al. (2008), Pötschke et al. (2002)]. However, a clear transition from the PS-like behavior to the plateau-like one can be hardly detected, being the evolution of the shape of the curves rather gradual. As a result, no further information can be collected from the Han plot.

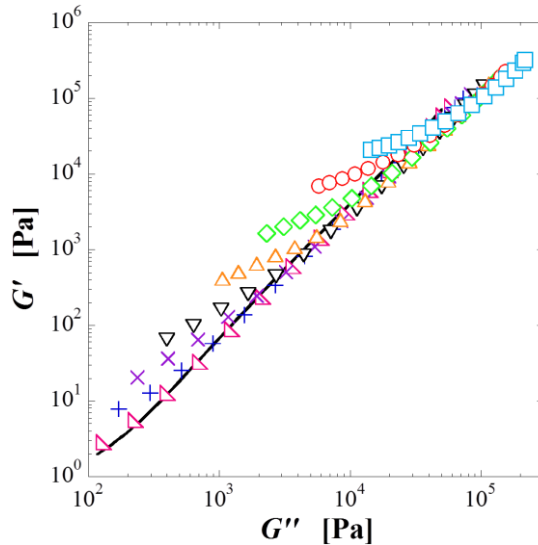


**Figure 5.9** Elastic modulus as a function of viscous modulus for the neat PS (solid line) and PS/GNPs nanocomposites at different composition. From bottom to top:  $\Phi = 0.009$ , 0.014, 0.018, 0.024, 0.029, 0.036, 0.037, 0.049.

The third criterion is the Cole-Cole plot of the imaginary viscosity,  $\eta''$ , versus the real viscosity,  $\eta'$ , which is analogous to the one used in dielectric spectroscopy [Friedrich and Braun (1992), Cole and Cole (1941)]. The Cole-Cole plot of the neat PS matrix and the GNP-based nanocomposites at different composition is shown in Figure 5.10. The curves of the neat polystyrene and the nanocomposites containing low GNP loading present a regular semi-arc, representative of materials which can be described by a single relaxation time or a narrow distribution. This clearly indicates that the presence of low amounts of nanoplatelets has almost no influence on the relaxation behavior of the PS, and the rheological characteristics of the matrix dominate the behavior of the nanocomposites. On the contrary, at intermediate filler content the plots are partitioned into two regions: a semi-curved arc at low viscosities (left hand side of the plot), corresponding to the local dynamics of polystyrene chains, and a linear or rigid end at higher viscosity, related to the long-term relaxation of the nanoparticles. At higher contents, the first region progressively disappears, and the linear region dominates the plots suggesting that the long-range motion of polymer chains is drastically restrained. Generally, the appearance of the linear region is ascribed to the formation of a space-spanning network of nanoparticles. According to Figure 5.10, the composition at which the network builds up is in the  $\Phi$ -range between 0.018 and 0.024, in agreement with the results of the electrical conductivity measurements.

However, from the Cole-Cole plot the estimation of a more precise value of  $\Phi_c$  is not possible.

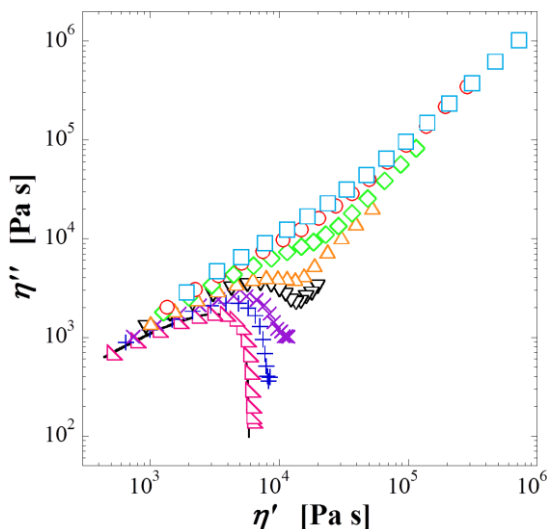


**Figure 5.10** Imaginary viscosity as a function of real viscosity for the neat PS (solid line) and PS/GNPs nanocomposites at different composition. From bottom to top:  $\Phi = 0.009, 0.014, 0.018, 0.024, 0.029, 0.036, 0.037, 0.049$ .

The fourth and last criterion is the van Gorp-Palmen plot of the phase angle,  $\delta$ , versus the complex modulus [van Gorp and Palmen (1998)], which is reported in Figure 5.11 for the PS matrix and the GNP-based nanocomposites at different filler content. In the neat polymer and the nanocomposite samples at low filler content the phase angle approaches a value of  $90^\circ$ , indicating the flow behavior of a viscoelastic fluid. As  $\Phi$  increases, a gradual yet moderate decrease in  $\delta$  in the low  $G^*$  range can be noticed. However, once reached a critical value of  $\Phi$ , the phase angle dramatically drops, denoting an increased elastic connotation. Such a behavior is commonly ascribed the rheological fluid to solid transition and thus suggest the formation of a percolating network of nanoparticles. The curves plotted in Figure 5.11 hint that the value of  $\Phi_c$  is between 0.024 and 0.029.

To summarize, with respect to the results of the electrical conductivity measurements, the  $\eta^*-G^*$  plot and the van Gorp-Palmen one overestimate the  $\Phi$  at which the liquid to solid transition takes place. The Han plot, instead, is not useful at all for the identification of  $\Phi_c$ . On the other hand, the Cole-Cole plot is the only criterion in agreement with the result of the electrical conductivity data, but it just gives the lower and upper bounds of  $\Phi_c$ , thus not allowing a more accurate estimation of the percolation threshold. Far from assessing the inability of the

presented rheological methods to accurately catch the liquid to solid transition in polymer nanocomposite, it is here important to stress their limits when dealing with nanoparticles characterized by low bending stiffness, such as the GNPs used in the present study.

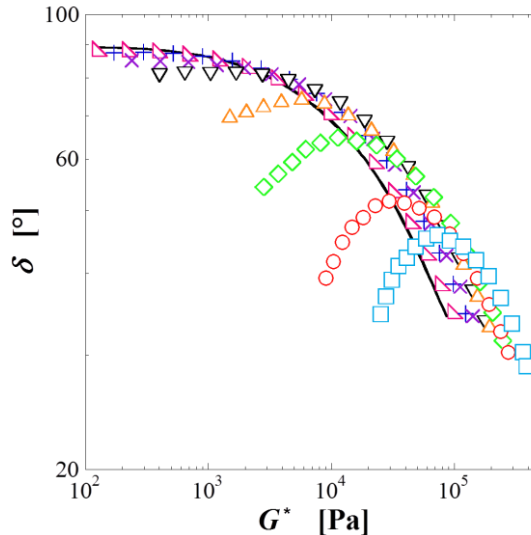


**Figure 5.11** Phase angle as a function of complex modulus for the neat PS (solid line) and PS/GNPs nanocomposites at different composition. From bottom to top:  $\Phi = 0.009, 0.014, 0.018, 0.024, 0.029, 0.036, 0.037, 0.049$ .

## 5.4 Predictive feature of the two-phase model

The apparent discrepancy between viscoelastic and electrical measurements can be ascribed to the low bending stiffness of the GNPs. Such nanoparticles form a three-dimensional structure which is too tenuous to be detected through conventional dynamic-mechanical spectroscopy, at least at low filler loadings. To overcome such a restriction, the two-phase model recently proposed to describe the linear viscoelasticity of polymer nanocomposites above  $\Phi_c$  by Filippone et al. (2010) can be exploited.

The underlying physics of the two-phase model indeed is based on the independent responses of only two main dynamical species: the predominantly viscous polymeric matrix and an elastic particle network. According to such a physical picture, at low frequency the response of the nanocomposite is dominated by the filler network, which exhibits a  $\omega$ -independent elastic modulus. On the other hand, the polymer dynamics prevail at high frequency, where the filler simply

causes an apparent increase of the moduli due to hydrodynamic contributions (see also § 5.3.1).

The two-phase model allows the building of a master curve for the elastic modulus, by properly identifying a pair of shift factors for each  $G'$  curve. The aim of this section is to disclose the predictive feature of the model in recognizing the elasticity of weak elastic networks of particles. In the following, the procedure towards the building of the master curve of  $G'$ , which is the main output of the model, is briefly retraced.

The first step is accounting for the hydrodynamic effects. In non-Newtonian liquids filled with micrometer-sized particles, Gleissle and Hochstein (2003) quantitatively accounted for hydrodynamic interactions by introducing an amplification factor,  $B(\Phi)$ , which accounts for the reduction of the effective gap distance available for the suspending medium due to the presence of the particles. In the case of polymer nanocomposites, the underlying physics is essentially the same, and the amplification factor can be easily estimated as the ratio between the complex modulus of the filled sample and that of the neat matrix,  $B(\Phi) = G^*(\Phi)/G_{PS}^*$ , in the high  $\omega$  range, that is where the behavior of the polymer matrix governs the rheological response (see Figure 5.12). Note that the consistency of the adopted procedure has been already verified by Filippone et al. (2010) for PS-based nanocomposite filled with fumed silica nanoparticles.

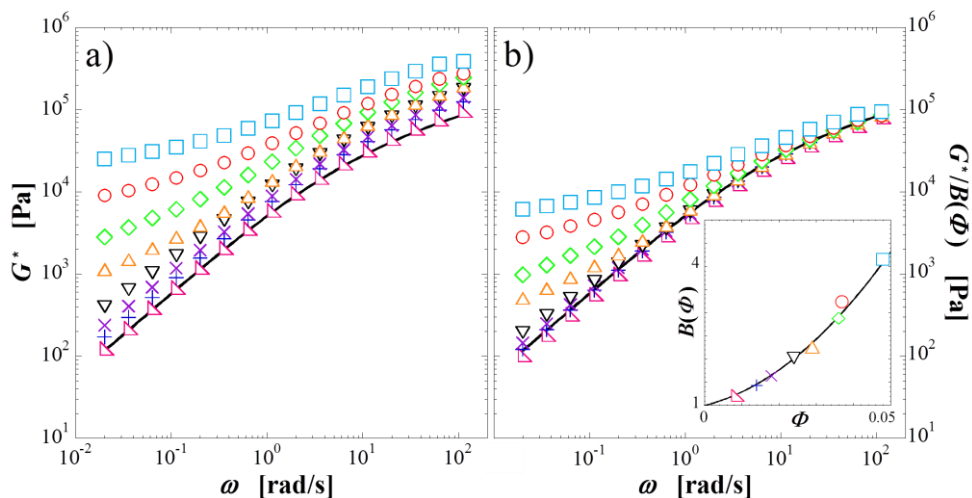


**Figure 5.12** Frequency-dependent complex modulus (a) as measured and (b) divided by the amplification factor for the neat PS (solid line) and PS/GNPs nanocomposites at different composition. From bottom to top:  $\Phi = 0.009, 0.014, 0.018, 0.024, 0.029, 0.036, 0.037, 0.049$ . The inset in (b) shows the amplification factor as a function of filler volume fraction (solid line is a guide for the eye).

The second and last step envisages the identification of the horizontal ( $a_\Phi$ ) and vertical ( $b_\Phi$ ) shift factors for the scaling of the  $G'$  curves. The shift factors are defined as the coordinates of the points at which the network elasticity, identified as the low-frequency plateau of the elastic modulus,  $G'_0(\Phi)$ , equals the viscous modulus of the neat polymer properly amplified to account for hydrodynamic effects,  $B(\Phi) \cdot G''_{PS}$ . This can be easily accomplished for the samples at  $\Phi \geq 0.036$ , in which the low-frequency plateau of the elastic modulus can be clearly recognized, allowing to start building the  $G'$  master curve, as shown in Figure 5.13.

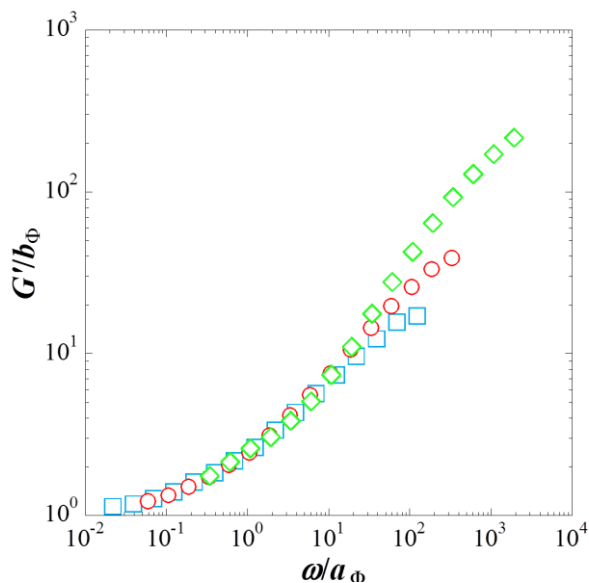


**Figure 5.13** Master curve of  $G'$  of the PS/GNPs nanocomposites at  $\Phi \geq 0.036$ .

The collapse of the moduli is excellent over about three decades of scaled frequencies, corresponding to the region in which non-continuum effects are predominant. The non-superposing tails at high dimensionless frequency,  $\omega/a_\Phi$ , do not invalidate the consistency of the scaling, being a consequence of the intrinsic viscoelastic feature of the polymer matrix, which governs the high-frequency behavior. It is important to stress that the overlay of the  $G'$  curves of Figure 5.13, is not obtained by looking for their partial superposition, being instead a direct consequence of the precise physical meaning of the shift factors. The two-phase model indeed reflects the physical picture of a filler network that scales along the viscous modulus of the neat matrix. Consequently, a constraint exists on the choice of the scaling factors: the relation  $b_\Phi = b_\Phi(a_\Phi)$  has to follow the same functional dependence as  $G''_{PS}(\omega)$  (Figure 5.14).

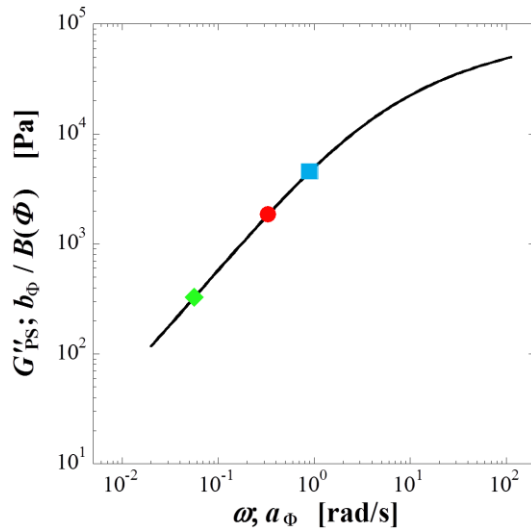


**Figure 5.14** Functional dependence of  $b_\Phi/B(\Phi)$  vs.  $a_\Phi$  for the samples at  $\Phi \geq 0.036$ . The solid line is the viscous modulus of the neat polymer.

The precise physical meaning of the shift factors confers a predictive ability to the two-phase model. Specifically, once built by referring to the samples at  $\Phi$  high enough to clearly identify the  $G'_0$  of the corresponding networks, the master curve can be exploited to infer the elasticity of more tenuous networks. This is exactly the case of the samples at  $0.024 \leq \Phi \leq 0.029$ , for which the electrical conductivity data indicate the presence of a continuous filler network across the matrix (see Figure 5.6), but an a priori estimation of the shift factors is difficult since the exact determination of the values of  $G'_0(\Phi)$  is questionable. Nonetheless, by referring to the master curve based on the samples at  $\Phi \geq 0.036$ , the pairs  $(a_\Phi; b_\Phi)$  for the samples at lower  $\Phi$  can be univocally determined. This concept is clarified for the sample at  $\Phi = 0.029$ , for which three curves of  $G'/b_\Phi$ , corresponding to three possible pairs of shift factors, are plotted together with the master curve obtained for the samples at higher filler content (Figure 5.15). Note that because the network elasticity is too weak to intercept the amplified viscous modulus of the matrix within the investigated frequency range, terminal Maxwellian behavior has been assumed for the neat polymer ( $G'' \sim \omega^1$ ). The positioning of each  $G'$  curve on the master curve is unambiguous: the interrelationship between the shift factors establishes a precise track in the plane  $G'/b_\Phi - \omega/a_\Phi$  for the the curve to be scaled. Evidently, only one curve (red diamonds) partially lies onto the master curve and thus the corresponding shift factors are taken for granted. The same procedure has been performed for the sample at  $\Phi = 0.024$ . As a result, the complete master curve for all the samples at  $\Phi \geq 0.024$  is finally obtained, as shown in Figure 5.16.

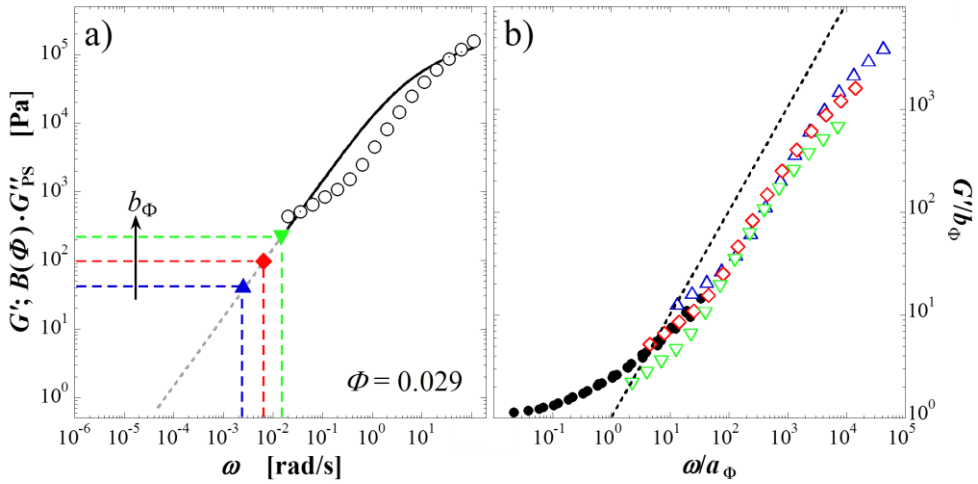


**Figure 5.15** (a) Possible pairs of scaling factors and (b) resulting scaled curves of  $G'$  for the PS/GNPs sample at  $\Phi = 0.029$ . In (a), empty symbols are the  $G'$  of the nanocomposite. The solid and dashed lines are the  $G''$  of PS: experimental data and extrapolated terminal behavior. In (b), the data are superimposed on the master curve of the samples at higher filler contents (full circles). The dashed line is the track on which the point at the lowest frequency of the curve to be scaled must move with changing the pair  $(a_\Phi; b_\Phi)$ .

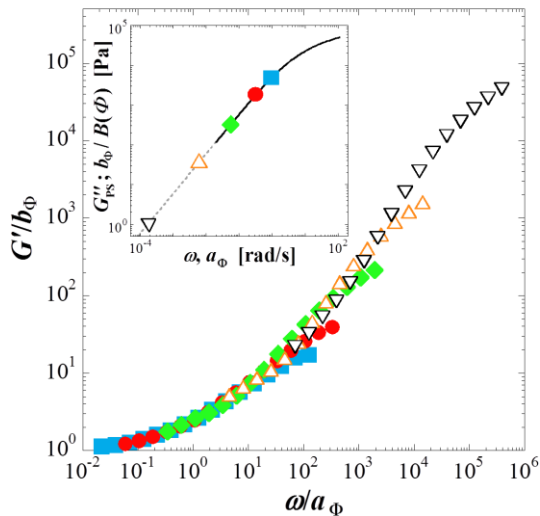


**Figure 5.16** Master curve of  $G'$  of the PS/GNPs nanocomposites at  $\Phi \geq 0.024$ . In the inset, functional dependence of the shift factors (solid line is the viscous modulus of the neat polymer). Full symbols corresponds to values estimated starting from  $G'_0$ ; open symbols to values inferred according to the two-phase model.

On the other hand, in obedience to physics of the two-phase model, the scaling of the  $G'$  curves of samples below  $\Phi_c$  onto the master curve is not allowed. To highlight this evidence, the procedure adopted for the nanocomposites at  $\Phi = 0.029$  and  $0.024$  is performed on nanocomposites at lower  $\Phi$ , as shown in Figure 5.17 for a representative sample.

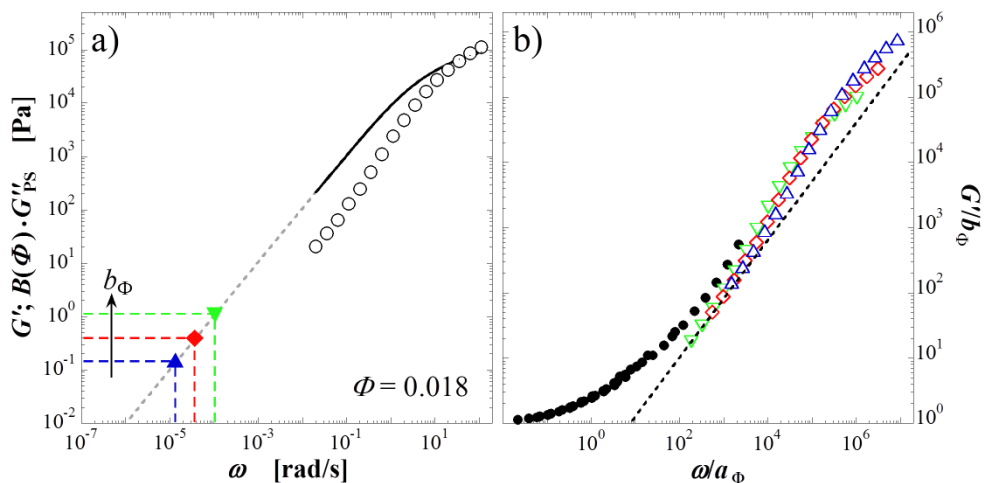


**Figure 5.17** (a) Possible pairs of scaling factors and (b) resulting scaled curves of  $G'$  for the PS/GNPs sample at  $\Phi = 0.018$ . In (a), empty symbols are the  $G'$  of the nanocomposite. The solid and dashed lines are the  $G''$  of PS: experimental data and extrapolated terminal behavior. In (b), the data are superimposed on the master curve of the samples at higher filler contents (full circles). The dashed line is the track on which the point at the lowest frequency of the curve to be scaled must move with changing the pair ( $a_\Phi$ ;  $b_\Phi$ ).

Whatever the pair of shift factors is, no superposition can be found (Figure 5.17b). Actually, the “track” on which the point at the lowest frequency of the curve to be scaled must move clearly indicates that it does not exist any pair of ( $a_\Phi$ ;  $b_\Phi$ ) which permits to partially overlap the  $G'$  curve of the sample at  $\Phi = 0.018$  on the master curve. The two-phase model thus set the lower and upper bounds of the percolation threshold as  $\Phi = 0.018$  and  $0.024$ , respectively, in agreement with the electrical conductivity experiments.

Besides strengthening the result of the electrical conductivity measurements, the two-phase model allows to precisely set the network elasticity of all the samples above  $\Phi_c$ , as  $b_\Phi = G'_0(\Phi)$ . This facilitates the identification of  $\Phi_c$ , which must be sought in a range of compositions which is inferiorly limited by the highest  $\Phi$  of the non-scalable  $G'$  curves, that is  $\Phi = 0.018$ . The next paragraph addresses the goal of the accurate estimation of the percolation threshold.

## 5.5 Estimation of the percolation threshold

The two-phase model applies for samples with filler contents greater than a critical value, which represents the minimum particle volume fraction necessary for the formation of a space-spanning network. The good quality of the obtained master curve reveals the common nature of the networks for all the samples above  $\Phi_c$ : increasing the  $\Phi$  results in an increased number of elements in the network, which becomes more robust while keeping its overall structure unaltered. According to the percolation theory, the network elasticity grows with  $\Phi$  as:

$$G'_0 = k(\Phi - \Phi_c)^\nu \quad (5.1)$$

where  $k$  and  $\nu$  are two constants, the latter being related to the stress-bearing mechanism [Stauffer and Aharony (1992)]. Owing to the two-phase model, the values of  $G'_0(\Phi)$  can be set as the vertical shift factors used for the building of the master curve. Equation 5.1 has been thus fitted to the  $b_\Phi = G'_0(\Phi)$  data setting  $k$  and  $\nu$  as fitting parameters while keeping  $\Phi_c$  constant. The procedure has been repeated for different values of  $\Phi_c$  in the range  $0.018 < \Phi < 0.024$ , corresponding to the samples of the first non-scalable and the last scalable  $G'$  curves, respectively. Adopting such a procedure, the highest value of the coefficient of determination,  $R^2$ , has been attained for a value of  $\Phi_c = 0.0200$ , which is consequently taken as the rheological percolation threshold for the PS/GNPs nanocomposites. The resulting power-law dependence of the network elasticity is shown in Figure 5.18.

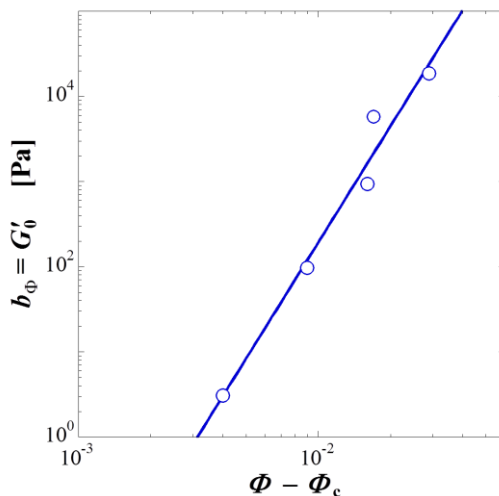


**Figure 5.18** Power law dependence of the network elasticity on the reduced filler content,  $\Phi - \Phi_c$ , setting  $\Phi_c = 0.0200$ . Solid line is the fitting to Equation 5.1.

Theoretically, the value of the critical exponent  $\nu$  ranges between 2.1 and 3.75 depending on the mechanism through which the particles resist to stress [Arbabi and Sahimi (1993), Sahimi and Arbabi (1993)]. In addition, values of  $\nu$  lower than 2.1 are indicative of polymer-bridged particle networks, whereas  $\nu$  higher than 3.75 have been observed when strong interactions establish directly between the particles [Surve et al. (2006)]. Therefore, the computed value of  $\nu = 4.54$  is consistent with the picture of GNPs interacting among them in the network without the mediation of the polymer. However, a thorough assessment of the actual stress bearing mechanism would require a targeted analyses.

Analogously to the network elasticity, the electrical conductivity of the nanocomposite samples is expected to exhibit critical behavior just above the percolation threshold:

$$\sigma = \sigma_0 (\Phi - \Phi_c^{\text{el}})^t \quad (5.2)$$

where  $\Phi_c^{\text{el}}$  represent the electrical percolation threshold and  $\sigma_0$  and  $t$  are two constants [Stauffer and Aharony (1992)]. Equation 5.2 is fitted to the electrical conductivity data adopted the same procedure used for the linear viscoelastic data and, again, the value of  $\Phi_c^{\text{el}}$  which returns the highest coefficient of determination is taken as definitive. The result of the best fitting procedure of the conductivity data is shown in Figure 5.19 and the corresponding parameters are compared with those concerning the rheological data in Table 5.1.

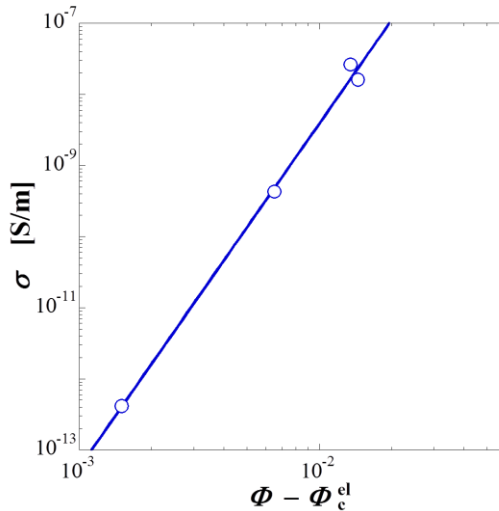


**Figure 5.19** Power law dependence of the electrical bulk conductivity on the reduced filler content,  $\Phi - \Phi_c^{\text{el}}$ , setting  $\Phi_c^{\text{el}} = 0.0225$ . Solid line is the fitting to Equation 5.2.

**Table 5.1** Best fitting parameters ( $k$ ,  $\nu$ ) of Equation 5.1 and ( $\sigma_0$ ,  $t$ ) of Equation 5.2 and corresponding values of percolation threshold.\*\*

$\Phi_c$	$k$ [Pa]	$\nu$	$R^2$
0.0200	2.29E+11	4.54	0.9710
$\Phi_c^{el}$	$\sigma_0$ [S/m]	$t$	$R^2$
0.0225	1.83 E+01	4.84	0.9953

The highest value of  $R^2$  is attained for  $\Phi_c^{el} = 0.0225$ , which is in good agreement with its rheological counterpart, since electrical percolation generally occurs at filler contents slightly higher than those required for rheological one [Potts et al. (2011)]. It can be finally noticed that, excluding the case of systems obtained by in situ polymerization, in which  $\Phi_c$  as low as 0.005 can be reached, the computed value of percolation thresholds, both the rheological and the electrical one, are comparable or even lower than those recently reported in the literature for GNP-based nanocomposites [Sengupta et al. (2011)].

---

\*\* Slight differences with the values reported in Filippone et al. (2012) are due the different number of available experimental data and to approximations in the estimation of the filler content in volume fraction.

# Generalization of the two-phase model: a unifying approach for the linear viscoelasticity of polymer nanocomposites\*

*In this chapter a general description of the linear viscoelasticity of polymer nanocomposites differing in the nature of the nanoparticles and polymer matrix is provided. To begin, preliminary considerations about the rheological implications stemming from the nanometric size of the filler phase in polymer nanocomposites are reported (§ 6.1). Then, a wide variety of polymer nanocomposite systems is analyzed to show that a unifying approach for their viscoelasticity is possible irrespective of the nature of pristine nanoparticles (§ 6.2) and the degree of polymer-filler affinity (§ 6.3). The complex relaxation spectrum of polymer nanocomposites above the percolation threshold is demonstrated to be satisfactorily described in terms of only two main populations of dynamical species: the free polymer matrix and an elastic three-dimensional network, which can be either formed by bare clusters or mediated by a fraction of adsorbed polymer. In the end, possible general trends in the stress bearing mechanisms of the different kinds of network considered are also discussed (§ 6.4).*

## 6.1 Prefatory notes

Polymer nanocomposites can be described as suspensions of particles and particle aggregates dispersed in a polymer medium. Dealing with nanoparticles, however, implies very large polymer-particles interfacial areas, very small wall-to-wall inter-particle distances and relevant filler mobility. Indeed, nanoparticles can experience significant Brownian motions even in highly viscous mediums such as polymer melts. As a result, polymer nanocomposites behave as “living systems” which evolve towards more favorable states in relatively short timescales (see Part I for details). Specifically, the hydrodynamic forces, developed during the intense mixing step, break up the initial aggregates down to small clusters of primary particles. On the other hand, above the melting or glass transition temperature of the polymer matrix, such clusters are inclined to reassemble into bigger structures.

---

\* Part of the results has been published in «Filippone G and Salzano de Luna M, “A unifying approach for the linear viscoelasticity of polymer nanocomposites”, *Macromolecules* 45, 8853-8860 (2012)».

Depending on filler content, interaction potential and applied stress, the latter may span the whole space, eventually resulting in the arrest of the particle dynamics [Trappe et al. (2001)]. The flocculation process can be appreciated by monitoring the time evolution of the linear viscoelastic moduli (see Part I for details). An example is given in Figure 6.1 for four polymer nanocomposites based on different nanoparticles, in which the filler content is above the percolation threshold.

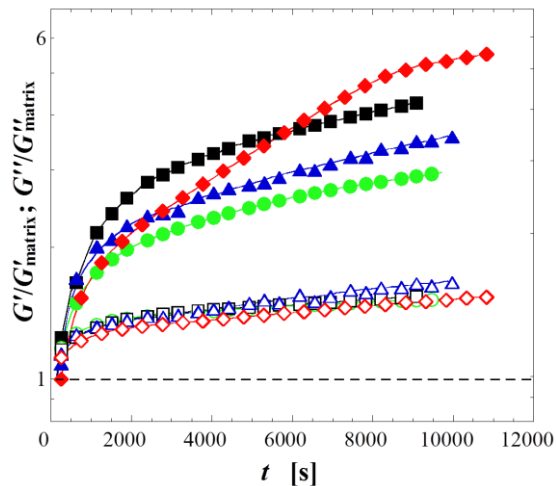


**Figure 6.1** Time evolution of elastic (full symbols) and viscous (empty symbols) moduli at  $0.1 \text{ rad s}^{-1}$  normalized over the corresponding values of the neat matrix for nanocomposites based on spherical nanoparticles (red diamonds), stiff (green circles) and flexible (blue triangles) plate-like nanoparticles and rod-like nanoparticles (black squares).

All the systems share the same qualitative behavior: the elastic modulus increases during the earlier stage, then it reaches a steady state value; a similar trend is noticed for the viscous modulus, but the changes are much less pronounced. The differences in the growth kinetics reflect the different mobility of the flocculating clusters, which is ultimately related to their initial size and shape and to the matrix viscosity. Irrespective of the nature of the primary particles, however, once reached the steady state all the systems can be depicted as three-dimensional networks of nanoparticle aggregates interspersed with the host polymer. It can be argued that such a common origin of the microstructure of polymer nanocomposites imply a universal macroscopic rheological response. Consequently, the goal of the present study is to show that the rheological two-phase model proposed by Filippone et al. (2010) for non-interacting nanocomposites based on spherical filler can be generalized to a wide variety of polymer nanocomposites, proving that the underlying physics is the same irrespective of the nature of polymer and filler.

The Chapter is organized as follows. A first generalization of the two-phase model is provided for a series of nanocomposites filled with nanoparticles differing among them in the size, shape and chemistry, yet all exhibiting negligible interactions with the polymer phase. Then, the analysis is extended to other systems, taken from the literature, in which the nature of the polymer matrix is different and also the entity of the polymer-particle affinity. The successful validation of a unifying approach for the linear viscoelasticity of different polymer nanocomposites allow the building of a master curve of the elastic modulus for each investigated system. This guarantees an accurate estimation of the percolation threshold for all the nanocomposite families, allowing to contour possible general trends in the stress bearing mechanisms of the different kinds of network.

## **6.2 Generalizing the two-phase model: nanoparticles nature**

The viscoelastic behavior of polymer nanocomposites arises from the complex interplay of the responses of the neat polymer matrix and, once the filler content exceeds the percolation threshold,  $\Phi_c$ , that of the space-spanning filler network. Although essentially elastic, the network also exhibits slow dissipative relaxation dynamics because of space rearrangements of the clusters [Wolthers et al. (1997)]. Therefore, both the filler and matrix phases of polymer nanocomposites are viscoelastic by nature.

The two-phase model represents a successful attempt towards a simple interpretation of the origin of the viscoelasticity in polymer nanocomposites. The model indeed suggests to neglect the viscous connotation of the filler network and the elastic one of the polymer. Under this assumption, the viscous connotation of the nanocomposite is totally encompassed in the matrix, whereas the entire elasticity derives from the filler and scales with its content. At this point, to confer even more generality to the model, a further clarification is necessary. Rather than made of single nanoparticles, the network has to be considered as composed by bigger structures into which the nanoparticles have reassembled under the effect of Brownian motion and interparticle attraction. Actually, filler aggregation phenomena take place in the polymer nanocomposites above the melting or glass transition temperature of the polymer matrix, as evidenced in Figure 6.1. Consequently, it is essential to zoom out from the length scale of the single nanoparticles, focusing instead on the effective building block which constitute the filler network, that is the clusters of nanoparticles. Ultimately, the only two populations of dynamical species which have to be considered in the two-phase model are the polymer matrix, whose dynamics, hydrodynamic effects apart, are not affected by the filler, and the three-dimensional network made by clusters of nanoparticles, which is unable to relax (at least in the investigated time window). A graphical representation of such a simplifying idea is given in Figure 6.2.

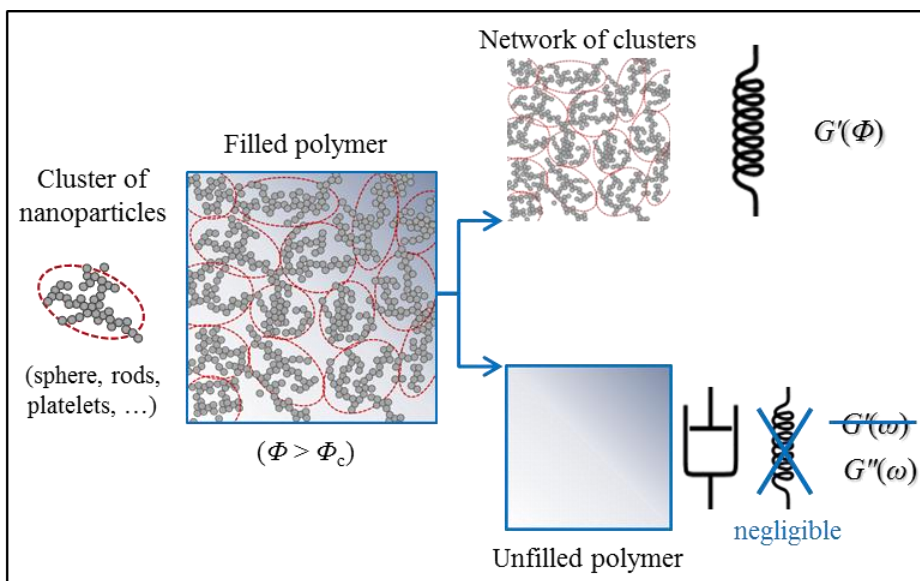


**Figure 6.2** Schematic representation of the origin of viscoelasticity in polymer nanocomposites above the percolation threshold.

A relevant consequence of the underlying physical picture of Figure 6.2 is that the two-phase model should work irrespective of the size and shape of the pristine particles, which simply represent the basic constituents of the filler clusters which compose the network.

To support such a conjecture, four nanocomposite systems are studied, differing among them for the kind of the primary particles. In detail, three families of polymer nanocomposites at different filler volume fraction,  $\Phi$ , have been prepared, each based on polystyrene (PS) and filled with a different kind of nanoparticles: graphite nanoplatelets (GNPs, the same discussed in Chapter 5), organo-modified montmorillonite, (O-Clay, Cloisite<sup>®</sup> 15A) and multi-walled carbon nanotubes (MWCNTs). Literature data on a system based on the same PS matrix and filled with fumed silica nanoparticles ( $\text{SiO}_2$  fumed) are further considered [Filippone et al. (2010)]. Note that, at this point, only non-interacting systems are considered, that is nanocomposites characterized by negligible polymer-particle interactions. Linear viscoelastic measurements have been carried out on the prepared nanocomposite families. At the end of the time scans the linear viscoelastic moduli are stable enough to obtain a reliable rheological fingerprint of the samples through reproducible frequency scan experiments. The elastic,  $G'$ , and viscous,  $G''$ , moduli are shown as a function of frequency,  $\omega$ , in Figure 6.3. Note that the data of the PS/GNPs samples already shown in § 5.3 are reported again for convenience.

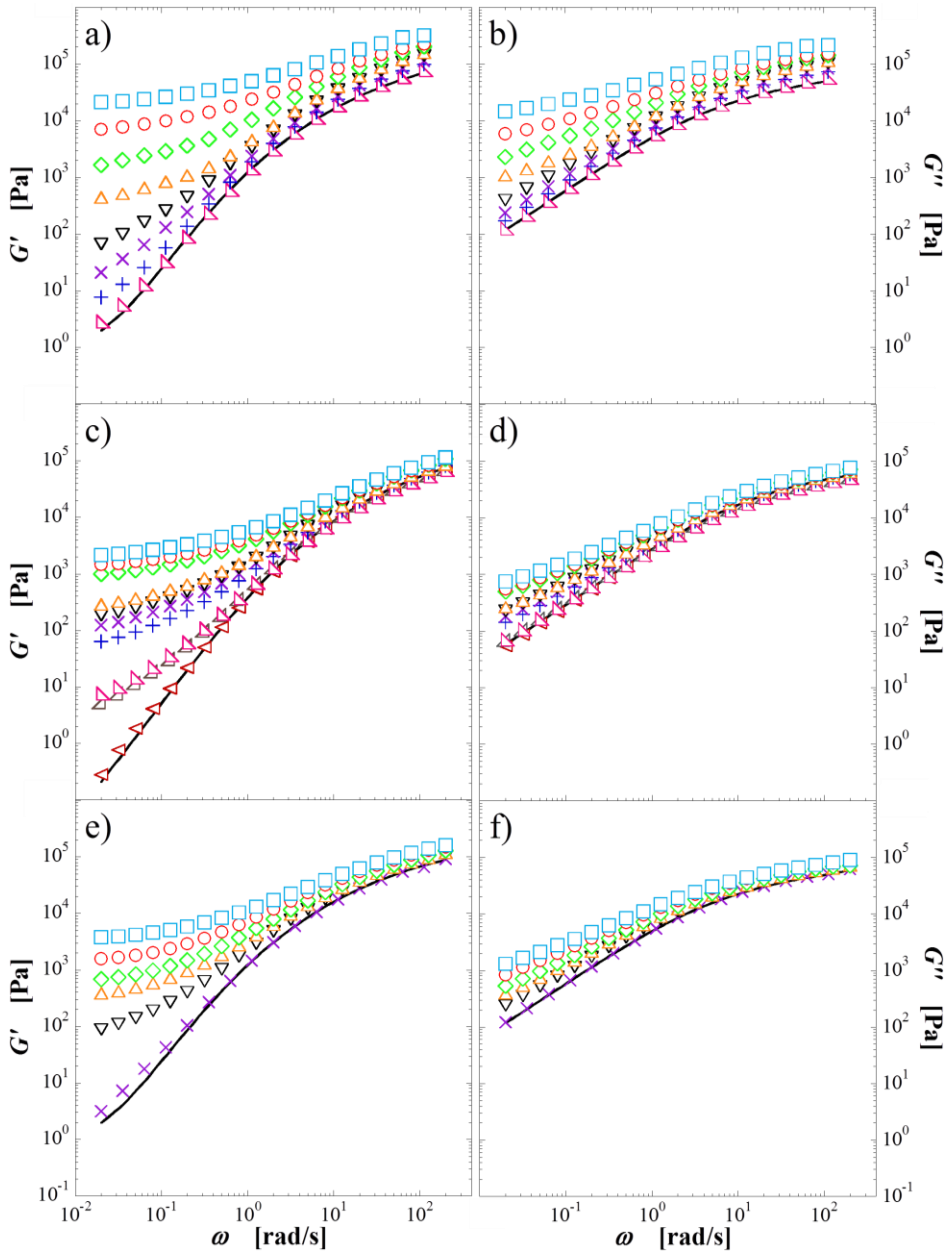


**Figure 6.3** Frequency-dependent (a, c, e) elastic and (b, d, f) viscous moduli of PS-based nanocomposites filled with (a, b) GNPs (c, d) O-Clay and (e, f) MWCNTs. From bottom to top: (a, b)  $\Phi = 0.009, 0.014, 0.018, 0.024, 0.029, 0.036, 0.037, 0.049$ ; (c, d)  $0.0007, 0.0044, 0.0060, 0.0094, 0.0110, 0.0127, 0.0132, 0.0163, 0.0189, 0.0265$ ; (e, f)  $0.0003, 0.0020, 0.0035, 0.0045, 0.0065, 0.0086$ . The solid lines refer to the neat PS matrix.

The systems share the same qualitative behavior, peculiar of many polymer nanocomposites. Briefly, both moduli of the filled samples monotonically increase with  $\Phi$  in the whole range of investigated frequencies, the effect being more pronounced on  $G'$  which is more sensitive to the presence of the filler than its viscous counterpart. The polymer dynamics prevail at high frequency, where the filler simply causes an apparent increase of the viscoelastic moduli due to hydrodynamic interactions among the clusters of nanoparticles. At low frequency, instead, the response of the nanocomposites is dominated by the filler phase. Indeed, the flattening of  $G'$  at low  $\omega$  indicates the occurrence of a liquid- to solid-like rheological transition due to the formation of a space-spanning network throughout the polymer matrix.

According to the two-phase model, once the filler volume fraction exceeds the percolation threshold, the contributions of the polymer phase and that of the network of clusters can be separated. Because of the independency of the responses of polymer and network, the building of master curves of  $G'$  for the samples at different composition is possible. Briefly, first the empirical amplifying factors  $B(\Phi)$  have to be estimated to account for the reduced gap available to the fluid because of the presence of the solid particles. Then, reflecting the physical picture of the two-phase model, the horizontal and vertical shift factors to build the master curve are identified by the coordinates of the point in which the network elasticity equals the viscous feature of the matrix, properly “corrected” to erase the mere hydrodynamic effects.

The master curves of the PS-based nanocomposites filled with either GNPs or O-Clay or MWCNTs are reported in Figure 6.4, together with that of the system filled with fumed silica taken from the literature.

For completeness, the amplifying factors,  $B(\Phi)$ , and the  $G''(\omega)$  curves of the pure matrices on which the shift factors ( $a_\Phi$ ;  $b_\Phi$ ) used to build the master curves lie are reported in the Appendices at the end of the dissertation, together with the corresponding numerical values.

The excellent quality of the scaling of all the master curves in Figure 6.4 confirms the validity of the basic assumptions of the two-phase model, which thus is proved to be able to describe the linear viscoelasticity of polymer nanocomposites irrespective of the nature of the embedded filler phase. It is important to stress that the overlay of the  $G'$  curves is not obtained by looking for their partial superposition, being instead a direct consequence of the precise physical meaning of the shift factors. Vice versa, once built the master curve by referring to the samples at  $\Phi$  high enough to clearly identify the network elasticity,  $G'_0$ , the master curve itself can be exploited to infer the elasticity of more tenuous networks which build up in the samples at lower filler content. Such a predictive feature of the two-phase model has been already demonstrated and discussed in Chapter 5. Here, it is just exploited to obtain the complete master curves of Figure 6.4 for all the samples above the percolation threshold.

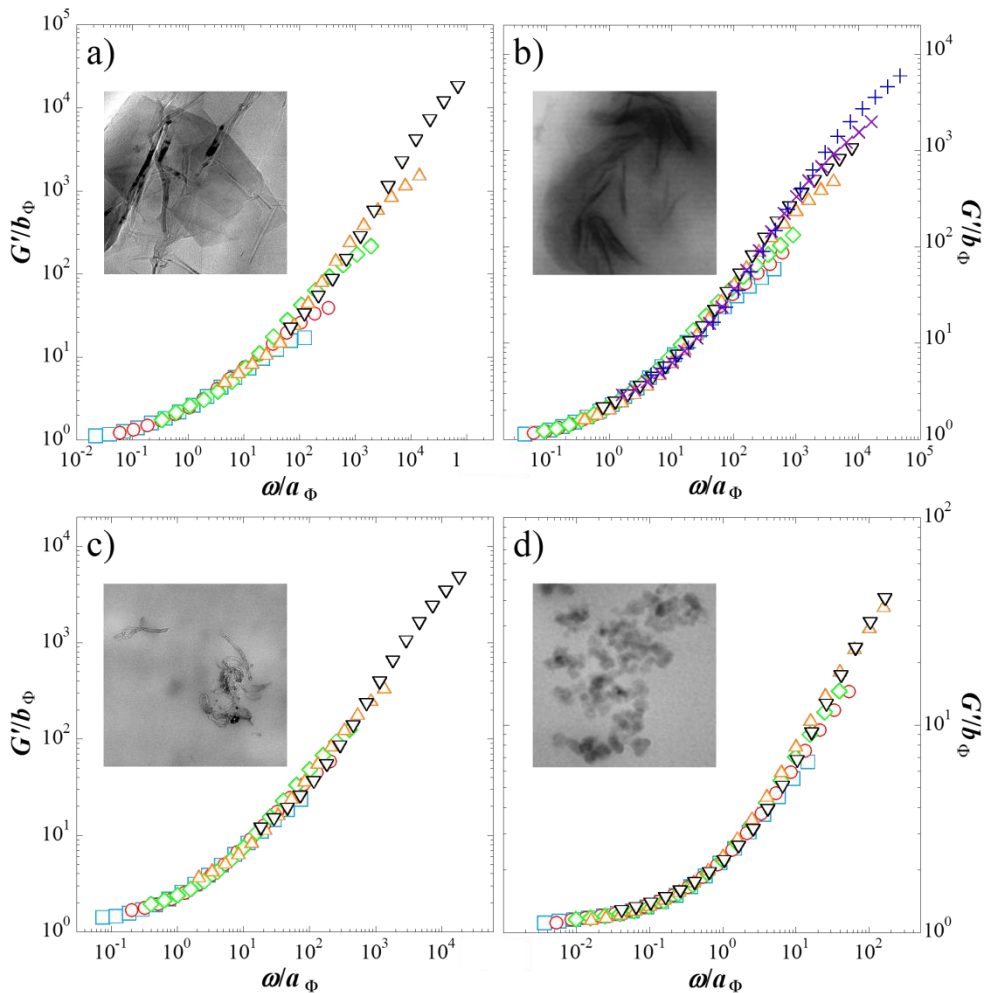


**Figure 6.4** Master curves of  $G'$  of (a) PS/GNPs nanocomposites at  $0.024 \leq \Phi \leq 0.049$ , (b) PS/O-Clay nanocomposites at  $0.0094 \leq \Phi \leq 0.0265$ , (c) PS/MWCNTs nanocomposites at  $0.0020 \leq \Phi \leq 0.0086$  and (d) PS/SiO<sub>2</sub> fumed nanocomposites at  $0.024 \leq \Phi \leq 0.041$ . Data of PS/SiO<sub>2</sub> samples the are taken from Filippone et al. (2010). The insets are TEM images which are representative of the clusters of nanoparticles embedded in the PS matrix for each considered nanocomposite system.

Concerning the conditions of the measurements, rheological data obtained at different temperature,  $T$ , are reported in Figure 6.4. It has to be pointed out that, if negligible polymer-particle interactions exist, then the network elasticity simply originates from mechanical interactions among bare clusters. In such a case, the

temperature is thus expected not to affect the network modulus appreciably, whereas it clearly influences the high-frequency behavior dominated by the polymer. This holds for all the investigated systems and is demonstrated in Figure 6.5 for a representative nanocomposite sample filled with MWCNTs.

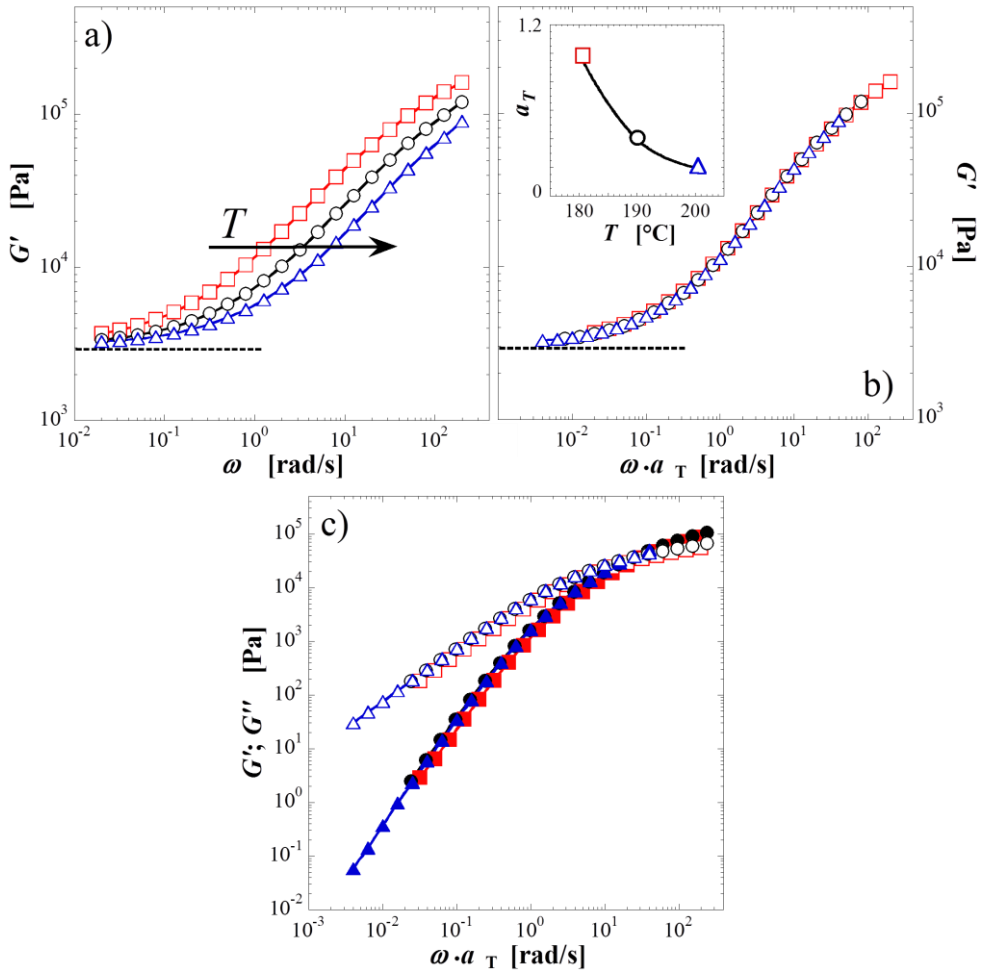


**Figure 6.5** (a) Frequency-dependent  $G'$  of a PS/MWCNTs sample at  $\Phi = 0.0086$  obtained at three different temperatures:  $T = 180$  °C (squares),  $190$  °C (circles) and  $200$  °C (triangles). (b) Overlay of the curves of part (a) obtained by shifting them along the log frequency axis by an empirical factor  $a_T$  (reported in the inset). (c) Master curves of  $G'$  (full symbols) and  $G''$  (empty symbols) of the neat PS at the reference temperature  $T = 180$  °C obtained using the same horizontal shift factors  $a_T$  shown in the inset of part (b); symbols are the same as in part (a).

The low-frequency plateau does not change with temperature, consequently the shift of the curves along the log frequency axis by a factor  $a_T$  causes their overlap (Figure 6.5b). In addition, using the same empirical factors a master curve of the linear viscoelastic moduli of the neat polymer is generated according to the time-temperature superposition principle (Figure 6.5c). This confirms the independence of the responses of the cluster network and the polymer. Therefore, the increase of the temperature in nanocomposites characterized by weak polymer-particle interactions can be interpreted as an increase of the filler content, being its effect essentially the same. It results indeed in a widening of the frequency range in which the cluster network prevails over the matrix. Consequently, the master curves of  $G'$  obtained at different temperatures can be correctly compared, as evidenced in Figure 6.6 for the four families of investigated nanocomposites.

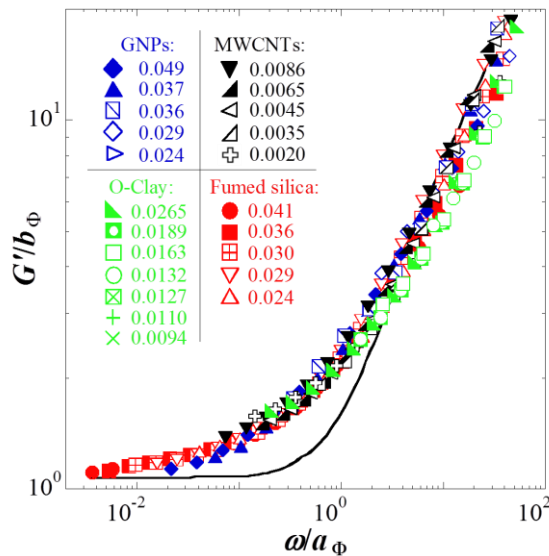


**Figure 6.6** Master curves of  $G'$  of four different nanocomposite systems based on the same PS matrix tested at different temperatures: PS/GNPs at  $T = 180$  °C (blue) and PS/MWCNTs (black) at  $T = 180$  °C, PS/O-clay at  $T = 190$  °C (green) and PS/SiO<sub>2</sub> fumed at  $T = 200$  °C (red). The filler volume fractions are listed in the inset for each system. The continuous line represents the elastic modulus of an ideal nanocomposite sample in which the  $\omega$ -independent network elasticity simply adds up to the elastic modulus of the neat PS matrix.

All the data collapse on a single master curve, which means that common dynamics characterize the networks of clusters irrespective of the nature of the primary particles. Specifically, a frequency-independent elasticity, reminiscent of purely elastic solids, emerges at  $\omega/a_\phi \ll 1$ , reflecting the only contribution to the

nanocomposite elasticity which stems from the cluster network. In contrast, the polymer elasticity dominates the response at  $\omega/a_\phi \gg 1$ , and all the samples share the relaxation dynamics of the common PS matrix. As a consequence, the nonscalable tails at high dimensionless frequency reflect the polymer relaxation processes and do not invalidate the good overall quality of the scaling. The transition between the two regimes occurs as a gradual slowing down of the relaxation dynamics. According to the two-phase model, at  $\omega/a_\phi \sim 1$  the cluster network and the polymer matrix equally contribute to the nanocomposite elasticity. Actually, the nanoparticles slow down the polymer dynamics even in case of weak polymer-particle interactions by way of confinement effects and topological constraints. As a consequence, the relaxation spectrum in the intermediate regime reflects the relaxation of the PS matrix in the nanocomposite, which is somehow different from that of the unfilled polymer to which the two-phase mode refers. This concept is clarified by the continuous line in Figure 6.6, which represents the elastic modulus of an ideal sample in which the  $\omega$ -independent network elasticity simply adds up to the  $G'(\omega)$  of the unfilled PS according to the simplified picture of the model. In such a case the transition is evidently much sharper than that observed in the real polymer nanocomposites, proving the retardation effect of the filler on the polymer dynamics. Surprisingly, however, neither the size nor the shape of the pristine nanoparticles noticeably affect the shape of the curves in the intermediate regime. This means that the single nanoparticles play a secondary role in determining the relaxation spectrum of the nanocomposite, which essentially reflects the interplay between the filler in its aggregated state and the host polymer.

### 6.3 Generalizing the two-phase model: polymer nature and polymer-particle interactions

The key assumption of the two-phase model is the coexistence of two main dynamical species with distinct relaxation timescales: the free polymer and a three-dimensional structure which is unable to relax, at least within the experimentally accessed timescales. As confirmed in the previous paragraph, this picture confers wide generality to the two-phase model, since the nature of latter phase is not strictly defined. To support such a conclusion, several polymer nanocomposites taken from the literature are considered, differing among them not only in terms of filler size, shape and chemistry, but also in the matrix viscosity, presence of compatibilizing agents and degree of polymer-filler affinity. The main features of each system are summarized in Table 6.1 and the corresponding master curves of the elastic modulus are reported in Figure 6.7. For completeness, the amplifying factors and the  $G''(\omega)$  curves of the pure matrices on which the shift factors used to build the master curves lie are reported in the Appendices at the end of the dissertation, together with the corresponding numerical values.

**Table 6.1** Main features of the investigated systems taken from the literature.

Filler	Polymer matrix	$\eta_0$ of the polymer <sup>a</sup> and testing $T$	Polymer-particle interaction	$\Phi^b$ of the scaled $G'$ curves	Reference
Colloidal Silica (SiO <sub>2</sub> )	Poly(ethylene oxide) (PEO)	$\eta_0=2.0 \times 10^5$ Pa·s; $T=75$ °C	Strong	0.02; 0.03; 0.04	Zhang and Archer (2002)
Fumed Silica (SiO <sub>2</sub> )	Poly(ethylene oxide) (PEO)	$\eta_0=2.1 \times 10^4$ Pa·s; $T=110$ °C	Good	MC: 0.048; 0.062; 0.071; 0.075 FD: 0.034; 0.044; 0.047; 0.062	Capuano et al. (2012)
Organo-modified clay (O-Clay)	Poly( $\epsilon$ -caprolactone) (PCL)	$\eta_0=1.5 \times 10^4$ Pa·s; $T=80$ °C	Unspecified; supposed to be good	0.015; 0.025; 0.051	Lepoittevin et al. (2002)
Organo-modified clay (O-Clay)	Linear low density polyethylene (LLDPE) + compatibilizer	$\eta_0=6.1 \times 10^3$ Pa·s; $T=160$ °C	Unspecified; supposed to be good	0.011; 0.016; 0.026; 0.042; 0.053	Durmus et al. (2007)
Single-walled carbon nanotubes (SWCNTs)	Unsaturated polyester resin (UPR)	$\eta_0=2.0 \times 10^0$ Pa·s; $T=20$ °C	Supposed to be good by the authors	0.00147; 0.00183; 0.002; 0.0025	Kayatun and Davis (2009)
Single-walled carbon nanotubes (SWCNTs)	Poly(methyl methacrylate) (PMMA)	$\eta_0=7.7 \times 10^3$ Pa·s; $T=200$ °C	Supposed to be good by the authors	0.0014; 0.0034; 0.0069; 0.014	Du et al. (2004)

<sup>a</sup> When not explicitly specified in the reference paper, the zero-shear rate viscosity of the neat polymer,  $\eta_0$ , has been estimated as the dynamic viscosity  $\eta' = G'' \cdot \omega$  in the limit of low frequency.

<sup>b</sup> When not expressed in volume fraction in the reference paper,  $\Phi$  is calculated using the mass fraction and the density value indicated by the authors or in the technical datasheet.

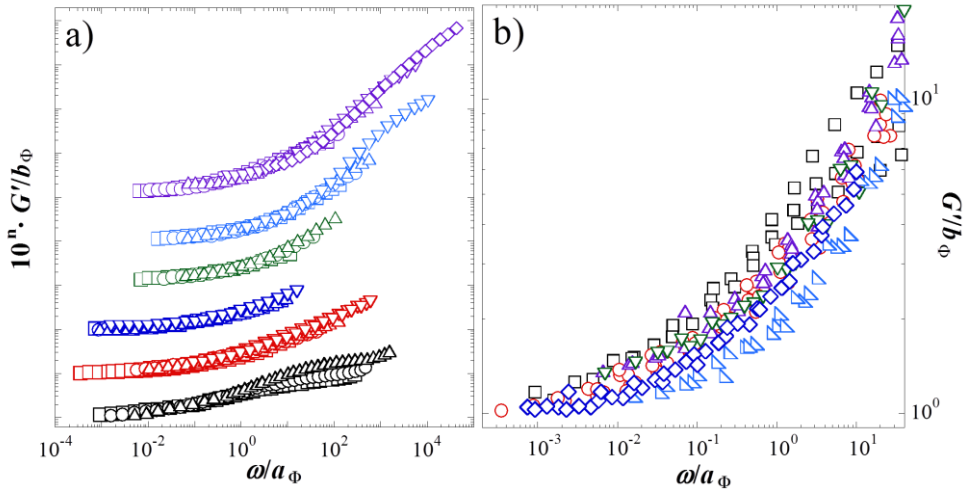


**Figure 6.7** (a) Master curves of  $G'$  for the nanocomposite systems described in Table 6.1. From bottom to top: Zhang and Archer (2002), Capuano et al. (2012), Kayatin and Davis (2009), Lepoittevin et al. (2002), Du et al. (2004) and Durmus et al. (2007). The master curves have been vertically shifted for sake of clarity. Different symbols are used for each composition. Increasing the  $\Phi$ : squares, circles, triangles, inverted triangles, diamonds. (b) Detail of the master curves shown in part (a) without vertical shifting. Only one out of two experimental points is reported. A single symbol has been used for each master curve: squares for Zhang and Archer (2002), circles for Capuano et al. (2012), inverted triangles for Lepoittevin et al. (2002), triangles for Durmus et al. (2007), diamonds for Kayatin and Davis (2009), and half-squares for Du et al. (2004). Colors are the same as in part (a).

Excluding the high-frequency regime, the collapse of the  $G'$  data sets on the corresponding master curves is extremely good for each system. Particularly noticeable is the result for nanocomposites in which good polymer-particle affinity is expected due to either the filler surface chemistry or the presence of a compatibilizing agent. This clearly indicates that the two-phase model works even in the case of polymer-mediated filler networks. Regardless of the presence of a fraction of chains linked to the particle, indeed, most of the polymer retains its own characteristic dynamics, which remain much faster than those of the hybrid network, thus restoring the underlying physics of the two phase model.

The overlay of the master curves of the various systems taken from the literature is shown in Figure 6.7b. Each data set approaches the common horizontal asymptote  $G'/b_\Phi = 1$  with its own characteristic dynamics. Keeping in mind the negligible effect of nanoparticle size and shape on the relaxation spectrum of the nanocomposite, the scattering of the data at  $\omega/a_\Phi \sim 1$  can be primarily ascribed to the peculiar dynamics of the polymer in each of the selected systems. In particular,

the different relaxation spectra of the various matrices bring about different shapes of the  $G'$  curves at high and intermediate values of  $\omega/a_\phi$ . In addition, in the systems with non-negligible polymer-particle interactions, the specific dynamics of the polymer chains adsorbed onto the nanoparticle surface also affect the relaxation modes of the nanocomposite [Solomon et al. (2001)]. Moreover, an influence of the testing temperature on the network elasticity is expected in polymer-mediated cluster networks, and this could imply additional changes in the relaxation spectra. As a consequence, despite the common elementary principles on the basis of the melt state relaxation processes, and unless comparing systems with similar polymer matrices and typology of network, the building of a universal master curve of the elasticity of polymer nanocomposites is precluded by the specificity of the each system.

## 6.4 Network elasticity and stress-bearing mechanisms

The two-phase model applies for samples with filler volume fractions greater than a critical concentration  $\Phi_c$ . Such a threshold represents the minimum particle volume fraction necessary for the formation of a space-spanning network, which can be either formed by bare clusters or mediated by a fraction of adsorbed polymer. According to the percolation theory, the network is expected to exhibit critical behavior just above  $\Phi_c$ , its elasticity growing with  $\Phi$  as:

$$G'_0 = k(\Phi - \Phi_c)^\nu \quad (6.1)$$

where  $k$  and  $\nu$  are two constants, the latter being related to the stress-bearing mechanism [Stauffer and Aharony (1992)].

The values of  $\Phi_c$  are estimated by adopting the same procedure described in Chapter 5. Briefly, Equation 6.1 is fitted to the vertical shift factors for the building of the master curves,  $b_\phi = G'_0$ , setting  $k$  and  $\nu$  as fitting parameters while keeping  $\Phi_c$  constant. The procedure is repeated for different  $\Phi_c$  in a range of composition inferiorly and superiorly limited by the highest  $\Phi$  of the  $G'$  curves which cannot be scaled on the corresponding master curve and the lowest  $\Phi$  of the scalable  $G'$  curves, respectively. Hence the percolation threshold is identified as the value of  $\Phi_c$  which returns the maximum coefficient of determination,  $R^2$ .

The parameters obtained through the best fitting procedure are reported for all the investigated systems, that is the experimental nanocomposite families and those taken from the literature, in Table 6.2. Note that, for the nanocomposite systems taken from the literature, the percolation threshold declared by the authors is also provided. In addition, the power-law dependences of the network elasticity resulting from the best fitting procedure are shown in Figure 6.8 for all the investigated nanocomposite families.

**Table 6.2** Percolation threshold  $\Phi_c$  and fitting parameters  $k$  and  $\nu$  of the percolation scaling law for all the investigated systems.\*\*\*

System	$\Phi_c$ (estimated)	$\nu$	$k$ [Pa]	$\Phi_c$ (reported in the reference)
PS+GNPs [Chapter 5]	0.020	4.54	$2.3 \times 10^{11}$	-
PS+O-clay	0.0076	2.34	$3.1 \times 10^7$	-
PS+MWCNTs	0.0012	2.62	$9.5 \times 10^8$	-
PS+SiO <sub>2</sub> fumed [Filippone et al. (2010)]	0.015	2.80	$5.9 \times 10^8$	0.015
PEO+SiO <sub>2</sub> colloidal [Zhang and Archer (2002)]	0.012	1.11	$1.5 \times 10^7$	> 0.01
PEO+SiO <sub>2</sub> fumed (melt mixed samples) [Capuano et al. (2012)]	0.041	1.74	$3.8 \times 10^7$	0.041
PEO+SiO <sub>2</sub> fumed (freeze dried samples) [Capuano et al. (2012)]	0.0029	1.59	$2.7 \times 10^7$	0.0029
PCL+O-clay [Lepoittevin et al. (2002)]	0.006	1.78	$5.0 \times 10^7$	> 0.005
LLDPE+compatibilizer +O-clay [Durmus et al. (2007)]	0.006	3.07	$1.8 \times 10^8$	~ 0.01
UPR+SWCNTs [Kayatin and Davis (2009)]	0.00055	2.07	$9.3 \times 10^7$	~ 0.001
PMMA+SWCNTs [Du et al. (2004)]	0.00133	0.92	$6.2 \times 10^5$	~ 0.0008

\*\*\* Slight differences with the values reported in Filippone and Salzano de Luna (2012) are due the different number of available experimental data and to approximations in the estimation of the filler content in volume fraction.

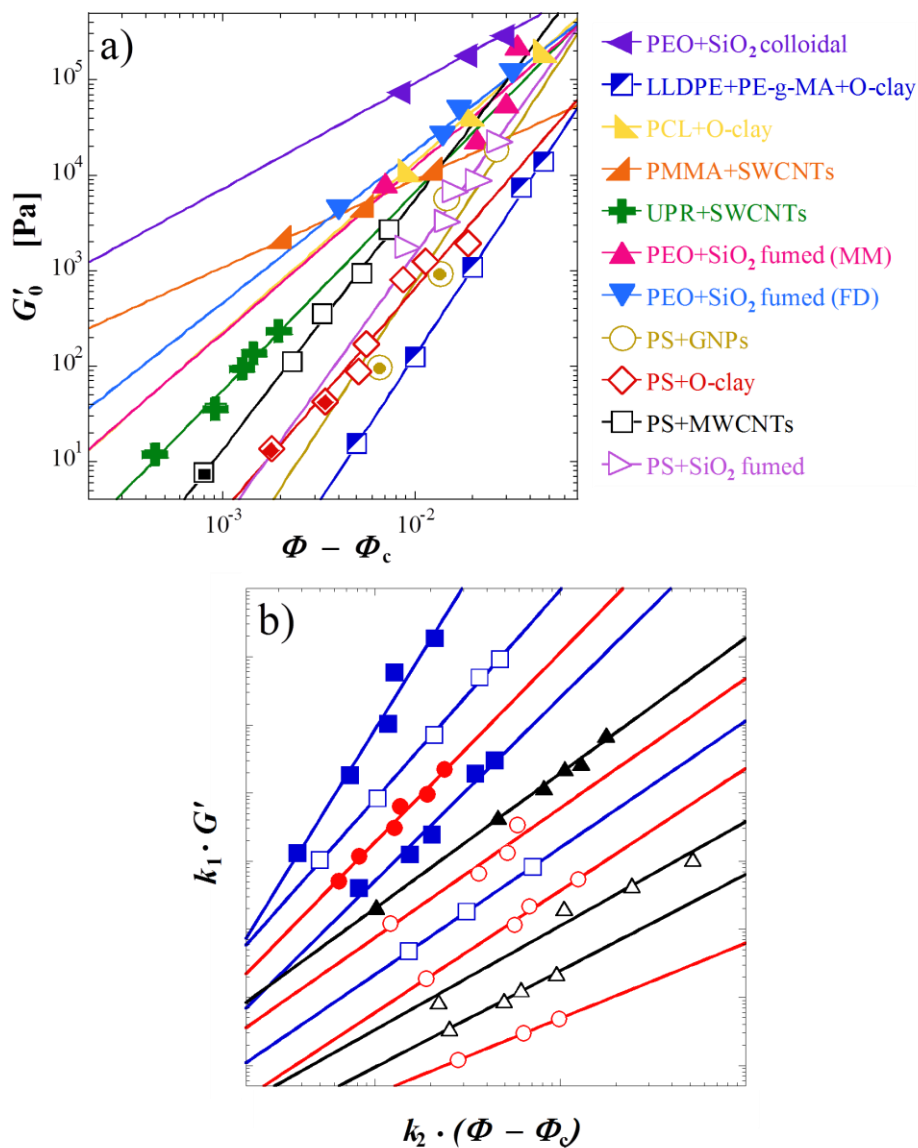


**Figure 6.8** (a) Power law dependence of  $G'_0$  on the reduced filler content,  $\Phi - \Phi_c$ , for all the investigated systems. Concentric symbols represent the values of network elasticity which have been inferred from the master curve as described Chapter 5. (b) Same curves of part (a) rescaled for the sake of clarity by empirical shift factors. The systems have been classified according to the type of filler: spherical (red circles), disk-like (blue squares) and rod-like nanoparticles (black triangles); degree of polymer-particle affinity: weak (full symbols) and strong (empty symbols).

For each system, the elasticity well follow the growth with filler content predicted by Equation 6.1. The concentric symbols, deduced by exploiting the predictive feature of the master curve, result well aligned to those at higher  $\Phi$ , supporting the reliability of the adopted procedure. Moreover, the agreement between the estimated and declared  $\Phi_c$  is generally good.

Trying to classify the systems, the data have been rescaled by an empirical pair of horizontal and vertical factors ( $k_1$ ;  $k_2$ ) without altering the scaling features, as shown in Figure 6.8b. Referring to the kind of filler, different colors and symbols have been used to discriminate the systems based on spherical, disk-like and rod-like nanoparticles. Nonetheless, trends which clearly relate the shape of the primary nanoparticles to the scaling of the elasticity can be hardly identified. On the other hand, another distinguishing feature of the nanocomposite families is the degree of polymer-particle interaction. The value of the critical exponent  $\nu$  partially reflects the degree of polymer-filler affinity, being it related to the specific stress-bearing mechanism. Indeed, if good polymer-filler affinity exists, polymer bridging can result in long-lived bonds between the particles which contribute to the stress transfer. Comparing different kinds of polymer-nanoparticle gels, Surve et al. (2006) suggested a universal trend with  $\nu \approx 1.88$  for polymer-mediated particle networks, in contrast to systems with strong particle-particle interactions which may exhibit elasticity exponents as high as  $\nu = 5.3$ . In line with these conclusions, the data can be reasonably divided in two groups depending on the degree of polymer-filler interaction. The classification can be interpreted in terms of critical exponents, as suggested by the aforementioned authors. Specifically, different values of  $\nu$  are expected to characterize non-interacting and interacting nanocomposites. The investigated systems exhibit values of  $\nu$  ranging between about 0.9 and 4.5. In detail, almost all the systems in which good affinity is declared or presumed have lower values of the critical exponent (empty symbols in Figure 6.8b), confirming that general trends can be recognized if referring to the degree of polymer-particle interactions.

Another interesting evidence emerges when looking at the absolute values of the network elasticity (see Figure 6.8a). In the immediate vicinity of  $\Phi_c$  the elasticity of the networks which form in the absence of noticeable polymer-particle interactions is generally lower. The strength of percolating networks reflects a complex interplay between energetic and structural features. The steepness of the interaction potential sets the attractive force between the network elements, but the mechanical strength ultimately depends on the way in which they are arranged in the space. It is possible that the better dispersion of the clusters in case of good polymer-particle affinity may result in finer networks, which are more effective in bearing the stress than the fractal structures forming just above  $\Phi_c$  in non-interacting polymer nanocomposites.

## **Robustness of the two-phase model: extension to nanocomposites based on a biphasic polymer matrix\***

*In this chapter the ability of the two-phase model in describing the linear viscoelasticity of complex fluids other than nanocomposites based on a homogenous polymer phase is proved. Focusing on nanocomposites based on biphasic polymer matrices, a preliminary overview of the rheological implications arising from the multiphasic nature of the host matrix is firstly provided (§ 7.1). Then the linear viscoelastic response of nanocomposites based on a biphasic polymer matrix is studied, using a reference system based on a single phase matrix to highlight the effect of the presence of liquid-liquid interfaces where the filler is inclined to gather (§ 7.2). It is demonstrated that the two-phase model is able to capture the viscoelasticity of the filled blend irrespective of the presence of the additional polymer phase (§ 7.3). On the other hand, percolation and fractal models are shown to reveal subtle and yet meaningful differences in terms of stress-bearing mechanisms and structure of the building blocks which constitute the filler network forming in the biphasic system above a certain filler content (§ 7.4).*

### **7.1 Prefatory notes**

In polymer nanocomposites increasing the filler volume fraction,  $\Phi$ , eventually results in the arrest of the relaxation dynamics. Such a phenomenon is ascribed to the formation of a three-dimensional network, made of particles or clusters of particles, which spans throughout the polymeric matrix. Although the filler and polymer phases are both viscoelastic by nature, Chapter 6 demonstrates that the complex  $\Phi$ -dependent relaxation spectrum of polymer nanocomposites can be simply described in terms of only two main families of dynamical species. The basic idea of the two-phase model is that the viscoelasticity of nanocomposite above the filler percolation threshold,  $\Phi_c$ , can be split into the independent

---

\* Part of the results has been published in «Filippone G, Causa A, Salzano de Luna M, Sanguigno L, Acierno D, “Assembly of plate-like nanoparticles in immiscible polymer blends - Effect of the presence of a preferred liquid-liquid interface”, *Soft Matter* 10, 3183-3191 (2014)».

responses of the network, assumed as deriving from the collection of clusters of nanoparticles, and the unfilled polymer. In addition, the network phase is considered the only responsible for the elastic connotation of the nanocomposite, while the entire viscous connotation is ascribed to the polymer, considered purely viscous. The simple underlying physics of the two-phase model bestows wide generality on it. Consequently, besides capturing the viscoelasticity of polymer nanocomposites at filler loadings higher than the percolation threshold, the analysis is expected to be useful to describe a wide variety of other kinds of complex fluids in which a superposition of the elasticity of the components is possible.

The linear viscoelastic response of multiphasic fluid systems, such as immiscible polymer blends, is characterized by an additional elastic contribution with respect to homogenous fluid media, which arises because of interfacial relaxation processes. Such systems thus represent a perfect candidate to verify the possibility of extending the approach of the two-phase model to other complex fluids. In particular, the present study deals with nanocomposites based on a biphasic polymer matrix with drop-matrix morphology, in which the characteristic timescale of the relaxation of the dispersed phase coincides with that at which the elasticity of the filler network prevails over the response of the unfilled polymer melt. The aim is to provide a reliable description of the viscoelastic response of such materials exploiting the two-phase model, irrespective of the presence of the additional source of elasticity given by the polymeric drops.

The Chapter is organized as follows. The viscoelastic response of the neat biphasic polymer system is deeply studied. The investigation focuses on polymer blends exhibiting drop-matrix morphology, in which an additional elastic source exists due drop shape relaxation processes under the influence of interfacial tension. Then, the rheological implications stemming from the addition of nanoparticles are analyzed and the ability of the two-phase model in describing the viscoelasticity of the biphasic nanocomposites, irrespective of the presence of a dispersed polymer phase, is proved. The validity of the approach is explained by the prevalence of the elastic contribution of the filler network over that related to the interfacial relaxation in the investigated regime. Finally, percolation and fractal models are used to highlight the effect of the presence of the polymeric drops on the superstructures formed by the filler phase at relatively high loadings.

## **7.2 Linear viscoelasticity of the neat biphasic polymer system**

The study focuses on a model biphasic polymer system based on polystyrene (PS) and poly(methyl methacrylate) (PMMA). The constituents have been selected because they are both amorphous, otherwise crystallinity compromises the link between melt- and solid-state morphology, making *ex post* microscopic analyses unreliable. In addition, PS and PMMA share a glass transition temperature of about

100°C, facilitating the preparatory steps for transmission electron microscopy (TEM) analyses.

From a rheological point of view, a dispersion of two immiscible liquids displays an enhanced elastic response at low frequency,  $\omega$ . This additional elasticity arises because deformed droplets relax back to a spherical shape under the influence of interfacial tension. The relaxation time of the process scales with  $(R \cdot \eta_m) / \gamma_{12}$ , where  $R$  is the radius of a spherical droplet,  $\eta_m$  is the viscosity of the matrix phase and  $\gamma_{12}$  represents the interfacial tension between the two constituents. For typical polymer blends the relaxation time can be on the order of seconds. This behavior is most easily probed by measuring the viscoelastic moduli in small-amplitude oscillatory shear flow. Using a small strain, indeed, ensures that the droplet remains nearly spherical and that the stress response is linear in strain. Experiments show that droplet breakup and coalescence are negligible during these experiments [Tucker and Moldenaers (2002)], making the interpretation of the  $\omega$ -dependent response straightforward. The linear viscoelastic behavior of PS/PMMA blends at different contents of PMMA is reported in Figure 7.1 in terms of frequency dependence of the elastic,  $G'$ , and viscous,  $G''$ , shear moduli.

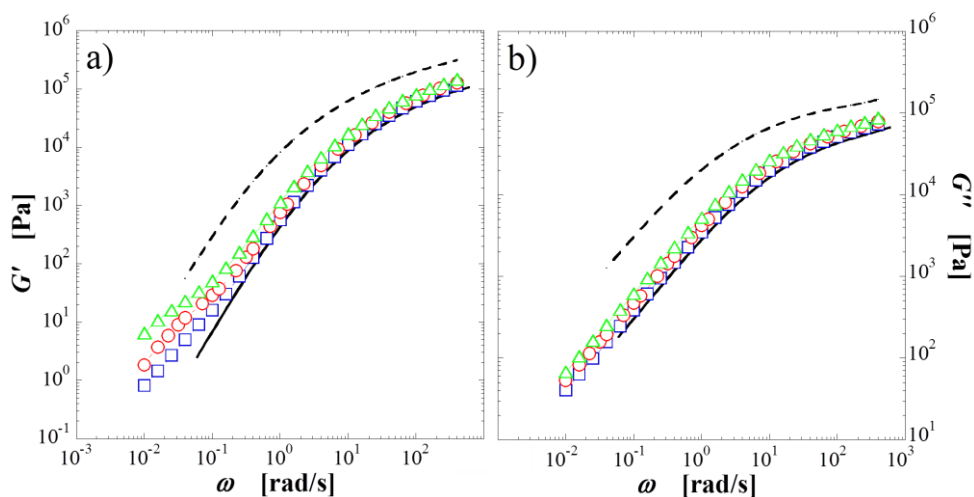


**Figure 7.1** Frequency-dependent (a) elastic and (b) viscous moduli of biphasic PS/PMMA polymer blends at different weight composition: 85/15 (squares), 75/25 (circles) and 65/35 (triangles). The solid and dashed lines refer to the neat PS and PMMA, respectively.

The main effect of the dispersed phase is to increase the storage modulus  $G'$  at low frequency. The critical frequency of this effect is governed by the relaxation time of the droplets,  $\tau_D$ . Because the elastic relaxation times of the matrix and droplet fluids are much shorter than  $\tau_D$ , the droplet contribution appear as a distinct

“shoulder” in the frequency-dependent curve of  $G'$ , which is readily apparent on the curves of the blends in Figure 7.1a. On the other hand, the presence of the droplets has only a very small effect on the viscous modulus.

The Palierne model predicts the linear viscoelastic moduli of a blend with drop-matrix morphology once the interfacial tension and the radius of the dispersed phase are known [Palierne (1990)]. Although Palierne theory can be written for a distribution of droplet sizes, for most cases it is sufficient to use the volume-average droplet radius,  $R_v$  [Graebling et al. 1993]. Using the average drop radius has a negligible effect on the predictions as long as the polydispersity  $R_v/R_n$  is less than about two,  $R_n$  being the number-average drop radius. In the paper by Palierne the expression of the complex modulus of the blend,  $G_b^*$ , is provided, whereas the relations for the elastic,  $G'_b$ , and viscous,  $G''_b$ , moduli of the blend are given by Lacroix et al. (1996):

$$G'_b = \frac{1}{D} [G'_c (B_1 B_2 + B_3 B_4) - G''_c (B_1 B_4 - B_2 B_3)] \quad (7.1)$$

$$G''_b = \frac{1}{D} [G'_c (B_1 B_4 - B_2 B_3) - G''_c (B_1 B_2 + B_3 B_4)] \quad (7.2)$$

where  $G'_c$  and  $G''_c$  are the elastic and viscous moduli, respectively, of the neat continuous-phase and the constants  $D$  and  $B_i$  are given by:

$$D = (C_2 - 2\Phi_D C_4)^2 + (C_1 - 2\Phi_D C_3)^2 \quad (7.3)$$

$$B_1 = C_1 - (2\Phi_D C_3) \quad (7.4)$$

$$B_2 = C_1 + (3\Phi_D C_3) \quad (7.5)$$

$$B_3 = C_2 - (2\Phi_D C_4) \quad (7.6)$$

$$B_4 = C_2 + (3\Phi_D C_4) \quad (7.7)$$

where  $\Phi_D$  is the volume fraction of the dispersed-phase in the biphasic system and the coefficients  $C_i$  are given by:

$$C_1 = 40 \frac{\gamma_{12}}{R_v} (G'_c + G'_d) + 38 (G'_d{}^2 - G''_d{}^2) + 48 (G'_c{}^2 - G''_c{}^2) + 89 (G'_c G'_d - G''_c G''_d) \quad (7.8)$$

$$C_2 = 40 \frac{\gamma_{12}}{R_v} (G''_c + G''_d) + 96(G'_c G''_c) + 76(G'_d G''_d) + 89(G''_c G'_d - G'_c G''_d) \quad (7.9)$$

$$C_3 = 4 \frac{\gamma_{12}}{R_v} (2G'_c + 5G'_d) - 16(G'^2_c - G''^2_c) + 19(G'^2_d - G''^2_d) - 3(G'_c G'_d - G''_c G''_d) \quad (7.10)$$

$$C_4 = 4 \frac{\gamma_{12}}{R_v} (2G''_c + 5G''_d) - 32(G'_c G''_c) + 38(G'_d G''_d) - 3(G''_c G'_d - G'_c G''_d) \quad (7.11)$$

where  $G'_d$  and  $G''_d$  are the elastic and viscous moduli, respectively, of the neat dispersed-phase.

Among the biphasic systems shown in Figure 7.1, the one made of PS/PMMA 85/15 by weight has been selected for the present, since its restrained excess elasticity makes it a good candidate to test the robustness of the two-phase model. To get a deeper insight into the viscoelasticity of the selected biphasic system, the experimental data can be interpreted in the light of the predictions of the Palierne model (Equations 7.1 and 7.2). For such a purpose, looking back to Equations 7.1-7.11 it emerges that some preliminary calculations are necessary:

- (i) to get an analytical expression for the elastic and viscous moduli of both the PS and PMMA phase, which have to be substituted into  $G'_c$ ,  $G''_c$  and  $G'_d$ ,  $G''_d$ , respectively;
- (ii) to estimate the number-average and volume-average radius of the PMMA drops;
- (iii) to evaluate the interfacial tension for the PS/PMMA system;
- (iv) to convert the weight composition of the blend in volume fraction.

The analytical expression of the viscoelastic moduli has been obtained by simply fitting the frequency-dependent experimental moduli of the neat polymeric phases to the well-known generalized Maxwell model. Specifically, such a model the data have to be fitted to the following forms of elastic and viscous moduli of the Maxwell model for a series of  $n$  terms:

$$G'_{\text{PS or PMMA}} = \sum_{i=1}^n J_i \frac{U_i^2 \omega^2}{1 + U_i^2 \omega^2} \quad (7.12)$$

$$G''_{\text{PS or PMMA}} = \sum_{i=1}^n L_i \frac{Y_i \omega}{1 + Y_i^2 \omega^2} \quad (7.13)$$

where  $J_i$  and  $L_i$  represent the elastic and viscous moduli of the  $i$ -th element of the Maxwell series, respectively, and  $U_i$  and  $Y_i$  are the corresponding relaxation times. The values of the parameters obtained using Equations 7.12 and 7.13 are reported for the neat PS and PMMA in the Appendices at the end of the dissertation.

Then, the size of the PMMA drops has been estimated by analyzing micrographs of the PS/PMMA blend obtained by scanning electron microscopy (SEM) analyses on the cryo-fractured surface of samples previously etched with formic acid to selectively remove the PMMA phase. The image analysis leads to a value of  $R_v = 0.895 \mu\text{m}$  and  $R_v/R_n = 1.94$  (see Chapter 3 for details). As a result, the volume-average radius can be used as representative size of the PMMA drops. In addition, from thermodynamic calculations based on theoretical models a value of  $1.48 \text{ mN/m}$  has been obtained for the interfacial tension between PS and PMMA (see Chapter 3 for details). Finally, according to the Palierne model the volume fraction of PMMA,  $\Phi_{\text{PMMA}}$ , have to be used in place of the weight fraction. A value of  $\Phi_{\text{PMMA}} = 0.132$  has been found for the PS/PMMA system 85/15 by weight (see Chapter 3 for details).

Once all the necessary values are available, the comparison between the predictions of Palierne model and the experimental moduli of the PS/PMMA system can be easily performed. The predicted and experimental viscoelastic moduli are shown in Figure 7.2 for the biphasic PS/PMMA system at a composition of 85/15 by weight.

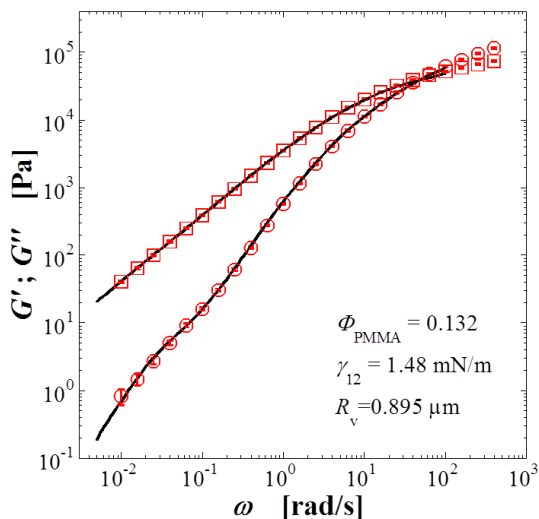


**Figure 7.2** Comparison of the viscoelastic moduli measured (symbols) and predicted by the Palierne model (solid lines) for the PS/PMMA blend (85/15 by weight): elastic (circles) and viscous (squares) moduli. The error bars represent the standard deviations over three independent measurements. The parameters of the Palierne model are reported in the plot.

A good agreement exists between predicted and measured moduli, which supports the reliability of the performed rheological measurements.

### 7.3 Linear viscoelasticity of the nanocomposites

The main goal of the present study is demonstrating that the two-phase model can satisfactorily describe the viscoelastic response of nanocomposites based on biphasic polymer matrix, in which an additional source of elasticity exists. For such a purpose, different amounts of an organo-modified montmorillonite, (O-Clay, Cloisite® 15A) have been added to the PS/PMMA (85/15 by weight) matrix previously introduced. As demonstrated in Chapter 3, in which the same nanocomposites based on a PS/PMMA matrix have been studied, the O-Clay preferentially locates at the polymer-polymer interface (see § 3.3). In addition, such a filler possesses a bending stiffness high enough to overcome the interfacial elasticity, making the particles clearly discernible via conventional rheological analysis.

The TEM micrographs of a representative diluted PS/PMMA/clay sample is shown in Figure 7.3.

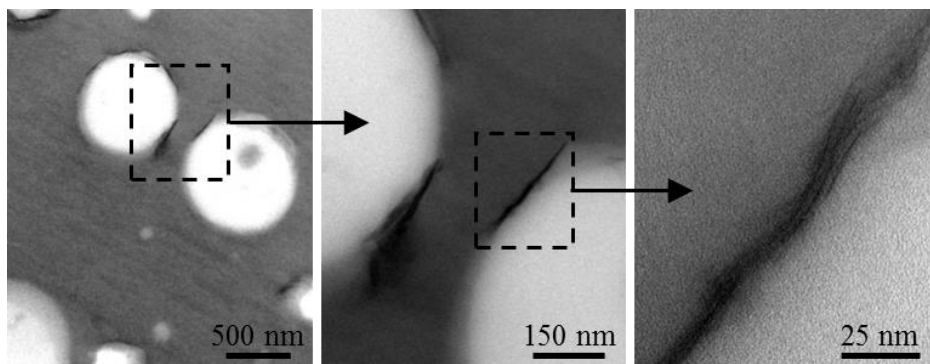


**Figure 7.3** TEM micrographs at different magnifications of the PS/PMMA/O-Clay sample at  $\Phi = 0.0032$ .

Micrometric PMMA drops are suspended in the PS matrix and the filler is mostly confined at the surface of irregularly-shaped droplets. This is consistent with the expectations of wettability calculations, which express the thermodynamic propensity of the O-Clay to gather at the polymer-polymer interface in the PS/PMMA matrix. It is worth noting that the high bending stiffness of the particles prevails over the interfacial tension of the drops, which adapt to the clay even in case of partial coating of the drop.

After the thermal annealing, the linear viscoelastic moduli are stable enough over time to perform reproducible frequency scan experiments. A reference system based on pure PS allows to highlight the role of the preferred polymer-polymer interface on the structuring of the filler in the melt. The elastic and viscous moduli are shown as a function of frequency in Figure 7.4 for the nanocomposites based on the monophasic matrix, PS/O-Clay samples, and those based on the biphasic one, PS/PMMA/O-Clay samples, at different  $\Phi$ .

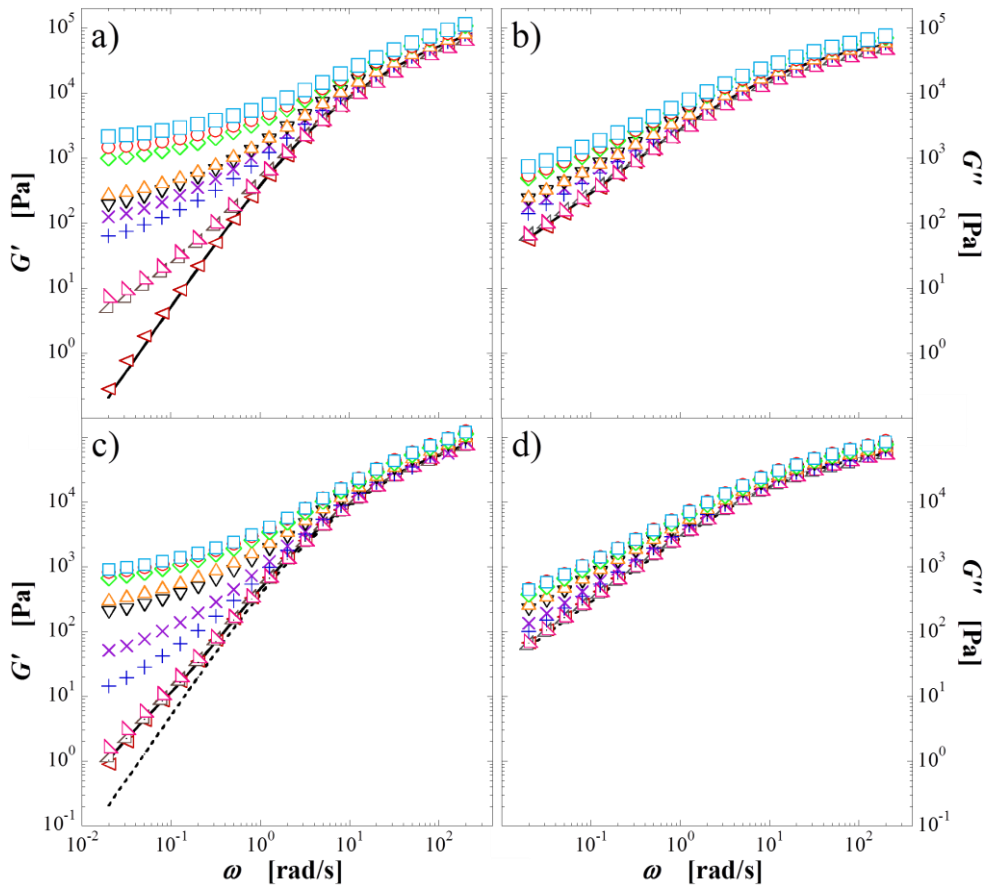


**Figure 7.4** Frequency-dependent (a, c) elastic and (b, d) viscous moduli of (a, b) PS/O-Clay and (c, d) PS/PMMA/O-Clay nanocomposites at different composition. From bottom to top: (a, b)  $\Phi = 0.0007, 0.0044, 0.0060, 0.0094, 0.0110, 0.0127, 0.0132, 0.0163, 0.0189, 0.0265$ ; (c, d)  $\Phi = 0.0018, 0.0032, 0.0061, 0.0075, 0.0093, 0.0132, 0.0166, 0.0205, 0.0212, 0.0224$ . In part (a, b), solid lines refer to the neat PS matrix. In part (c, d), solid lines refer to the neat PS/PMMA matrix and the dashed lines to the neat PS.

The neat PS is predominantly viscous throughout the investigated frequency range. The continuous PS phase governs the high-frequency behavior of the unfilled PS/PMMA blend, whereas the enhanced elasticity at low frequency reflects the shape relaxation of the PMMA droplets (see also Figure 7.3). Concerning the influence of the filler, the O-Clay radically affects the relaxation spectra. The effect is qualitatively the same for the two systems: a slight increase of the moduli occurs at high frequency, the overall shape of the curves remaining essentially unaltered; over longer timescales the filler gradually slows down the relaxation dynamics. The flattening of  $G'$  at low frequency reflects a gradual transition from liquid- ( $G'' \gg G'$ ) to solid-like behavior ( $G' > G''$ , weak  $\omega$ -dependence), which is commonly observed in polymer nanocomposites and generally ascribed to the formation of meso-structure of nanoparticles within the host medium.

Intriguingly, the filler has negligible effect in the PS/PMMA/O-Clay nanocomposites at  $\Phi < 0.0075$ . Such a composition is close to the threshold above which the elasticity starts to increase over time during the thermal annealing process due to filler flocculation phenomena (see Chapter 3 for details). At higher filler content, instead,  $G'$  begins to flatten out reaching a low-frequency plateau, in analogy to the nanocomposites based on the homogeneous PS matrix. In Chapter 3, the value of  $\Phi \sim 0.0075$  has been found to roughly correspond to the composition at which the available PS/PMMA interface is almost saturated by the O-Clay nanoparticles. In other words, the filler anchored to the PMMA drops, that is devoid of sufficient mobility in the melt, does not appreciably affect the overall viscoelasticity imparting solid-like features to the matrix. On the other hand, once exceeded such a filler content, the particles are not anymore constrained at the polymer-polymer interface and they start to randomly enrich the continuous PS phase. In this scenario, the O-Clay particles affect the relaxation spectra of the biphasic host matrix in a manner somehow analogous to the system based on the monophasic matrix. The study of the superstructures into which the particles can assemble, after the constraint represented by the interface has been saturated, is addressed in the next paragraph.

## 7.4 Filler network in the mono- and biphasic matrices

Above a certain filler content necessary for the saturation of the polymer-polymer interface, the relaxation dynamics of the PS/PMMA/O-Clay samples are reminiscent of those observed in the nanocomposites based on the homogeneous PS matrix. Morphological analyses have been performed to visualize the structures formed by the filler at relatively high loadings. The TEM micrographs of two samples exhibiting a comparable low-frequency plateau of the elastic modulus are compared in Figure 7.5.

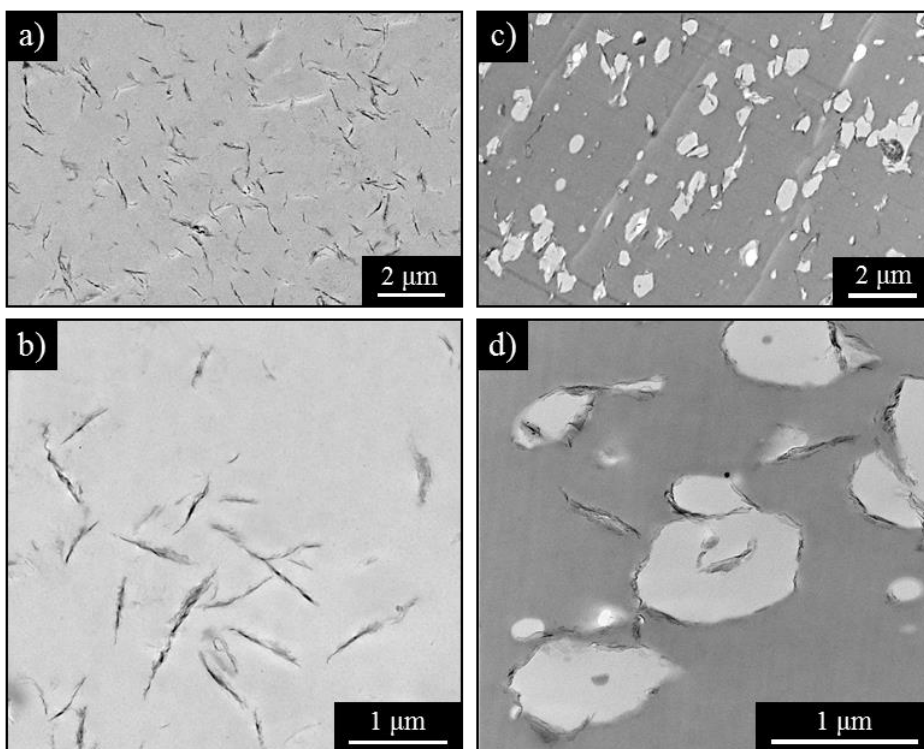


**Figure 7.5** TEM micrographs of the samples at  $\Phi = 0.0132$ : (a, b) PS/O-Clay and (c, d) PS/PMMA/O-Clay.

The clay tactoids are randomly suspended in the host matrix in the PS/O-Clay sample. The considerable lateral dimension of such structures are due to hydroxylated edge-edge interactions between silicate layers [Sinha Ray et al. (2003)]. The random assembly of the O-Clay results in micron-sized flocs, which in turn assemble into a three-dimensional network that spans large section of the sample. Larger portions of matrix are devoid of clay in the PS/PMMA/O-Clay sample: most of the particles either adhere at the surface of the drops or are trapped within drop clusters. Nonetheless, long-range connectivity of the particles can be identified also in the nanocomposite based on the biphasic matrix (Figure 7.5d). The main difference with the PS/O-Clay system is that here the particle flocs embed the PMMA domains.

After the constraint represented by the polymer-polymer interface has been saturated, the similarities in the rheological responses suggest that the viscoelasticity of the PS/PMMA/O-Clay system can be interpreted by referring to the simple two-phase model, which has proved to satisfactorily describe the linear viscoelasticity of homopolymer-based nanocomposites above the percolation

threshold (see Chapter 6). Briefly, for nanocomposites based on a single polymer phase, the coexistence of two independent populations of dynamical species is assumed: a fraction of free polymer, whose dynamics are not affected by the filler, and a three-dimensional network based on flocs of nanoparticles. The polymer-phase accounts for the viscous feature of the nanocomposite, whereas the network-phase is the only responsible for the marked elasticity which emerges at low frequency. However, when the suspending medium is a biphasic fluid, such as an immiscible blend, an additional contribution arises at low frequency because of the interfacial elasticity. Nonetheless, it can be argued that the latter is not so important to invalidate the assumption that the network-phase encompasses the entire elasticity of the nanocomposite. The physical picture of the “revised” two-phase model in the case of biphasic polymer matrix is sketched in Figure 7.6.

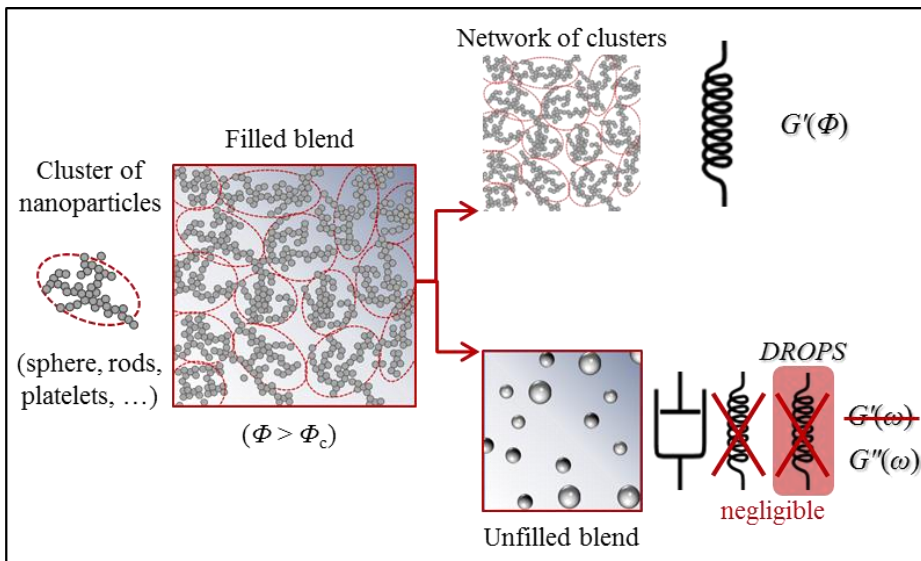


**Figure 7.6** Representation of the interpretation of the viscoelasticity according to the two-phase model for samples based on a biphasic matrix above the percolation threshold.

If the assumptions in Figure 7.6 are consistent, the two-phase model holds also for the nanocomposite samples based on the PS/PMMA matrix. The  $G'$  curves of the filled blends at different  $\Phi$  can be thus scaled on a single master curve, and the elasticity of the filler networks which set up in the system based on the biphasic matrix can be precisely estimated and studied apart. The key steps for identifying the horizontal,  $a_\Phi$ , and vertical,  $b_\Phi$ , shift factors to build the master curve of  $G'$  in the case of the PS/PMMA/O-Clay system are summarized in the following:

(i) accounting for hydrodynamic effects related to the presence of the filler by introducing an amplification factor,  $B(\Phi)$ : it represents the ratio between the complex modulus  $G^*(\Phi)$  of the filled sample and that of the neat matrix (neat PS for the PS/O-Clay nanocomposite systems, unfilled PS/PMMA blend for the PS/PMMA/O-Clay ones) in the high-frequency range;

(ii) amplifying the viscous modulus of the pure matrix (again, neat PS for the PS/O-Clay nanocomposite systems, unfilled PS/PMMA blend for the PS/PMMA/O-Clay ones) by the factors  $B(\Phi)$ ;

(iii) identifying  $a_\Phi$  and  $b_\Phi$  as the coordinates of the point at which the network elasticity,  $G'_0(\Phi)$ , identified as the low-frequency plateau of the elastic modulus, equals the amplified viscous modulus of the pure matrix,  $B(\Phi) \cdot G''(\omega)$ .

The master curves of the PS/O-Clay and PS/PMMA/O-Clay systems are shown in Figure 7.7. For completeness, the amplifying factors,  $B(\Phi)$ , and the  $G''(\omega)$  curves of the pure matrices on which the shift factors ( $a_\Phi$ ;  $b_\Phi$ ) used to build the master curves lie are reported in the Appendices at the end of the dissertation, together with the corresponding numerical values.

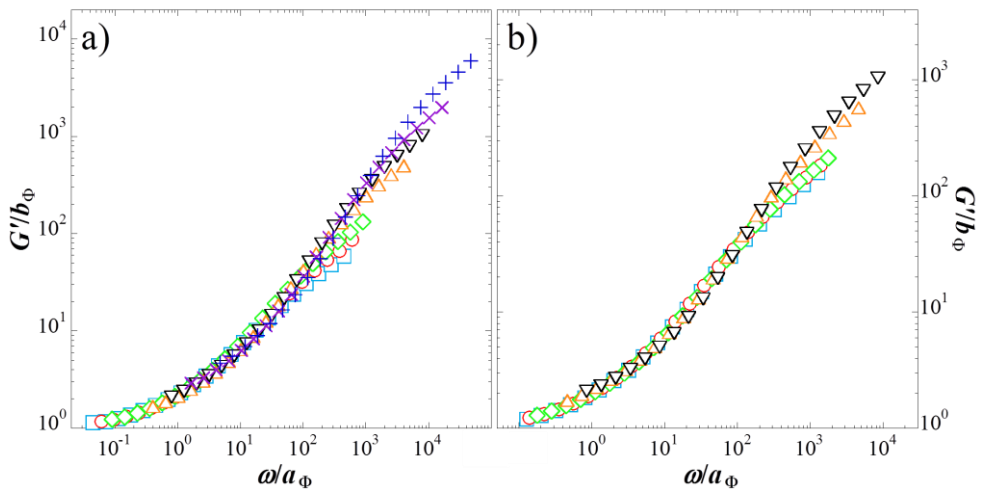


**Figure 7.7** Master curves of  $G'$  for (a) the PS/O-Clay samples at  $\Phi \geq 0.0094$  and (b) the PS/PMMA/O-Clay samples at  $\Phi \geq 0.0132$ .

In both the systems the collapse of the moduli is excellent over about three decades of low scaled frequencies,  $\omega/a_\Phi$ , which demonstrates the effectiveness of the two-phase model even in case of biphasic polymer matrices. The non-superposing tails at high  $\omega/a_\Phi$  reflect the dynamics of the unfilled matrices, so their presence does not compromise the overall quality of the scaling. The ability of the two-phase model in capturing even the viscoelasticity of the nanocomposite

samples based on the biphasic PS/PMMA matrix can be understood thinking about the different sources of elasticity in such materials. Actually, there are three contributions to the elastic response in the PS/PMMA/O-Clay samples above the filler percolation threshold: (i) the intrinsic elasticity of the neat continuous PS phase,  $G'_{\text{PS}} = G'_c$ ; (ii) the elasticity ascribable to the filler network,  $G'_0(\Phi)$ ; (iii) the excess elasticity due to the shape relaxation processes of the PMMA drops,  $G'_{\text{interface}}$ . It is worth noting that the contribution of the elasticity of the dispersed PMMA phase,  $G'_{\text{PMMA}} = G'_d$ , to the overall elasticity of the biphasic system is essentially negligible, being responsible for only a slight vertical shift of the whole  $G'_b$  curve. This is evidenced in Figure 7.8, in which the frequency-dependent  $G'_b$  has been calculated in the case of three different curves of  $G'_d$ , according to the Palierne model. Note that for the sake of comparison, the elastic moduli of the blends have been estimated keeping constant the other viscoelastic moduli of the neat constituents, that is  $G''_d$ ,  $G'_c$  and  $G''_c$ .

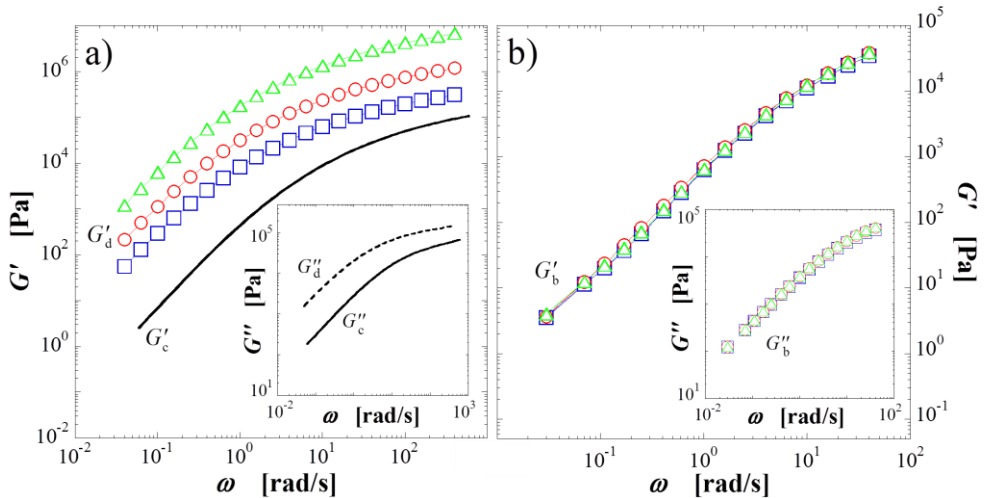


**Figure 7.8** (a) Three curves for the elastic modulus of the dispersed phase and (b) corresponding predictions for the elastic modulus of a blend according to the Palierne model (the material-related parameters are those of the investigated PS/PMMA blend). Symbols are the same as in part (a). The solid line in part (a) is the elastic modulus of the continuous phase used in the Palierne model. The viscous moduli are reported in the insets.

It clearly emerges that variations in  $G'_d$  over about one order of magnitude (Figure 7.8a) do not imply appreciable changes in the elastic modulus of the blend (85/15 by weight), the three  $G'_b$  curves of Figure 7.8b being practically indistinguishable. Note also that the viscous modulus of the blend is even less affected (inset of Figure 7.8b). Consequently, the frequency-dependent elastic

response of the PS/PMMA/O-Clay samples can be correctly considered as resulting from the interplay among only the three previously identified elastic contributions:  $G'_{\text{PS}}$ ,  $G'_0(\Phi)$  and  $G'_{\text{interface}}$ . The comparison of the relative participation of such contributions to the elastic modulus of the nanocomposites based on the biphasic matrix in the investigated frequency range is useful to shed light on the reason why the two-phase model works in the case of the PS/PMMA/O-Clay system.

The first contribution ( $G'_{\text{PS}}$ ) is easy to obtain since it merely represents the frequency-dependent elastic modulus of the PS matrix. The second one, instead, corresponds to the value of the vertical shift factor used to build the master curve of the PS/PMMA/O-Clay system, that is  $G'_0(\Phi) = b_\Phi$ . It scales with the filler volume fraction and it is frequency-independent. Finally, the third contribution ( $G'_{\text{interface}}$ ) can be evaluated as:

$$G'_{\text{interface}} = G'_{\text{PS/PMMA}} - G'_{\text{components}} \quad (7.14)$$

where  $G'_{\text{components}}$  represents the elasticity of the components of the biphasic system without any interfacial effects and  $G'_{\text{PS/PMMA}}$  is the elastic modulus of the PS/PMMA blend ( $G'_{\text{PS/PMMA}} = G'_b$ ) [Vermant et al. (2004)]. According to Yu et al. (2010), in the linear viscoelastic regime the relative contribution of the two polymers can be extrapolated from the Palierne model in the limit of zero interfacial tension as:

$$G'_{\text{components}} = G'_c \frac{1 + 3\Phi_D H}{1 - 2\Phi_D H} \quad (7.15)$$

where the parameter  $H$  is equal to:

$$H = \frac{G'_d - G'_c}{2G'_d - 3G'_c} \quad (7.16)$$

The evaluation of the interface elasticity of the PS/PMMA/O-Clay system presumes the knowledge of the rheological response of the bulk polymer phases with the actual filler content deriving from the particle distribution. However, the preferential localization of the filler at the polymer-polymer interface, at least for  $\Phi < \Phi_c$ , makes the amount of filler contained in the bulk phases of these samples low enough to reasonably assume that their bulk rheology is not significantly affected by the particles. Hence, the interface elasticity of the filled blends can be estimated by simply using the elastic moduli of the neat PS and PMMA as  $G'_c$  and  $G'_d$ , respectively, in Equation 7.16. The measured/estimated elastic moduli which participate to the overall elasticity of the PS/PMMA/O-Clay system are shown in Figure 7.9 as a function of frequency. Note that, for the network elasticity, the

lowest available value has been chosen, that is the one which refers to the lowest  $\Phi$  of the scalable  $G'$  curves of the PS/PMMA/O-Clay samples (see Figure 7.7).

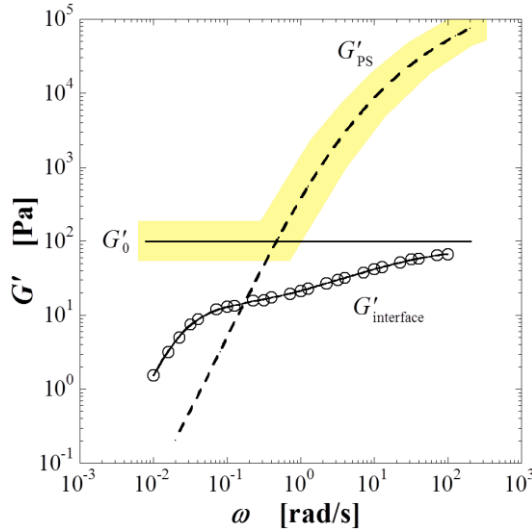


**Figure 7.9** Elastic modulus of continuous PS phase (dashed line), filler network elasticity for the sample at  $\Phi = 0.0132$  (solid line) and elasticity of the PS/PMMA interface (symbols) as a function of frequency.

Although the value of  $G'_0$  in Figure 7.9 corresponds to the lowest available one, it clearly emerges that the network elasticity prevails in the low frequency region, whereas the elasticity of the neat PS phase dominates the high frequency range (highlighted area in Figure 7.9). Consequently, the elastic contribution ascribable to the PMMA drops (interfacial effects) is hindered throughout the investigated frequency window. Such a result perfectly fits the underlying idea of the two-phase model, which indeed succeeds in capturing the viscoelastic response of the studied polymer nanocomposites even in the presence of an extra elastic contribution, such as those based on a biphasic polymer matrix.

Another interesting evidence emerges if the master curves of the two systems in Figure 7.7 are plotted together, as shown in Figure 7.10. Surprisingly, both systems approach the plateau at low  $\omega/a_\Phi$  following the same trend. The polymer-phase governs the behavior at  $\omega/a_\Phi \gg 1$ . Since the fastest relaxation modes of the blend are essentially those of the PS, the overlay at high  $\omega/a_\Phi$  is not unexpected. Instead, the superposition at  $\omega/a_\Phi \sim 1$  is more surprising. In such an intermediate frequency range the network- and polymer-phase equally contribute to the system elasticity. Actually, the nanoparticles slow down the polymer dynamics even in case of weak

polymer-particle interactions, so the contributions of the two phases are not merely additional. Moreover, in this regime the polymer-phase of the PS/PMMA/O-Clay system exhibits an extra elastic contribution due to the polymer-polymer interface. The complex interplay among the various sources of elasticity makes it difficult to discern the various contributions. Nonetheless, the main elastic features of the filler network prescind from the presence of drops of a dispersed phase embedded in it.

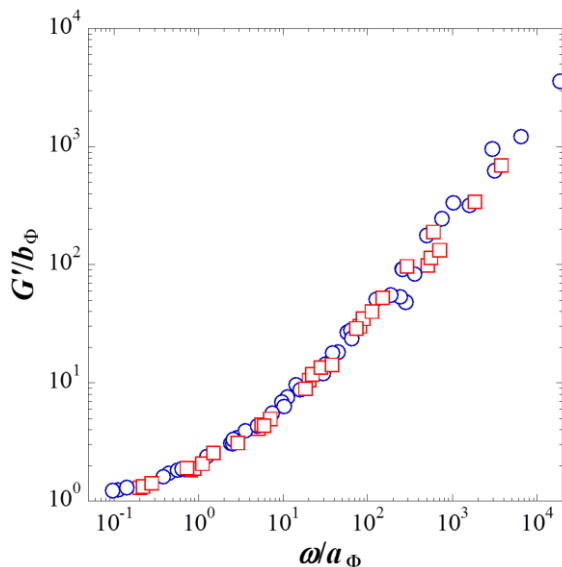


**Figure 7.10** Overlay of the two master curves reported in Figure 7.7: PS/O-Clay (circles) and PS/PMMA/O-Clay (squares) samples. Only one out of three points is reported.

## 7.5 Elasticity and structure of the filler networks

Despite the presence of a second polymer phase in the form of drops, which bring about an additional elastic contribution, the relaxation spectrum of the PS/PMMA/O-Clay samples has been satisfactorily described in terms of only two dynamical species, exactly as in the case of nanocomposites based on a single phase polymer matrix. The building up of a three-dimensional filler network above  $\Phi_c$  has been found to influence the relaxation dynamics of the polymeric matrix irrespective of the presence of dispersed drops of PMMA embedded in it. The evidenced similarities suggest that the structure of the network in the biphasic matrix can be studied using the same approaches often employed for particulate gels in homogeneous fluids. As a result, a quantitative comparison between the structures of the networks which form in the mono- and biphasic matrices can be

performed by referring to the percolation theory. The latter predicts the network elasticity to grow with  $\Phi$  as:

$$G'_0 = k(\Phi - \Phi_c)^\nu \quad (7.17)$$

where  $k$  and  $\nu$  are two constants, the latter being related to the stress-bearing mechanism [Stauffer and Aharony (1992)]. To precisely identify the percolation threshold, Equation 7.17 has been fitted to the experimental data of  $G'_0(\Phi)$  for different possible values of  $\Phi_c$ . The percolation threshold is thus taken as the one that returns the highest coefficient of determination,  $R^2$ . The advantage of using the two-phase model is double: first, the  $\Phi_c$  can be sought in a restricted composition range, whose inferior limit is the highest  $\Phi$  of the non-scalable  $G'$  curves; second, the values of  $G'_0(\Phi)$  can be accurately estimated even for samples whose network is too weak to cause the arrest of the relaxation dynamics in the investigated frequency range (see Chapter 5 for details). In such cases, the elasticity is usually conjectured presuming a plateau of  $G'$  at not accessible very low frequencies. This procedure may thus result in non-trivial errors when referring to theoretical models. Differently, any presumption is avoided referring to the master curve, whose vertical shift factors  $b_\phi$  exactly correspond to the  $G'_0$  values. The power-law dependences of the network elasticity obtained through the best fitting procedure is shown in Figure 7.11 for the two systems and the corresponding parameters are summarized in Table 7.1

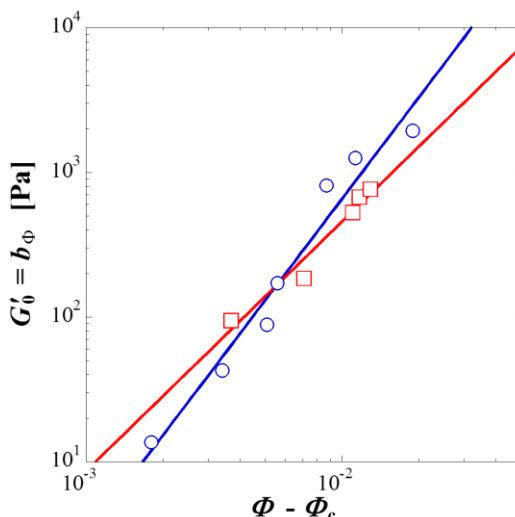


**Figure 7.11** Power law dependence of the network elasticity on the reduced filler content,  $\Phi - \Phi_c$ , setting  $\Phi_c = 0.0076$  for the PS/O-Clay system (circles) and  $\Phi_c = 0.0095$  for the PS/PMMA/O-Clay one (squares). Solid lines are the fittings to Equation 7.17.

**Table 7.1** Best fitting parameters ( $k, \nu$ ) of Equation 7.17 and corresponding values of percolation threshold for the PS/O-Clay and PS/PMMA/O-Clay systems.

System	$\Phi_c$	$k$ [Pa]	$\nu$	$R^2$
PS/O-Clay	0.0076	$3.1 \times 10^7$	2.34	0.9599
PS/PMMA/O-Clay	0.0095	$1.3 \times 10^6$	1.73	0.9582

The higher value of  $\Phi_c$  found for the PS/PMMA/O-Clay system is ascribed to the presence of PMMA drops, which gather the clay tactoids and restrict their allowed space configurations. Once the polymer-polymer interface has been saturated, the added particles are able to rearrange in the reduced volume outside the coated drops, easily connecting them to form a space-spanning filler network, which also embeds the PMMA phase. Concerning the critical exponents, the elasticity of the network in the biphasic matrix results less dependent on the reduced filler content,  $\Phi - \Phi_c$ , reflecting a different structure of the network made of nanoparticle clusters.

Further insight about this matter can be gathered by considering that the stress transfer takes place across an elastic backbone of particle aggregates. Modelling a gel of colloidal particles as a collection of fractal flocs, or equivalently fractal clusters of nanoparticles, Shih et al. (1990) developed a scaling theory which relates the elastic constant and the limit of linearity,  $\gamma_{cr}$ , of the network to the fractal dimension of the flocs. Such properties are predicted to scale with the filler content as  $G'_0 \sim \Phi^A$  and  $\gamma_{cr} \sim \Phi^B$ . The exponents  $A$  and  $B$ , which are functions of the fractal dimensions of the cluster of particles,  $d_f$ , and floc backbone,  $x$ , depend on the stress bearing mechanism. Specifically, two limit situations are considered: in the so-called “strong-link regime” the network elasticity is dominated by the inter-floc links, whereas in the “weak-link regime” the intra-floc elasticity governs the mechanical response.

In the scientific literature, attempts to apply the Shih’s model to homopolymer/clay nanocomposites led to reasonable values of  $d_f$ , but physically unacceptable values of  $x$  [Durmus et al. (2007), Vermant et al. (2007)], which should be higher than unity to ensure the connectivity of the network. Taking for granted the latter requisite, Wu and Morbidelli (2001) admitted the existence of intermediate situations by introducing a third parameter  $\alpha$  ranging between 0 (strong-link) and 1 (weak-link). For three-dimensional systems the expressions of the exponents  $A$  and  $B$  thus become:

$$A = \frac{\beta}{3 - d_f} \quad (7.18)$$

$$B = \frac{3 - \beta - 1}{3 - d_f} \quad (7.19)$$

where the parameter  $\beta$  is given by:

$$\beta = 1 + (2 + x)(1 - \alpha) \quad (7.20)$$

where  $\alpha$  varies between 0 and 1, representing the variable introduced by Wu and Morbidelli (2001) to distinguish intermediate configuration in between the two extremes of strong-link ( $\alpha = 0$ ) and weak-link ( $\alpha = 1$ ) regimes.

The model by Wu and Morbidelli (2001) is here exploited to go deeper into the analysis of the two kinds of networks which form in the PS/O-Clay and PS/PMMA/O-Clay systems. Note that for such an analysis samples at  $\Phi \geq 0.0110$  for the PS/O-Clay system and at  $\Phi \geq 0.0132$  for the PS/PMMA/O-Clay one are considered, that is well above the corresponding percolation thresholds as established by the model.

The values of the limit of linearity have been estimated by performing strain sweep experiments at low frequency ( $\omega = 0.1$  rad/s). The elastic modulus as a function of the percentage of imposed strain,  $\gamma$ , is shown in Figure 7.12 for the PS/O-Clay and PS/PMMA/O-Clay samples. The values of  $\gamma_{cr}$  have been conventionally set as the strain at which  $G'$  decreases by about 5% with respect to its low-strain plateau value. The as-estimated  $\gamma_{cr}$  values are reported in Table 7.2.

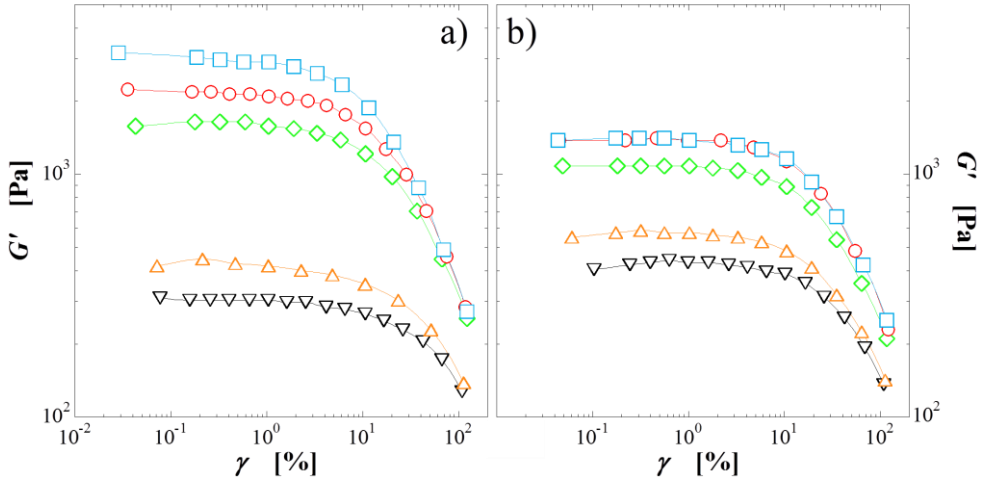


**Figure 7.12** Strain-dependent  $G'$  for (a) the PS/O-Clay and (b) the PS/PMMA/clay samples considered according to the Wu and Morbidelli model. From bottom to top:  $\Phi =$  (a) 0.0110, 0.0127, 0.0163, 0.0189, 0.0265; (b) 0.0132, 0.0166, 0.0205, 0.0212, 0.0224.

**Table 7.2** Estimated values of the limit of linearity for the PS/O-Clay and PS/PMMA/clay samples at different filler volume fraction.

PS/O-clay		PS/PMMA/O-clay	
$\Phi$	$\gamma_{cr}$ [%]	$\Phi$	$\gamma_{cr}$ [%]
0.0265	4.7	0.0224	7.2
0.0189	7.4	0.0212	8.1
0.0163	9.1	0.0205	9.5
0.0127	20.2	0.0166	12.3
0.0110	31.3	0.0132	18.2

By fitting the experimental data to the scaling laws  $G'_0 \sim \Phi^A$  and  $\gamma_{cr} \sim \Phi^B$ , the exponents  $A$  and  $B$  are obtained, as shown in Figure 7.13.

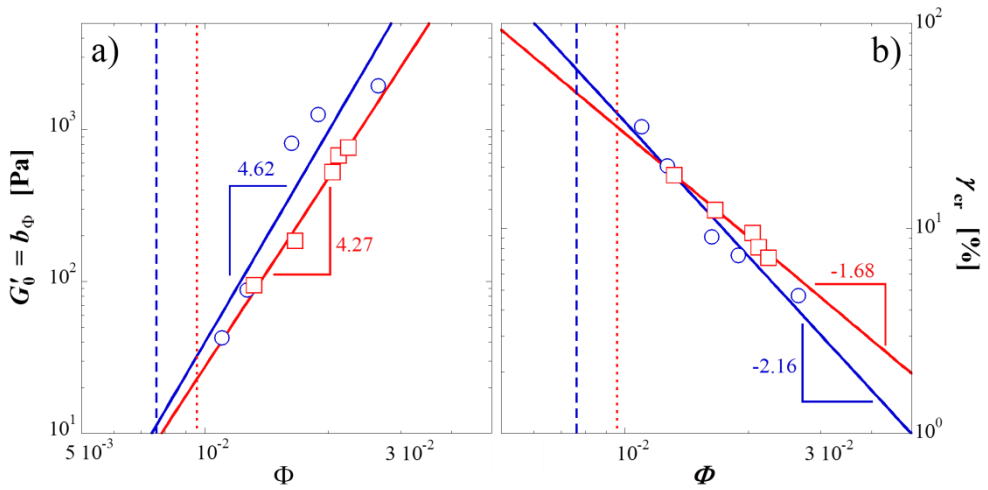


**Figure 7.13** (a) Elasticity of the filler network and (b) limit of linearity as a function of filler volume fraction for the PS/O-Clay (circles) and PS/PMMA/ O-Clay (squares) systems. Solid lines are the power law fitting curves. Dashed and dotted lines indicate the percolation thresholds of the PS/O-Clay and PS/PMMA/ O-Clay systems, respectively.

By substituting in Equations 7.18 and 7.19 the values of  $A$  and  $B$  corresponding to the best fittings of the experimental data, the fractal dimension of the clusters of nanoparticles and the parameter  $\alpha$  for the PS/O-Clay and PS/PMMA/O-Clay systems are finally calculated (Table 7.3). Note that a reasonable value of the

tortuosity of the network,  $x = 1.3$ , has been presumed, as the results are essentially the same by assuming values of  $x$  other than 1.3, and yet higher than 1.

**Table 7.3** Values of the fractal dimension of the nanoparticle clusters and of the parameter  $\alpha$  for the PS/O-Clay and PS/PMMA/O-Clay systems.

System	$d_f$	$\alpha$
PS/O-Clay	$2.19 \pm 0.01$	$0.16 \pm 0.01$
PS/PMMA/O-Clay	$2.17 \pm 0.08$	$0.28 \pm 0.01$

The fractal dimensions of the two kinds of flocs are predicted to be almost the same, being comparable or a bit lower than those reported in the literature for O-Clay based networks [Durmus et al. (2007), Vermant et al. (2007)]. To substantiate such a result, image analysis has been carried out on sections of flocs identified in several TEM micrographs. The main steps of the procedure are summarized in the Appendices at the end of the dissertation. Briefly, the two-dimensional box counting fractal dimension,  $D_f$ , has been obtained from the plot reporting the total number of square boxes containing more than a certain fraction of black pixels in the binarized image,  $N_{\text{box}}$ , as a function of the box size,  $L_{\text{box}}$ . The opposite of the slope represents  $D_f$ . An example of the outcome is given in Figure 7.14.

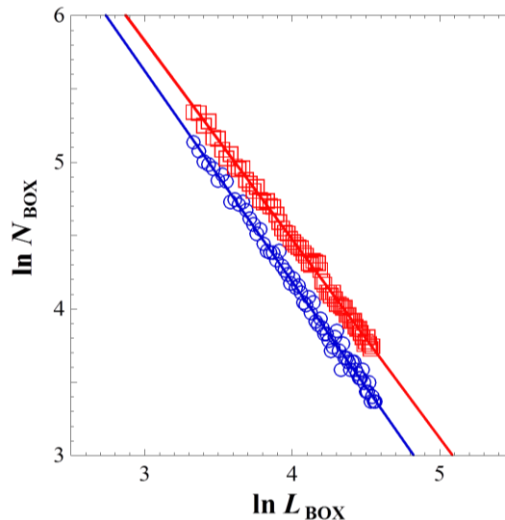


**Figure 7.14** Number of boxes as a function of box size for the PS/O-Clay (circles) and PS/PMMA/O-Clay (squares) systems. Solid lines are linear fittings.

Repeating the image analysis over about fifteen flocs taken from several TEM micrographs and averaging returns the data summarized in Table 7.4. Note that the fractal dimensions obtained exploiting the Wu and Morbidelli model are reported as well for the sake of comparison.

**Table 7.4** Two-dimensional fractal dimensions for the PS/O-Clay and PS/PMMA/O-Clay systems compared to the fractal dimensions by Wu and Morbidelli model..

<b>System</b>	<b><math>D_f</math> Image analysis</b>	<b><math>d_f</math> Wu&amp;Morbidelli model</b>
PS/O-Clay	$1.36 \pm 0.06$	$2.19 \pm 0.01$
PS/PMMA/O-Clay	$1.28 \pm 0.08$	$2.17 \pm 0.08$

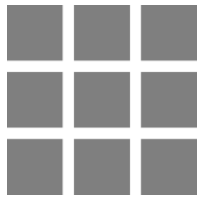
The values of  $D_f$  of the two systems are comparable, corroborating the predictions of the Wu and Morbidelli model. The image analysis confirms a slightly lower fractal dimension of the flocs in the biphasic matrix, but the computed values of  $D_f$  are too close to be interpreted as a clear sign of a more opened structure.

On the other hand, a subtle and yet statistically significant difference instead emerges when comparing the values of the parameter  $\alpha$  obtained exploiting the Wu and Morbidelli model (see Table 7.3). Actually, such a parameter quantifies the relative importance of inter- and intra-floc links. Both systems exhibit values of  $\alpha$  close to the extreme of the strong-link regime ( $\alpha \rightarrow 0$ ), meaning that the flocs are soft and behave as weak springs. However, the comparison indicates that the clusters in the PS/PMMA/O-Clay system are a bit stronger, or alternatively the inter-floc links are a bit weaker. The first possibility reflect some extra elasticity of the drops and drop clusters in which the flocs are embedded; this contribution, which has revealed to be negligible when modelling the viscoelasticity of the nanocomposite, stiffen the flocs as little as needed to slightly unbalance the system towards the weak-link regime. On the other hand, the organo-clay stacks lying on the surface of the PMMA drops form curvy flocs. The latter could interact among them more weakly than in the PS/O-Clay systems, in which hydroxylated edge-edge interactions are more likely to occur.

In any case, it is interesting to remark the agreement with the picture given by Shih et al (1990). In the strong-link the individual flocs are allowed to grow starting from low particle concentration, which is congruent with what happens in a system without the constraint of the polymer-polymer interface such as our PS/O-Clay. On the opposite, in the weak-link regime smaller and stronger flocs assemble to form the network at higher particle concentration. It is reasonable to expect

similar features in the PS/PMMA/O-Clay system, where the drops anchor the particles and provide additional elasticity to the clusters of particles.





**PART**  
**III**

**Structure-property  
relationships in polymer  
nanocomposites through  
rheological analyses**



# 8

## Current issues in the research on polymer nanocomposites

*In this chapter the state of the art regarding the understanding and prediction of the macro-scale properties of polymers reinforced with nanometer-sized inclusions is briefly surveyed. Illustrative examples of commercial polymer nanocomposites already available in the market are reported. And, in parallel, the growing interest in improved materials with “dialed-in” properties is discussed (§ 8.1). Then, the challenges in preparing spatially optimized dispersions of nanoparticles in polymer matrices are presented (§ 8.2). Finally, the focus moves on some relevant studies dealing with the use of rheological measurements for the analysis of the structure-property relationships in polymer nanocomposites (§ 8.3).*

### 8.1 Applications and future perspectives for polymer nanocomposites

The mixing of nanoparticles with polymers to form composite materials has been practiced for decades. From an historical perspective, the first example dates back to beginning of the XX Century when the clay-reinforced resin, known as Bakelite, was introduced [Baekeland (1909)]. Nonetheless, the broad scientific community was not galvanized by nanocomposites until the early 1990s, when reports by Toyota researchers revealed that adding mica to nylon produces a five-fold increase in the yield and tensile strength of the material [Usuki et al. (1993), Kojima et al. (1993)]. Subsequent developments have further contributed to the surging interest in polymer-nanoparticle composites. Since then, indeed, numerous polymer-nanoparticles formulations have been developed targeting a multitude of applications. In the electronics industry, researchers have exploited the electrical conductivity of carbon nanotubes or fullerene to design low-cost solar cells or anti-static composite materials, whereas titanium oxide nanoparticles have been used in photovoltaics and sensing devices [Ramasubramaniam et al. (2003), Thompson and Fréchet (2008)]. In the food industry, the addition of nanoclays along with antimicrobial additives to a polymer matrix improves the oxygen barrier properties of the final material, leading to applications in packaging films, bags and bottles [Lange and Wyser (2003), Duncan (2011)]. The biomedical field also explored the potential that polymer nanocomposites offer in tissue engineering, implants or

medical devices [Hule and Pochan (2007)]. Other relevant industrial applications include cosmetics, aircraft structures, military equipment and sporting and leisure goods. Although the reported examples of polymer nanocomposites and corresponding possible fields of applications are far from being exhaustive, it turns out that there is a lot that is still poorly understood about the underlying phenomena taking place during the production processes. Often, manufacturers are in the dark about the basic physics and principles to which the obtained performances have to be ascribed. As a result, beyond maximizing nanoparticle dispersion, the morphology of these materials is many times uncontrolled because of the huge number of involved parameters. No matter how, it is exciting to consider the extent to which nanoparticle-filled polymer materials can be directed to assemble into hierarchically ordered nanocomposites. In the last decade, the research of both academia and industry is truly moving in this direction. Indeed, unanticipated improvements of transverse and axial strength were reported in the presence of lamellar nanoparticles aligned along the carbon-fiber surface [Rice et al. (2001)]. Comparable shear moduli were obtained at only half of the volume fraction of particles if a web-like morphology is generated rather than random or hexagonal arrangement [Gusev and Rozman (1999)]. Other works on barrier properties [Gusev and Lusti (2001)] and mechanical reinforcement [Sheng et al. (2004)] also pointed to the importance of filler arrangement in achieving the maximum effect at the minimum loading. More recently, the possibility of controlling the spanning dimension of the percolating clusters using a combination of volume fraction and shear rate has been demonstrated [Zheng et al. (2007)]. In line with these results, huge dividends are expected in the structural and functional properties if processing ensures a prescribes nanoparticle spatial arrangement.

Although the design and production of targeted structures is still in its early stages, it will certainly lead to materials with new and/or optimized functionalities. Essential to meet this challenge is establishing guidelines for process optimization, discovering assembly methods that yield a desired structure, and understanding the structure-property relationships in order to predict the performance of a given architecture. With these in hand, nanoparticle/polymer mixtures hold promise for the fabrication of hierarchically ordered materials that have tailored structures and functionalities that span multiple length scales and dimensions. In this sense, opportunities to exploit the knowledge gained from fundamental research studies are among the future challenges in the polymer nanocomposites field.

## **8.2 Main challenges in the preparation of polymer nanocomposites**

The state of dispersion of the nanoparticles in the polymer matrix has a profound impact on the properties of the ultimate nanocomposite material.

Consequently, one of the scientific and technical challenges to overcome in order to achieve the desired properties is the control of the filler structure, intended as the spatial distribution of relative position and orientation of the nanoparticles. However, it has been often proved that imparting a prescribed space arrangement to the nanoparticles is not a straightforward process. Thermodynamics play an important role, but the flow during processing has also to be considered. Actually, the perceived difficulties can be mainly ascribed to the nanometric size of the filler itself. Although desirable to open a door for promising functional properties which cannot be realized by micrometer sized traditional fillers [Althues et al. (2007)], the nanoscale size of the additives brings about the occurrence of a series of phenomena which have to be taken into account during processing. Specifically, nanoparticles are subjected to relevant Brownian motion even in highly viscous mediums such as polymer melts. The self-diffusion time of a single particle,  $\tau_{SD}$ , that is the time required for the particle to move of a length equal to its radius, gives an idea about the relevance of such a phenomenon:

$$\tau_{SD} = \frac{6\pi\eta_m r^3}{k_B T} \quad (8.1)$$

where  $\eta_m$  is the viscosity of the suspending medium,  $r$  is the radius of the particle,  $k_B$  is the Boltzmann's constant and  $T$  is the temperature [Russel et al. (1989)].

Setting  $T = 400$  K and  $\eta_m \sim 10^3$  Pa s, as typical values for melted polymers, Equation 8.1 gives the noteworthy result that particles of few tens of nanometers experience appreciable Brownian motions on timescales of order of a  $10^1 \div 10^2$  seconds. Such durations are typically accessed in many transforming processes of the polymer industry. In addition, the difference in the surface energies between the polymer and filler phases leads to segregation of the particles, that is to the formation of agglomerates which are usually extremely difficult to break up into individual species. Wetting of the individual particles by the polymer segments is in fact unfavorable against particle-particle interaction for enthalpic reasons even if individual particles were present [Demir and Wegner (2012)]. Under the coupled effect of Brownian motion and particle-particle interactions, the nanoparticles are free to move and rearrange in the melt towards more favorable thermodynamic states. It emerges that the internal morphology of the polymer nanocomposites arise from the complex interplay of such phenomena which lead to local rearrangements of the filler in the melt during flow and even at rest. Whatever the ultimate filler structure is, it irretrievably affects the behavior of the host polymer matrix, dictating the macroscopic response of the nanocomposite.

As a matter of fact, the incorporation in polymer matrices of nanoparticles in a fully dispersed and stable state has been often proved to be rather difficult. Indeed, large variations in the properties have been found for systems of the same composition but prepared using different techniques. The irreproducibility of the

results, indeed, is in actuality one of the major drawback when dealing with polymer nanocomposites. Besides, it is well-established that, depending on the adopted compounding procedure, one may run into a different combination of technical advantages and disadvantages. Evidently, both the state in which nanoparticles are assembled into cluster and their shape affect material properties which are important for applications and processing [Starr et al. (2002), Starr et al. (2003)]. At the same time, there has been considerable interest in utilizing particle self-assembly as a “bottom-up” route to new material assembly [Glotzer and Solomon (2007), Lee et al. (2004), Tang et al. (2006)]. As a consequence, the possible underlying mechanisms for nanoparticle clustering have been investigated, considering the roles played by phase separation, as well as by self-assembly that may occur before, or in lieu of phase separation [Starr et al. (2001)]. Actually, although uniform nanoparticle dispersions are desired for many applications, particle aggregation can also be used to advantage. Consider CdSe nanorods functionalized with alkane ligands in PS. Because of the incompatibility of the ligands with the PS, the system phase separates into domains of PS and nanorods. If an electric field is applied to a solution of nanorods mixed with PS, the nanorods align in the direction of the applied field and, as solvent evaporates, the PS and oriented nanorods phase separate. Minimization of the interfacial energy between the domains drives a close packing or “self- corralling” of the nanorods into a hexagonal array oriented normal to the film surface [Ryan et al. (2006), Gupta et al. (2006)]. More in general, the ability to assemble particles into desired morphologies should allow us to dramatically increase the electrical conductivity of typically insulating polymers. Similarly, this ability to control particle self-assembly might permit us to synthesize a range of biomimetic materials.

Irrespective of the desired spatial configuration of the filler phase at the nano- and micro-scale, the take-home message is that the establishment of a consolidated route for the attainment of a prescribed morphology is certainly among the more necessary and yet demanding tasks in the polymer nanocomposite field. To meet this challenge, materials scientists and engineers call for a versatile tool which is sensible enough to the nanocomposite microstructure to make it possible to draw reliable relationships bridging the current gap of knowledge in the process-structure-property chain.

### **8.3 Filler state of dispersion through rheological analyses**

Recent scientific developments have contributed to boost the interest in polymer-nanoparticle composites and in their governing “rules”. In particular, the growing availability of nanoparticles of precise size and shape and the development of instrumentation to probe small length scales have spurred research aimed at probing the influence of the characteristics of the filler on the properties

of nanoparticle-polymer composites. The holy grail of any material scientist lies in the fundamental understanding of the phenomena occurring in nanoparticle-containing polymer systems at the micro- or submicron-scale and the properties of the nanocomposites originating therefrom. In this scenario, having at your disposal a characterization tool able to somehow match the nano- and micro-scale features to macro-scale evidences simply represent an undeniable privilege. However, monitoring the quality of nanoparticles dispersion within a composite system often gives rise to non-trivial problems.

Direct visualization of the space distribution of the filler phase within the host polymeric matrix guarantees an immediate insight in the microstructure of the sample. However, optical methods cut off below a length scale of about 0.5  $\mu\text{m}$ , while the nanofillers inherently belong to a smaller characteristic length. On the other hand, even though observation of individual nanoparticles can be performed, scanning and transmission electron microscopy methods can only provide the representative information for the selected fields of view. Hence, possible heterogeneities in the microstructure may go undetected. To obtain statistically relevant data a large number of images needs to be taken and analyzed, which is not always possible also because of the very laborious sample preparation. More fundamentally, these methods only provide a two-dimensional scan through the three-dimensional structure, which makes the image interpretation difficult when the constituent particles are anisotropic in shape [Zhang et al. (2008)]. They thus suffer from unavoidable difficulty in the interpretation of the global state of dispersion of the filler in the nanocomposite.

Scattering techniques, such as X-ray diffraction or small angle X-ray scattering, while offering statistically averaged data, are strongly model dependent and again fail to probe the large scale morphology, as reviewed by Schaefer and Justice (2007). The authors clearly showed how most techniques investigate only the local microstructure and emphasized that when measuring the quality of dispersion, one should also consider the large-scale structure of particles in nanocomposites. The obtained data indeed are still ambiguous with regard to correlating the information to the real dispersion space and its contribution to the target properties.

Another possibility lies in directly looking at the macroscopic properties such as the mechanical modulus or, when the nanofiller is conductive, the (di-)electrical properties [Song and Youn (2005), Pötschke et al. (2003)]. These methods offer a global view of the material performance, but need to be performed post factum, with limited possibility for in situ monitoring of the dispersion quality. Alternatively, rheology also provides an unified picture of the nanocomposite material. In addition, it plays a dual role in nanocomposite formulation and processing. First, rheological properties govern the flow behavior during melt-processing. Secondly, both linear and nonlinear rheological properties are very sensitive to changes in the particulate microstructure integrated over all length scales. Since they offer a means to assess the filler arrangement within the host

matrix directly in the melt state, they have hence been widely used as a complementary, indirect technique to monitor the quality of dispersion in different types of nanocomposite systems [Park et al. (2008), Lim et al. (2003)]. Rheological properties of nanoparticle-filled polymer melts have thus proved to provide essential information about the flocculated structure of the filler, which corresponds not only to the dispersing state of the filler itself, but also to the physical properties of composites, such as mechanical strength, electrical resistivity, heat conductivity, etc. Consequently, rheological measurements can be fruitfully exploited to define precious relationships which link the nano-and micro-scale structural variables to the macroscopic performances of the nanocomposite. As a matter of fact, much work has been performed in order to elucidate the effect of nanoparticle geometry and structure on the rheological properties. A wealth of experimental studies on the interrelationship between rheological properties and nanocomposite morphologies has already been accumulated [Wagener and Reisinger (2003), Ray and Okamoto (2003), Lee and Han (2003), Mitchell and Krishnamoorti (2002), Krishnamoorti and Yurekli (2001)]. Among the research studies on the rheology of polymer nanocomposite, a beaten path concerns the comparison of the effect of different dispersion states on the rheological behavior of the material. For example, Vermant et al. (2007) investigated to what extent rheological methods can be used in both a qualitative and a quantitative manner to compare nanocomposites resulting from slightly different preparation methods. Analogously, Zhu et al. (2009) studied the rheological features of samples based on the same components but prepared in a different manner, so as to alter the degree of filler dispersion, aiming to evaluate the sensitivity of the rheological characterization to structural differences. Moreover, Zhao et al. (2005) developed a rheological technique to analyze the morphology of clay particles in polymer nanocomposites. In addition to nanocomposites based on lamellar filler, such as those based on organo-modified clays previously mentioned, rheological measurements have been adopted also to estimate the filler dispersion in nanocomposite filled with carbon nanotubes [Zhang et al. (2008)] and silica nanoparticles [Jouault et al. (2009)]. In line with the previous studies, very recently Galindo-Rosales et al. (2011) investigated to what extent rheological properties in the melt state can be used to assess the quality of the filler dispersion in polymer nanocomposites. In detail, they systematically explore the effects of changes in dispersion quality on the rheological properties of model nanoparticle-polymer matrix systems. Different rheological methods, based on an evaluation of the evolution of the properties as a function of volume fraction, are compared and the authors evaluated if the different approaches ensure sufficient sensitivity. Besides demonstrating the suitability of the viscoelastic measurements in quantitatively assess state of dispersion of the nanoparticles, they also proposed a novel rheological method to infer the microstructure large-scale filler structures in nanocomposites.

Rheological analyses have thus been widely adopted to look into the quality of filler dispersion and into its overall microstructure in polymer matrices. The common objective is to shed light on the complex phenomena which eventually determine the filler nano- and micro-structures forming during processing. This is essential in order to reach the basic knowledge for becoming able to select materials and processes suitable to get nanocomposites with prescribed arrays of nanoparticles and hence targeted properties. Far from being exhaustive, the presented overview of the rheological studies just serves to point out that much work has been done in the field, and maybe more is ongoing. The general knowledge is going deeper and deeper and the paradigm of materials science, that is correlating the material properties to their structure over different length scales, seems to be handy.



## **Role of the morphology of primary aggregates of carbon nanotubes on their dispersibility in polymer melts\***

*In this chapter the dispersibility of unfunctionalized multi-walled carbon nanotubes in a polymer matrix is studied. The common difficulties related to the de-agglomeration and dispersion of carbon nanotubes during the mixing with the polymer are first highlighted (§ 9.1). Then the study is directed at the role of the morphology of the primary aggregates on the ease of dispersion of the nanotubes. To this aim, two kinds of multi-walled carbon nanotubes differing for the space arrangement of the nanotubes inside the aggregates are used. The morphological features of the fillers are illustrated (§ 9.2). Rheological analyses on the nanocomposites demonstrate that a hierarchical structure of loosely packed clusters of nanotubes ensures a superior dispersibility in the host polymer matrix, as also confirmed by dielectric spectroscopy and transmission electron microscopy (§ 9.3). Finally, it is verified that the high dispersibility is not achieved to the detriment of integrity of the nanotubes, the nanocomposites exhibiting also enhanced thermal stability and dynamic mechanical properties (§ 9.4).*

### **9.1 Prefatory notes**

Carbon nanotubes (CNTs) are an ideal candidate as filler for polymer nanocomposites of technological interest due to their extremely high stiffness, electrical and thermal conductivity. On the other hand, the large-scale synthesis of CNTs usually results into bundles of hundreds of microns formed by thousands of individual nanotubes held together by physical entanglements and Van der Waals forces. This prevents an efficient transfer of the CNT superior properties to the nanocomposite. Therefore, the commercial breakthrough of CNT-based nanocomposites requires the overcoming of the difficulties related to the de-agglomeration and dispersion of the primary aggregates during the mixing with the polymer. Basically, the dispersion of CNTs inside polymer melts starts with the

---

\* Part of the results has been published in «Salzano de Luna M, Pellegrino L, Daghetta M, Mazzocchia CV, Acierno D, Filippone G, “Importance of the morphology and structure of the primary aggregates for the dispersibility of carbon nanotubes in polymer melts”, *Compos Sci Technol* 85, 17-22 (2013)».

infiltration of polymer chains into the aggregates, which crack and erode, and it ends with the pulling out of single nanotubes in the late stages of the process [Alig et al. (2012)]. To expedite the dispersion, the surface of the nanotubes can be functionalized via a chemical reaction that enhances the affinity with the host polymer and/or reduces the tube-tube attractive forces [Sahoo et al. (2010)]. However, dealing with unfunctionalized nanotubes that are themselves easy to disperse would be preferred for a large-scale production of nanocomposites filled with carbon nanotubes [Grady (2010)]. To reach this goal, understanding the influence of the morphological features of the nanotubes and their aggregates on the dispersion process is of crucial importance.

Numerous studies compared the properties of polymer nanocomposites based on carbon nanotubes prepared through different synthesis methods [Krause et al. (2010a)], having different aspect ratios [Krause et al. (2011a), Shokrieh and Rafiee (2010)] and different morphology of the primary aggregates [Castillo et al. (2011), Morcom et al. (2010), Socher et al. (2011)]. A series of focused papers by Pötschke and co-workers ultimately correlated the ease of dispersion of carbon nanotubes in polymer melts to a low bulk density of the initial aggregates [Pegel et al. (2008), Krause et al. (2009), Krause et al. (2010b)]. The relationship, however, is not univocal, the bulk density being only one of many parameters which play a role in determining the actual dispersibility of the filler phase [Verge et al. (2012)]. Among others, this study focuses on the role of the morphology and structure of the primary aggregate, interpreted as the space arrangement of the CNTs over various length scales, from the texture of the grain down to the entanglements among the single nanotubes.

The Chapter is organized as follows. The morphological features of the investigated kinds of carbon nanotubes are first illustrated. Then, the state of dispersion of the filler within a polymer matrix is investigated through linear viscoelastic measurements, which allow the estimation of the filler percolation threshold. Further support is given by means of dielectric spectroscopy and morphological analyses. Finally, the macroscopic properties of the nanocomposites are characterized in order to ensure that the filler distribution in the host polymeric medium has not been achieved to the detriment of the nanotube integrity.

## **9.2 Morphology and structure of the primary aggregates**

Two kinds of carbon nanotubes have been selected to investigate the role of the morphology of the primary aggregates on the ease of dispersion of the filler in polymer melts. In detail, synthesized unfunctionalized multi-walled carbon nanotubes (MWCNTs, the same discussed in Chapter 6), whose grains exhibit a peculiar hierarchical structure, are compared with commercially available MWCNTs (Baytubes<sup>®</sup> C150P). To exclude the interference of additional

parameters other than the morphology of the primary aggregates, commercial nanotubes having similar features to the synthesized ones and only differently arranged in the primary aggregates have been carefully selected. The main features of the two types of particles (purity, length and diameter of the nanotubes etc.) are summarized in the Appendices at the end of the dissertation. Here, focusing on the morphology and structure of the primary aggregates of nanotubes, the normalized size distribution functions (SDF) of the dry powders are reported in Figure 9.1 for the two kinds of MWCNTs.

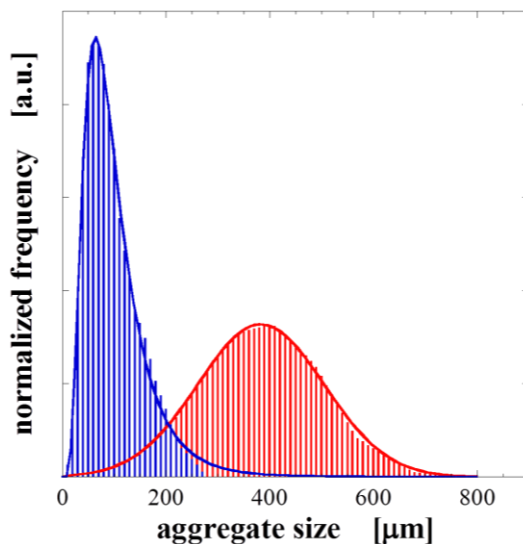


**Figure 9.1** Normalized size distribution functions of synthesized (blue) and commercial (red) CNT aggregates. Solid lines are Lognormal and Gaussian fittings, respectively.

The average size of the aggregates is much smaller for the synthesized particles. Such a parameter, however, is not strictly related to the dispersibility of CNTs in polymer matrices [Bai and Allaoui (2003)]. More importantly, the SDF of the commercial nanotubes results much wider. The small aggregates fill up the space between the big ones, thus affecting the value of bulk density of the powder. The latter is often erroneously taken as indicative of the bulk density of the single aggregate,  $\rho_a$ , which is instead known to be a relevant parameter in the dispersion process of CNTs [Krause et al. (2010b)]. However,  $\rho_a$  only partially reflects the actual space arrangement of the single nanotubes inside the aggregates, which ultimately governs the dispersibility. Scanning electron microscopy (SEM) images showing the internal structure of the two kinds of MWCNT aggregates at different magnifications are reported in Figure 9.2.

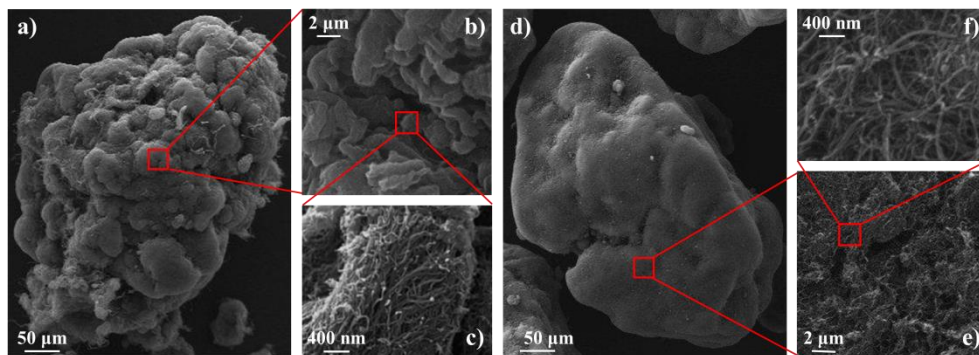


**Figure 9.2** SEM micrographs of the primary aggregates of the (a-c) synthesized and (d-f) commercial carbon nanotubes on different length scales.

The synthesized MWCNTs are in the form of loosely packed agglomerates with coarse-grained texture (Figure 9.2a), which is likely to facilitate the infiltration of the polymer in the earlier stages of melt mixing. Such an “opened” structure persists also on micro-scale (Figure 9.2b), reflecting the presence of interwoven bundles of combed yarns of nanotubes (Figure 9.2c). Such an aligned arrangement on nanoscale is expected to favor the pulling out of the nanotubes required for their individualization when melt mixed with polymer matrices. In contrast with the hierarchical structure of the synthesized particles, the aggregates of commercial MWCNTs appear as fine-textured blocks (Figure 9.2d), whose apparent dense structure is the result of a random arrangement of highly entangled nanotubes (Figure 9.2e-f) which are thus supposed to be difficult to unravel.

### 9.3 State of dispersion of the carbon nanotubes

The structural and morphological differences between the aggregates of the two kinds of fillers affect the quality of their dispersion within the host polymer. The dispersibility of the two kinds of nanotubes is investigated referring to a polystyrene (PS) matrix, which has been deliberately selected as its high chain stiffness is known to hinder the infiltration process within the pristine aggregates [Alig et al. (2012)]. The resulting polymer nanocomposites have been studied through rheological analyses. Before measurements, the samples have been annealed for about 2 hours at  $T = 220^{\circ}\text{C}$  in inert conditions. Driven by particle-particle attraction, the re-agglomeration of the filler eventually results in time-independent viscoelastic properties [Alig et al. (2008)], which have been studied as a function of the frequency. The elastic  $G'$ , and viscous,  $G''$ , shear moduli are shown as a function of frequency,  $\omega$ , in Figure 9.3 for the samples filled with

synthesized and commercial MWCNTs at different filler volume fractions,  $\Phi$ . Note that the data of the PS-based samples filled with the synthesized MWCNTs already shown in Chapter 6 are reported again for convenience.

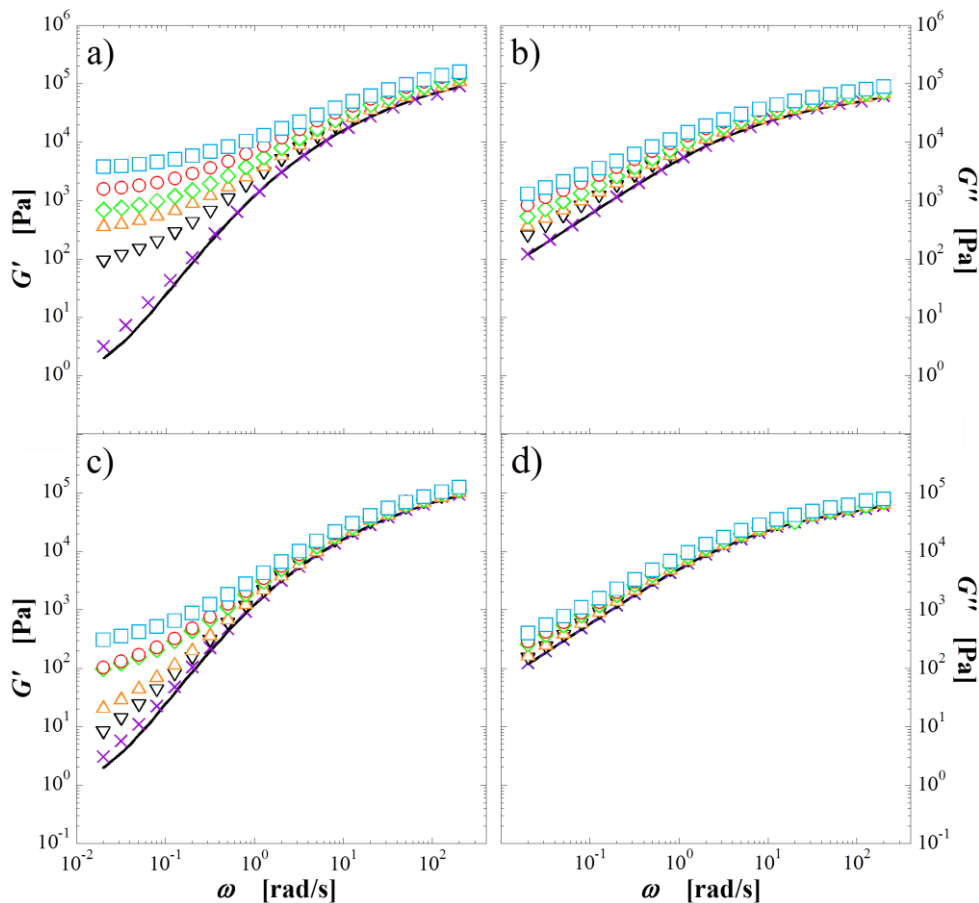


**Figure 9.3** Frequency-dependent (a, c) elastic and (b, d) viscous moduli of PS-based nanocomposites filled with (a, b) synthesized and (c, d) commercial MWCNTs at different composition. From bottom to top: (a, b)  $\Phi = 0.0003, 0.0020, 0.0035, 0.0045, 0.0065, 0.0086$ ; (c, d)  $\Phi = 0.0015, 0.0038, 0.0054, 0.0067, 0.0069, 0.0099$ . In each plot the solid line refers to the neat PS matrix.

The two systems share the same qualitative behavior, peculiar of many polymer nanocomposites. The elastic modulus, more sensitive than its viscous counterpart to the state of dispersion of the nanotubes, gradually flattens at low frequency, indicating the occurrence of a liquid- to solid-like rheological transition due to the

formation of an elastic network of carbon nanotubes. The comparison between the two families of curves reveals that higher contents of worse dispersed commercial nanotubes are required to obtain comparable enhancements of  $G'$  as those attained in the case of synthesized nanotubes.

A deeper insight into the quality of filler dispersion can be obtained looking at the values of the percolation threshold,  $\Phi_c$ , in the two systems. Actually, a good nanoscale dispersion is often related to a low  $\Phi_c$ . Indeed, the more effectively dispersed the filler is, the lower is the filler volume fraction necessary to form a three-dimensional space-spanning network. The two-phase model is exploited to accurately estimate  $\Phi_c$ . The model allows to build the master curves of  $G'$ , which then ensure to precisely set the elasticity of the network of each sample at  $\Phi > \Phi_c$ . The physical constraints invoked when building the master curve, indeed, allow to identify the samples whose filler content is below the percolation threshold. The obtained master curves of the PS/O-Clay and PS/PMMA/O-Clay systems are shown in Figure 9.4. For completeness, the amplifying factors,  $B(\Phi)$ , and the  $G''(\omega)$  curves of the pure matrices on which the shift factors ( $a_\Phi$ ;  $b_\Phi$ ) used to build the master curves lie are reported in the Appendices at the end of the dissertation, together with the corresponding numerical values.

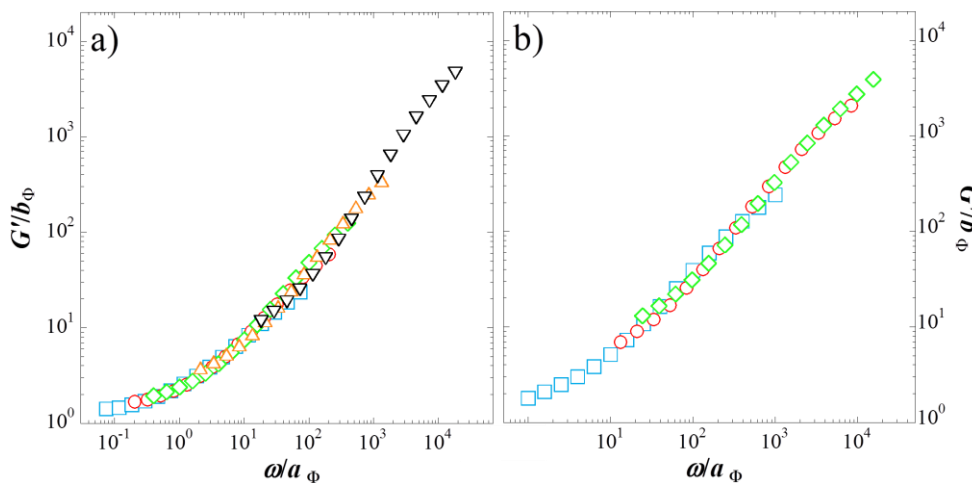


**Figure 9.4** Master curves of  $G'$  of (a) PS/synthesized MWCNTs nanocomposites at  $0.0020 \leq \Phi \leq 0.0086$  and (b) PS/synthesized MWCNTs samples at  $0.0067 \leq \Phi \leq 0.0099$ .

As expected in the light of the results of Chapter 6, the two-phase model perfectly works for both the nanocomposite families: the collapse of the moduli is excellent over more than three decades of scaled frequencies,  $\omega/a_\Phi$ , corresponding

to the region in which non-continuum effects are predominant. More importantly, for each system, the master curve facilitates the identification of the percolation threshold, which must be sought in the composition range which is superiorly limited by the lowest  $\Phi$  of the scalable  $G'$  curves and inferiorly limited by the highest  $\Phi$  of the non-scalable  $G'$  curves. Moreover, the vertical shifts factors,  $b_\Phi$ , used to build the master curves of  $G'$  unambiguously set the elasticity of the filler network of each scaled curve. The network elasticity,  $G'_0(\Phi)$ , monotonically increases with increasing the filler volume fraction, and according to the percolation theory, it is expected to exhibit critical behavior just above  $\Phi_c$ :

$$G'_0 = k(\Phi - \Phi_c)^\nu \quad (9.1)$$

where  $k$  and  $\nu$  are two constants, the latter being related to the stress-bearing mechanism [Stauffer and Aharony (1992)]. Equation 9.1 has been fitted to the network elasticity data,  $G'_0(\Phi) = b_\Phi$ , setting  $k$  and  $\nu$  as fitting parameters while keeping  $\Phi_c$  constant. The procedure has been repeated for different values of  $\Phi_c$  in the composition range recognized thanks to the master curve and the value of  $\Phi_c$  which returns the maximum coefficient of determination,  $R^2$ , is taken for granted. The power-law dependence of the network elasticity obtained through the best fitting procedure is shown in Figure 9.5 for the two nanocomposite families. The corresponding parameters are reported in Table 9.1.

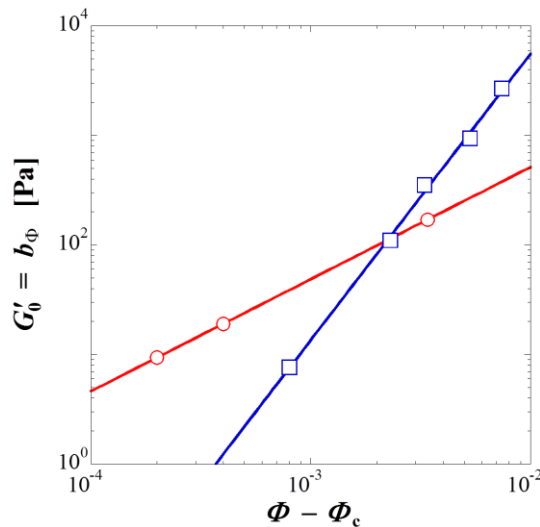


**Figure 9.5** Power law dependence of  $G'_0$  on the reduced filler content,  $\Phi - \Phi_c$ , obtained setting  $\Phi_c = 0.0012$  and  $0.0065$  for the nanocomposite systems based on synthesized and commercial MWCNTs, respectively. Solid lines are the fittings to Equation 9.1.

**Table 9.1** Best fitting parameters ( $k$ ,  $\nu$ ) of Equation 9.1 and corresponding values of percolation threshold for the two investigated families of nanocomposites.\*\*

System	$\Phi_c$	$k$ [Pa]	$\nu$	$R^2$
PS+synthesized MWCNTs	0.0012	$9.5 \times 10^8$	2.62	0.9979
PS+commercial MWCNTs	0.0065	$5.7 \times 10^4$	1.02	0.9998

The better dispersibility of the synthesized MWCNTs clearly emerges from the comparison of the percolation thresholds. Besides being more than five times lower than that of the commercial nanotubes, the percolation threshold of the system based on synthesized particles is among the lowest reported in the literature for polystyrene-CNT nanocomposites, irrespective of the adopted compounding technique [Bauhofer and Kovacs (2009)]. It is important to stress that such a result has been obtained without the optimization of the processing parameters, whose fine tuning is known to be important for enhancing the dispersion of carbon nanotubes inside polymer matrices [Villmow et al. (2010)].

Dielectric spectroscopy analyses have been performed to give further support to the rheological data. The real,  $\varepsilon'$ , and imaginary,  $\varepsilon''$ , parts of the complex permittivity have been monitored as functions of the frequency of the electrical field,  $f$ . Then the real part of the complex conductivity,  $\sigma'$ , which is a measure of the long range movements of the charge carriers, has been evaluated as:

$$\sigma' = \varepsilon'' \varepsilon_0 f \quad (9.2)$$

where  $\varepsilon_0$   $8.85 \times 10^{-12}$  F m<sup>-1</sup> is the permittivity of free space. The real part of the complex permittivity and the as-estimated values of  $\sigma'$  are shown as a function of the electrical frequency in Figure 9.6 for the samples based on synthesized and commercial MWCNTs at different filler loadings. For both families of nanocomposites, the curves of  $\varepsilon'$  are essentially flat, excluding the presence of significant dipolar contributions in the investigated frequency range. Nonetheless, a sudden increase in the values of the real part of the complex permittivity takes place at  $\Phi > 0.0003$  for the nanocomposites filled with synthesized nanotubes and at  $\Phi > 0.0054$  for the nanocomposites filled with commercial particles. Contextually, for the same samples the appearance of a low-frequency plateau of  $\sigma'$  (which means that  $\varepsilon'' \sim f^{-1}$ ) is indicative of an insulator to conductor transition,

\*\* Slight differences with the values reported in Salzano de Luna et al. (2013) are due the different number of available experimental data and to approximations in the estimation of the filler content in volume fraction.

which reflects the formation of a percolating network of conductive particles throughout the insulating polymer matrix [Pötschke et al. (2003)]. Dielectric spectroscopy analyses thus clearly strengthen the results of the rheological measurements. The system based on the synthesized MWCNTs, indeed, experiences the transition at a certain value of  $\Phi$  in the range  $0.0003 \div 0.0020$ , whereas the critical content of the commercial ones is sensibly higher, as it falls in the range  $0.0054 \div 0.0067$ .

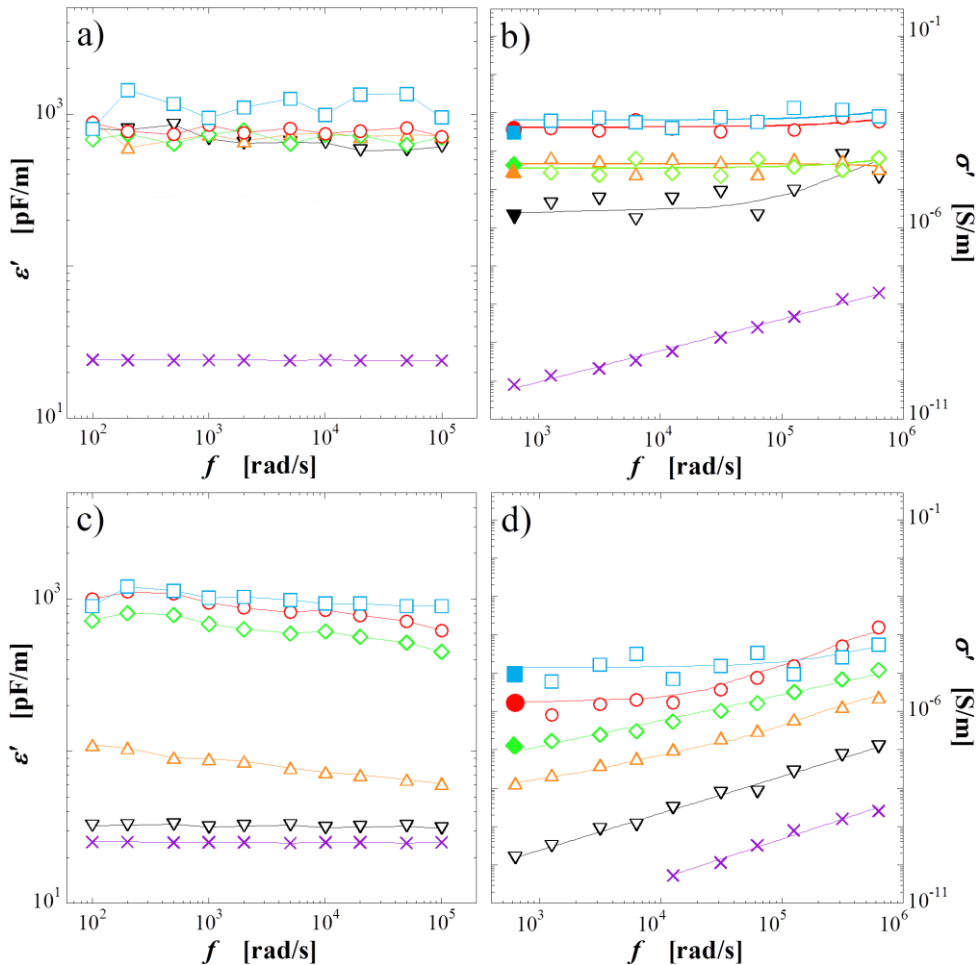


**Figure 9.6** Frequency-dependent real part of (a, c) the complex permittivity and of (b, d) the complex conductivity calculated by Equation 9.2 for the PS-based nanocomposites filled with (a, b) synthesized and (c, d) commercial nanotubes at different composition. In each graph, from bottom to top: (a, b)  $\Phi = 0.0003, 0.0020, 0.0035, 0.0045, 0.0065, 0.0086$ ; (c, d)  $\Phi = 0.0015, 0.0038, 0.0054, 0.0067, 0.0069, 0.0099$ . Lines are guides for the eye.

The percolation theory has been again exploited to estimate more accurately the thresholds. Similarly to the network elasticity, the DC conductivity,  $\sigma$ , grows with  $\Phi$  as:

$$\sigma = \sigma_0 (\Phi - \Phi_c^{\text{el}})^t \quad (9.3)$$

where  $\Phi_c^{\text{el}}$  represent the electrical percolation threshold and  $\sigma_0$  and  $t$  are two constants, the latter being related to the mechanisms of electrical transport [Stauffer and Aharony (1992)]. For the samples in which a plateau of the real part of complex conductivity is recognizable, Equation 9.3 has been fitted to the values of  $\sigma'$  at the lowest investigated frequency (corresponding to the full symbols in Figure 9.6b and Figure 9.6d), which can be taken as rough representations of the DC conductivity [Pötschke et al. (2003), Wang et al. (2013)]. The same fitting procedure used for the linear viscoelastic data is adopted and again the value of  $\Phi_c^{\text{el}}$  which returns the highest  $R^2$  is taken as definitive.

The power-law dependence of the values of  $\sigma'$  at the lowest investigated frequency obtained through the best fitting procedure is shown in Figure 9.7 for both the investigated nanocomposite families. The corresponding parameters are reported in Table 9.2.

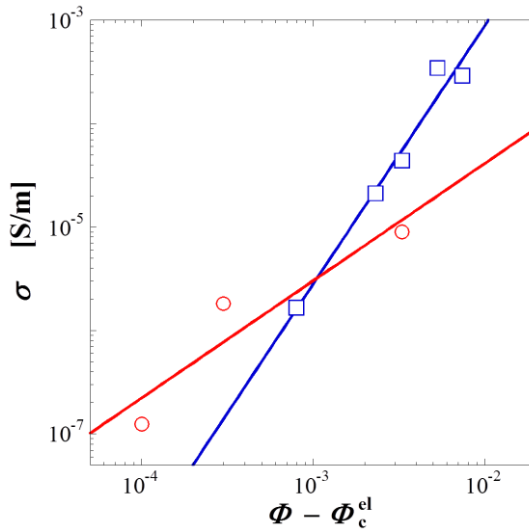


**Figure 9.7** Power law dependence of the electrical conductivity on the reduced filler content,  $\Phi - \Phi_c^{\text{el}}$ , setting  $\Phi_c^{\text{el}} = 0.0012$  and  $0.0066$  for the systems based on synthesized and commercial MWCNTs, respectively. Solid lines are the fittings to Equation 9.3.

**Table 9.2** Best fitting parameters ( $k$ ,  $\nu$ ) of Equation 9.1 and ( $\sigma_0$ ,  $t$ ) of Equation 9.3 and corresponding values of percolation threshold.<sup>\*\*\*</sup>

System	$\Phi_c^{el}$	$\sigma_0$ [S/m]	$t$	$R^2$
PS+synthesized MWCNTs	0.0012	$8.8 \times 10^3$	2.50	0.9683
PS+commercial MWCNTs	0.0066	$7.6 \times 10^{-3}$	1.13	0.8776

The electrical percolation thresholds reported in Table 9.2 perfectly agree with their rheological counterparts (see Table 9.1). Again, the value of  $\Phi_c^{el}$  for the system based on synthesized nanotubes is much lower than that related to the nanocomposites filled with commercial particles. More in general, the very low rheological and electrical percolation thresholds detected for the nanocomposites based on synthesized particles unambiguously reveal that the nanotubes are really well dispersed inside the host polystyrene matrix. Viscoelastic measurements and dielectric spectroscopy thus clearly agree in recognizing a key role of the structural and morphological features of the primary aggregates of carbon nanotubes in dictating their propensity to be easily dispersed in polymer melts. Specifically, it emerges that the hierarchical structure of the primary aggregates of synthesized MWCNTs facilitates both the infiltration of the polymer in the earlier stages of mixing and the pulling out of the nanotubes required for their individualization. Indeed, the results suggest that such a peculiar arrangement of the synthesized nanotubes within the aggregate brings about a superior dispersibility of the filler in polymer melts, even in the case of nanocomposites prepared by conventional melt mixing route.

Finally, the comparison between the values of the critical exponents  $\nu$  and  $t$  reported in Table 9.2 reveals that both the strength and electrical conductivity of the network grow with  $\Phi$  more rapidly for the synthesized MWCNTs. This is ascribed to the different structures of the percolating networks, which are based on distinct building blocks. To isolate the basic elements of the filler networks, transmission electron microscopy (TEM) analyses have been performed on two diluted samples with comparable viscoelastic and dielectric features. The micrographs are shown in Figure 9.8. Individualized nanotubes and small clusters can be noticed in the case of synthesized particles (Figure 9.8a), whereas the presence of bigger entangled hanks characterizes the sample based on commercial nanotubes (Figure 9.9b). The former, smaller and better distributed in the space, are

<sup>\*\*\*</sup> Slight differences with the values reported in Salzano de Luna et al. (2013) are due the different number of available experimental data and to approximations in the estimation of the filler content in volume fraction.

expected to be more effective in contributing to the mechanical and electrical properties of the network.

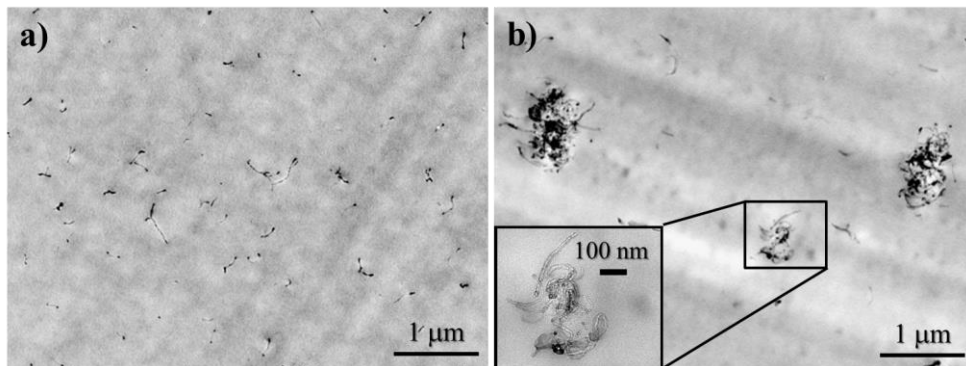


**Figure 9.8** TEM micrographs of the nanocomposites at (a)  $\Phi = 0.0003$  of synthesized nanotubes and (b)  $\Phi = 0.0015$  of commercial ones.

## 9.4 Macroscopic performances of the nanocomposites

The high dispersibility of the synthesized nanotubes is proved by a very low value of  $\Phi_c$ , comparable with those attainable through much more intensive mixing procedures. The filler percolation threshold, however, may hide nanotube breakage that compromises the macroscopic properties of the final nanocomposite [Lin et al. (2006)]. In addition, higher  $\Phi_c$  are not necessarily coupled with lower performances, the polymer nanocomposite properties being the result of a complex interplay among various features of the nanotubes [Castillo et al. (2011)].

To demonstrate that the very low percolation threshold detected for the samples based on synthesized MWCNTs has not been obtained to the detriment of the integrity of the nanotubes, the thermal and mechanical performances of the two families of samples have been investigated. Nanotube breakage, indeed, would negatively reflect on the macroscopic properties of the nanocomposites [Pegel et al. (2008)]. The results of thermal gravimetric analyses are reported in Figure 9.9. Specifically, the degradation paths of the two nanocomposite systems at different filler content have been interpreted in terms of onset of thermal degradation,  $T_{\text{onset}}$ , identified as the temperature at which a weight loss of 5 wt.% occurs, and temperature of maximum rate of degradation,  $T_{\text{max}}$ . Both  $T_{\text{onset}}$  and  $T_{\text{max}}$  are systematically higher for the nanocomposites based on synthesized nanotubes. A notable increase of  $T_{\text{onset}}$  of about  $10^\circ\text{C}$  is obtained upon addition of amounts of synthesized particles as low as  $\Phi = 0.0065$ . On the contrary, the presence of commercial MWCNT leads to values of  $T_{\text{onset}}$  is practically unaltered with respect

to the neat matrix. Similar trends can be noticed for  $T_{\max}$ . In addition, besides being systematically higher, both  $T_{\text{onset}}$  and  $T_{\max}$  grow with  $\Phi$  more rapidly for the nanocomposites based on the synthesized nanotubes. Again, such a higher sensitivity to filler content reflects a finer and more homogeneous dispersion of the particles.

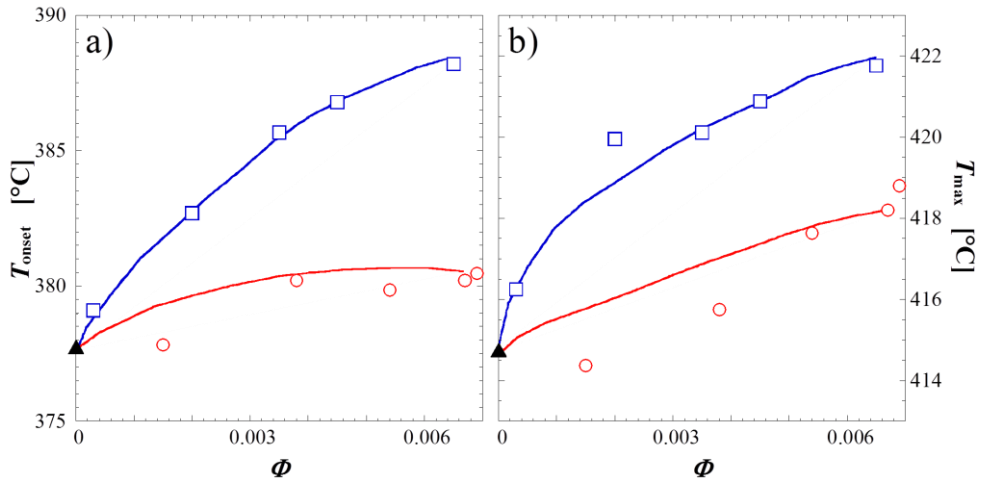


**Figure 9.9** (a) Onset of thermal degradation and (b) temperature of maximum rate of degradation as functions of filler volume fraction for the nanocomposites filled with synthesized (squares) and commercial (circles) MWCNTs. The full triangle represent the neat PS. The solid lines are guide for the eye.

Similar conclusions can be drawn for the dynamic-mechanical properties. The elastic,  $E'$ , and viscous,  $E''$ , flexural moduli are shown in Figure 9.10a as a function of temperature for the neat PS and two representative nanocomposites above their percolation thresholds. The overall effect of the two kinds of filler is similar, the moduli of the nanocomposites being higher than those of the neat polymer except for  $E''$  at low temperature. The high dispersibility of the synthesized particles ensures the same enhancements at much lower MWCNT loadings. Dealing with small amounts of particles is also desirable because too large amounts of filler can deteriorate the ultimate mechanical properties of the nanocomposite [Zhou et al. (2012)]. Focusing on the glassy modulus,  $E_g$ , which is reported in Figure 9.10b as a function of filler content, a faster growth with  $\Phi$  is still noticed for the samples based on the synthesized carbon nanotubes. Negligible enhancements of the mechanical properties are usually observed for melt processed MWCNT-filled composites, especially for brittle matrices such as polystyrene [Spitalsky et al. (2010)]. Nonetheless, a noticeable increase in  $E_g$  is obtained upon addition of only

very small amounts of synthesized MWCNTs, that is  $\Phi = 0.0020$ . It is important to stress that such a result is exclusively due to the reinforcing action of the filler phase. The amorphous nature of our matrix, indeed, excludes possible contributions of a crystalline phase which may enucleate in the proximity of the nanotube walls [Logakis et al. (2011)].

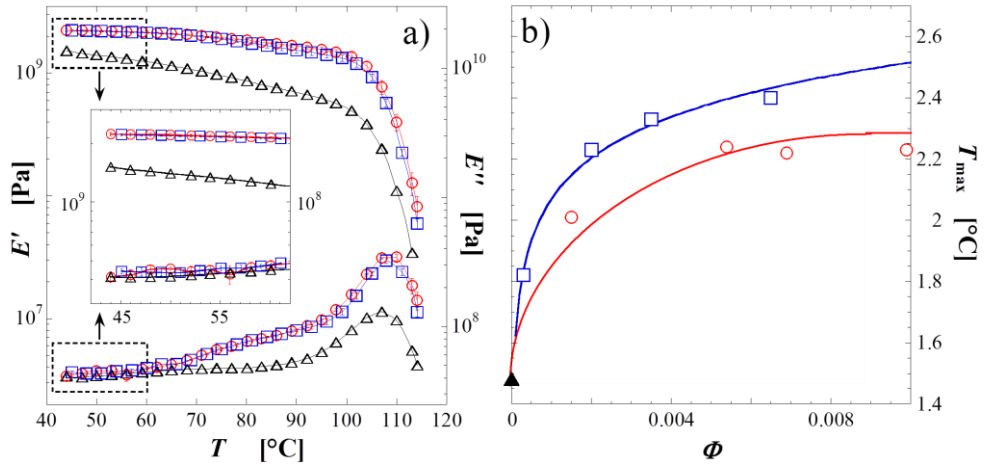


**Figure 9.10** (a) Temperature dependent elastic (up) and viscous (down) flexural moduli for the neat PS (triangles) and for nanocomposite at  $\Phi = 0.0020$  of synthesized MWCNTs (squares) and at  $\Phi = 0.0099$  of commercial ones (circles). (b) Glassy modulus as a function of filler content for the samples filled with synthesized (squares) and commercial (circles) MWCNTs. The full triangle represent the neat PS. The solid lines are guides for the eye.

# 10

## **Dispersing hydrophilic nanoparticles in hydrophobic polymers: nanocomposites by a novel template-based approach\***

*In this chapter a novel compounding approach for the dispersion of hydrophilic nanoparticles in hydrophobic polymers is proposed and its efficiency is proved. To begin, the difficulties related to the breakup of agglomerates of nanoparticles into individual species during the compounding with the polymer and to their uniform dispersion inside the matrix are introduced (§ 10.1). Then, melt mixing route is shown to be inadequate in the case of very low polymer-particle affinity (§ 10.2). A novel technique for the preparation of nanocomposites with highly dispersed filler phase is presented (§ 10.3). The procedure envisages the penetration of a well dispersed nanoparticle suspension inside a micro-porous matrix, obtained through selective extraction of a sacrificial phase from a finely interpenetrated co-continuous polymer blend. Finally, comparing the two families of nanocomposites, viscoelastic measurements prove that the proposed compounding technique, despite an uneven distribution on micro-scale, ensures a good quality of the filler dispersion (§ 10.4).*

### **10.1 Prefatory notes**

Polymer nanocomposites based on inorganic nanoparticles are a well-established field of research due to the interesting properties arising from such class of filler. In particular, besides improved mechanical, thermal and barrier properties, the control of the chemistry of the filler may provide new functionalities to the host matrix, allowing for the enlarging of the fields of application of polymeric materials in sectors such as automotive, micro-optics, micro-electronics, environment, health, energy and housing [Sanchez et al. (2011)].

The use of nanoparticles as filler for polymer matrices generally implies relevant problems in terms of dispersability [Jancar et al. (2010)]. Inorganic nanoparticles usually present hydrophilic characteristics, which bring about

---

\* Part of the results has been published in «Salzano de Luna M, Galizia M, Wojnarowicz J, Rosa R, Lojkowski W, Leonelli C, Acierno D, Filippone G, “Dispersing hydrophilic nanoparticles in hydrophobic polymers: HDPE/ZnO nanocomposites by a novel template-based approach”, Express Polym Lett 8, 362-372 (2014)».

substantial differences in terms of surface energy between the polymer matrix and the filler, leading to phase segregation. In addition, the high surface-to-volume ratio of nanoparticles typically results in small inter-particle distances, which makes van der Waals and electrostatic forces of major importance [Hiemenz and Rajagopalan (1997)]. As a consequence, nanoparticles are inclined to form agglomerates which can be extremely difficult to break up into individual species and to disperse uniformly inside the polymer matrix. The presence of such agglomerates impedes the efficient transfer of the beneficial properties of the filler related to its nanoscopic dimension to the host polymer, leading to materials with properties comparable to traditional micro-composites. As a result, it is undeniable that the control of the dispersion of nanoparticles inside polymer matrices is crucial to fully exploit the potential of polymer nanocomposites. In this sense, the use of a suitable compounding technique is strictly required [Demir and Wegner (2012)].

Various approaches have been proposed to manufacture well dispersed polymer nanocomposites based on inorganic fillers. Chemical modification of the nanoparticle surface, polymer-particle compatibilizing agents, in situ synthesis and/or polymerization are examples of possible strategies which have revealed to be effective in attaining a homogeneous filler dispersion [Chow et al. (2012), Peponi et al. (2011), Tyurin et al. (2010)]. On the other hand, the compounding approach for the large scale production of polymer nanocomposites typically involve unmodified nanoparticles which are directly incorporated in the polymer matrix, either in the melt or in solution. Melt mixing is the most time- and cost-effective technique, but it requires that the filler is used in powder form. Although produced in the nm-range and with a narrow size distribution, dry nanoparticles have the tendency to fuse together forming stable aggregates, suffering from further agglomeration during handling and/or storage [Nordström et al. (2010)]. The immediate advantage offered by solution mixing is a better filler dispersion [Agrawal et al. (2010)]. In this case the nanoparticles are in the form of colloidal dispersion, in which almost exclusively isolated primary particles are present. The major drawback of solution mixing is that it requires that the polymer matrix is dissolved in the same solvent of nanoparticles or in a medium soluble with them. Unless often unaffordable chemical modifications of the particle surface are made, the feasibility of solution mixing is hence limited to suitable polymer-particle pairs, and to polymers which are soluble in solvents of common use, thereby excluding, for example, polyolefins. In the light of the previous considerations, a novel template-based approach which capitalizes the high degree of filler dispersion of solution techniques eluding the issues related to the needing of specific solvents for the polymer has been conceived. The ultimate goal of the present work is to prove the ability of the proposed strategy to effectively disperse a hydrophilic filler, namely zinc oxide (ZnO) nanoparticles in a hydrophobic matrix, such as high density polyethylene (HDPE).

The Chapter is organized as follows. The properties of the nanocomposites obtained through conventional melt mixing are first examined. Rheological measurements relates the scarce performances of such samples to a poor degree of dispersion of the filler. Then, a novel compounding approach is presented. Specifically, each step is illustrated and discussed, motivating the choice of selected material and process-related parameters. The effectiveness of the proposed technique is finally assessed by linear viscoelastic measurements and morphological analyses.

## 10.2 Melt mixing route

Dispersing metal oxide nanoparticles in polymer mediums is a difficult task because of the large specific surface area of the filler and the incompatibility in surface characteristics with the matrix. Directly compounding polymer and dry nano-powders by melt mixing route is often inadequate, although the high shear and elongational stresses during extrusion break the clusters of primary nanoparticles reducing their average size. The minimum size of the aggregates depends on the applied stress and the composite Hamaker constant for two surfaces interacting through a medium [Baird and Collias (1995)], being in any case much larger than the size of the single primary nanoparticle. This is clearly shown in Figure 10.1, in which a scanning electron microscopy (SEM) image of dry ZnO nanoparticles is compared to that of a typical micron-sized aggregate suspended in the HDPE matrix for a melt mixed sample.

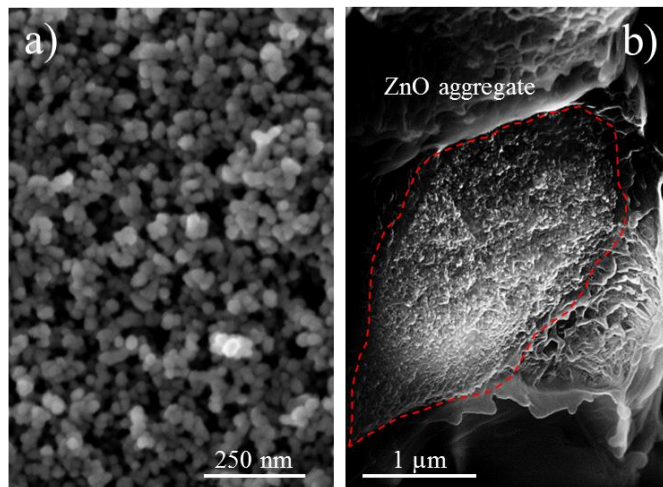


**Figure 10.1** SEM micrographs showing (a) pristine dry ZnO nanoparticles and (b) a detail of particle aggregate protruding from the fracture surface of a melt mixed nanocomposite.

The negligible polymer-particle enthalpic interactions are responsible for the aggregated state of the filler, which is expected to not appreciably affect the macroscopic properties of the resulting nanocomposite samples. To verify such a conjecture, the structural and functional properties of the melt mixed samples have been studied. First, possible effects of the particles on the crystalline structure of the HDPE matrix have been investigated through differential scanning calorimetry (DSC) measurements. The results are summarized in Table 10.1, in terms of onset,  $T_{m,onset}$ , and peak,  $T_{m,peak}$ , melting temperatures and crystallization temperature,  $T_c$ , for the neat HDPE and the nanocomposites samples at different filler volume fraction of ZnO nanoparticles,  $\Phi_{ZnO}$ . The degree of crystallinity,  $\chi_c$ , has also been evaluated.

**Table 10.1** Onset and peak melting temperatures, crystallization temperature and crystallinity of neat HDPE and melt mixed nanocomposites.

$\Phi_{ZnO}$	$T_{m,onset}$ [°C]	$T_{m,peak}$ [°C]	$T_c$ [°C]	$\chi_c^a$ [%]
neat HDPE	123.5	128.8	115.3	54.5
0.0027	122.3	128.5	116.0	54.3
0.0055	123.6	128.9	116.7	53.4
0.0090	122.7	128.7	116.6	52.5
0.0113	123.8	128.7	116.4	52.7

<sup>a</sup>  $\chi_c$  values are obtained by dividing the melting enthalpy,  $\Delta H_f$ , of each sample by the  $\Delta H_f$  of a 100% pure crystalline HDPE sample, taken as 293.1 J g<sup>-1</sup> [Wunderlich (1980)].

Whatever the content of ZnO nanoparticles is, the melting and crystallization behaviors remain almost constant. In addition, no evident changes are detected for the crystallinity, the samples sharing comparably high values of  $\chi_c$  (~50%).

Other technologically relevant properties of polymer nanocomposites are mechanical and barrier properties. The results of the tensile and permeability tests are reported in Figure 10.2 as a function of filler content. Neither the Young's modulus,  $E$ , nor the tensile strength,  $\sigma_{max}$ , appreciably change with respect to the unfilled matrix, whereas a drastic decrease of the elongation at break,  $\epsilon_{break}$ , occurs with increasing  $\Phi_{ZnO}$ . The detrimental effect on  $\epsilon_{break}$  noticed upon addition of the filler is due to the presence of nanoparticle aggregates, which are sites where cracks initiate on and significantly lowering the ultimate properties of the material [Tjong (2006)]. Analogously, also the barrier properties are negligibly affected by

the aggregated filler. The permeability to oxygen,  $P_{O_2}$ , and carbon dioxide,  $P_{CO_2}$ , of the melt mixed samples indeed slightly increase upon addition of ZnO nanoparticles, probably due to the scarce polymer-particle interfacial adhesion which enhances the overall free volume of the nanocomposite samples. Nonetheless, scarce improvements in the mechanical and barrier properties of ZnO-filled nanocomposites have been reported even in case of good dispersion of the filler due to the low aspect ratio of the nanoparticles [Hess et al. (2009)].

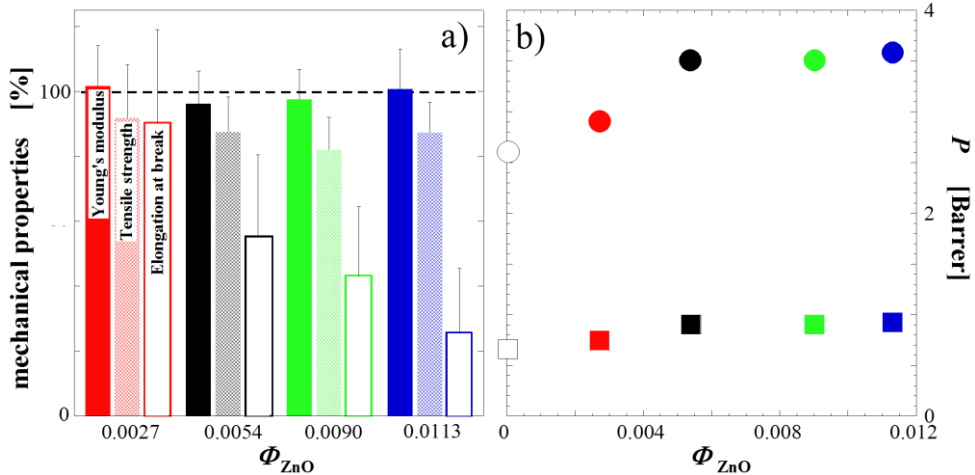


**Figure 10.2** (a) Mechanical properties of the melt mixed nanocomposites at different  $\Phi_{ZnO}$ : Young's modulus, tensile strength and elongation at break. (b) Barrier properties of the melt mixed nanocomposites at different  $\Phi_{ZnO}$ : permeability to oxygen (squares) and carbon dioxide (circles). Colors are the same as in part (a).

Actually, a more conclusive insight on the state of dispersion of the filler can be obtained through rheological measurements. In particular, linear viscoelastic analysis is an extremely sensitive tool to probe the material structure over various length scales, offering an integrated picture of composite samples with higher reliability of the results compared to other methods, such as the analysis of the mechanical and barrier properties, which are instead too sensitive to micron-scale inhomogeneity [Galindo-Rosales et al. (2011)]. If the viscosity of the melt is adequately low, nanoparticles, either isolated or in the form of aggregates, may experience relevant Brownian motions in polymer melts provided that they are sufficiently small [Romeo et al. (2009)]. Driven by particle-particle attraction, the filler flocculates in timescales which are proportional to the cubic power of the size of the aggregates [Larson (1999)]. Such structural rearrangements, if any, cause an enhancement of the elastic and viscous connotation during time, which eventually

alters the relaxation spectrum in a characteristic way. Specifically, both  $G'$  and  $G''$  significantly increase at low frequency, the effect being more pronounced on the elastic component. It is important to observe that noticeable alterations are expected even for very low filler contents and poor polymer-particle affinity [Acierno et al. (2007a)]. The time evolution of the elastic,  $G'$ , and viscous,  $G''$ , shear moduli at low frequency,  $\omega$ , and their frequency dependence are shown in Figure 10.3 for the neat polymer and the nanocomposites at different filler content.

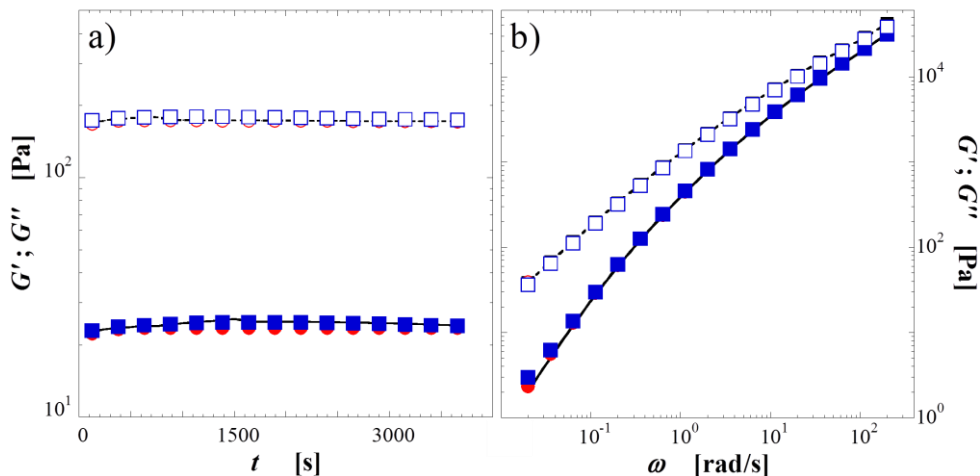


**Figure 10.3** (a) Time evolution and (b) frequency dependence of the elastic (full symbols) and viscous (empty symbols) moduli of the nanocomposite at  $\Phi_{\text{ZnO}} = 0.0027$  (circles) and  $\Phi_{\text{ZnO}} = 0.0113$  (squares). Solid and dashed lines represent the elastic and viscous moduli of the neat HDPE, respectively.

None of the rheological peculiarities of polymer nanocomposites can be recognized in the melt mixed samples of Figure 10.3, not even at relatively high ZnO contents (up to  $\Phi_{\text{ZnO}} \sim 0.01$ ). Indeed, the moduli of the filled samples exactly retrace those of the neat matrix, irrespective of the filler volume fraction. Such a behavior is rather reminiscent of that of conventional micro-composites at low filler volume fractions, in which the particles are too big to move and rearrange in the melt and the volume of polymer perturbed by the filler is not sufficient to affect the overall relaxation spectrum [Acierno et al. (2007b), Dorigato et al. (2010)]. From the analysis of the linear viscoelastic measurements, thus, it clearly emerges that the mediocre macroscopic performances of the melt mixed nanocomposites arise from a scarce quality of filler dispersion. Indeed, although being a widespread route to distribute and disperse nanoparticles in the form of dry powders within polymer matrices, unless using targeted processing expedients, melt compounding

is often inadequate in case of systems with very low polymer-particle affinity, such as the HDPE/ZnO nanocomposites considered here.

### 10.3 Template-based approach

The control of the dispersion of nanoparticles inside polymer matrices is crucial to fully exploit the potential of polymer nanocomposites. More specifically, a suitable compounding technique, which ensure the breakup of the filler aggregates down to particles with nanometric dimensions is strictly required to efficiently transfer the beneficial properties of the filler to the host polymer matrix. In this context, aiming at exploiting the advantages of solution techniques eluding the issues related to the needing of specific solvents, an alternative compounding method, namely the template-based approach, has been conceived. The underlying idea of the proposed method is to make a suspension of well dispersed ZnO nanoparticles to penetrate inside a microporous HDPE scaffold, obtained by selective extraction of a sacrificial phase blended with the HDPE. Poly(ethyleneoxide) (PEO) has been selected as sacrificial phase because it can be easily removed by solvent extraction in deionized water, just keeping the system under stirring to accelerate the process and without any further expedient. A prerequisite is that the starting polymer blend exhibits a co-continuous morphology. A blend composition of 50/50 by weight, in which the PEO phase forms a space-spanning framework that interpenetrates the HDPE, has been selected for such a purpose [Filippone et al. (2011)]. Once the PEO has been extracted, the remaining HDPE scaffold is dipped in a stable dispersion of almost isolated primary ZnO nanoparticles, which may penetrate into the micro-pores of the scaffold, thus remaining trapped inside the polymer. In order to optimize the process, the HDPE scaffold have to contain a thick network of tiny channels, i.e. the starting HDPE/PEO blend should exhibit a microstructure as fine as possible. In such a way, the trapped nanoparticles will finely distribute inside the host matrix. On the other hand, the penetration depth of the ZnO suspension inside the channels, which inversely scales with their diameter, must be preserved to ensure a homogeneous distribution along the sample thickness. Conciliating these two opposite requisites is a challenging task, which has been address through a judicial selection of the materials.

First of all, adding plate-like nanoparticles to a polymer blend is a clever expedient to promote and stabilize fine co-continuous morphologies in immiscible polymer blends. Drawing upon recent literature results, small amounts of organo-modified montmorillonite, (O-Clay, Cloisite<sup>®</sup> 15A) have been used to refine the morphology of the HDPE/PEO blend [Filippone et al. (2011)]. SEM micrographs showing the impact of the filler on the blend morphology are reported in Figure

10.4. For the sake of clarity, the PEO phase has been selectively removed by dipping the cryo-fractured surface of the sample in water.

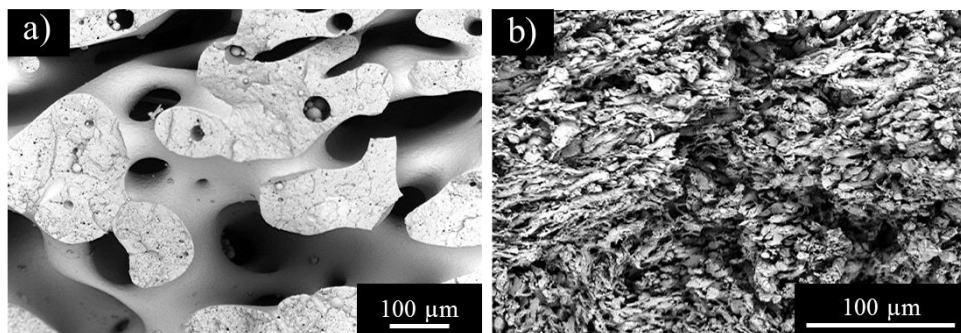


**Figure 10.4** SEM micrographs of (a) the neat HDPE/PEO blend and (b) the blend filled with  $\Phi_{\text{O-Clay}} = 0.0090$ .

The O-Clay induces a drastic downsizing of the polymer phases, and the HDPE scaffold remaining after the removal of PEO exhibits an irregular porous microstructure much finer than that of the unfilled sample.

On the other hand, besides refining the morphology, the penetration of the suspension of ZnO nanoparticles inside the channels of the HDPE scaffold has to be ensured. For this purpose, wettability arguments are invoked. A good affinity between the liquid phase of the suspension and the polymer template is required. The penetrating power of a liquid is equal to the distance which the liquid will penetrate in a capillary tube of unit radius in unit time, when flowing under its own capillary pressure. Such a “penetrativity” is also a function of the nature of the material composing the capillary and the liquid itself, being proportional to  $\cos\vartheta$ , where  $\vartheta$  represents the contact angle [Washburn (1921)]. To verify the relevance of the nature of the liquid medium, two different ZnO suspensions, one in water and the other in butyl acetate, have been employed. The wettability of HDPE films by the two selected liquids has been estimated by contact angle measurements, whose results are summarized in Table 10.2 (see also Figure 10.5).

**Table 10.2** Contact angle of water and butyl acetate on HDPE.

Testing liquid	$\vartheta$ [°]
Water	$96.5 \pm 3.4$
Butyl acetate	$15.7 \pm 2.7$

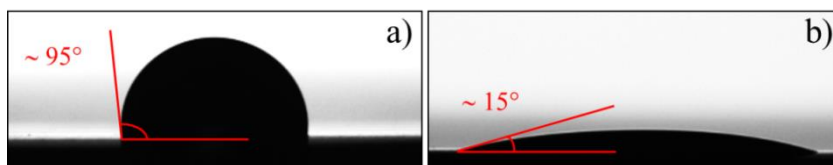


**Figure 10.5** Representative images of the contact angle measurements for HDPE films with (a) water and (b) butyl acetate.

The water contact angle is greater than  $90^\circ$ , hence water cannot penetrate inside the pores of the HDPE scaffold by simply capillary action. In contrast, the value of  $\theta \ll 90^\circ$  for butyl acetate indicates a much higher propensity of such a liquid to penetrate the pores inside the polymeric material. To support such a deduction, two porous samples have been dipped in a water-based suspension of ZnO suspension and in a butyl acetate-based one. Energy dispersive spectroscopy (EDS) is used to infer the presence of the ZnO nanoparticles in the fractured samples. The obtained images are shown in Figure 10.6.

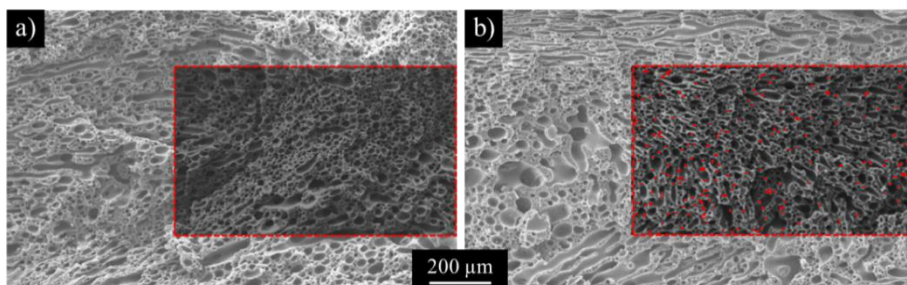


**Figure 10.6** SEM micrographs with the X-ray map of zinc partially superimposed for the blends after immersion in the ZnO suspension in (a) water and (b) butyl acetate.

The EDS mapping of the fracture surfaces of the HDPE scaffolds confirm the presence of ZnO nanoparticles in the porous sample dipped in the butyl acetate-based suspension. It is worth noting that the EDS analysis has been performed in the center of the disk, meaning that the ZnO suspension effectively penetrates deep inside the HDPE scaffold. On the contrary, the water-based suspension cannot access the inner parts of the sample due to the unfavorable contact angle, and no signal related to the filler has been detected. More quantitative proofs of the presence of ZnO nanoparticles come from the thermal gravimetric analyses performed on the HDPE scaffolds dipped into the two colloidal suspensions (see Table 10.3). A residual weight is noticed at high temperature, that is after the

volatilization of the polymer, in both the nanocomposites samples dipped in the different ZnO suspensions. Then, taking as the reference the residual of the PEO-free HDPE scaffold containing O-clay, more than 2 wt% of ZnO nanoparticles (corresponding to  $\Phi_{\text{ZnO}} \sim 0.004$ ) remains trapped in the sample dipped in the butyl acetate-based suspension, compared to little more than 0.5 wt% (corresponding to  $\Phi_{\text{ZnO}} \sim 0.001$ ) of the one immersed in the water-based suspension. In conclusion, all the results previously shown prove the ability of the proposed strategy to effectively entrap hydrophilic ZnO nanoparticles in the hydrophobic HDPE matrix.

**Table 10.3** Residual weight percentage at 700°C of the investigated samples.

<b>Sample</b>	<b>Residual [wt%]</b>
HDPE	0.01
PEO	1.71
HDPE/PEO	0.78
HDPE (PEO extracted)	0.15
HDPE/PEO+C15A	2.32
HDPE+C15A (PEO extracted)	1.68
HDPE+C15A+ZnO (water)	2.37
HDPE+C15A+ZnO (butyl acetate)	3.85

## 10.4 State of dispersion of the nanoparticles

Once the ZnO nanoparticles have been trapped in the HDPE scaffolds, the porous scaffolds are compacted to obtain dense samples. Such a last step of the procedure determines the ultimate space arrangement of the ZnO nanoparticles inside the polymer matrix. EDS analyses have been performed to localize the filler. The SEM micrographs with the X-ray maps of the zinc of the nanocomposites samples prepared by conventional melt mixing and by the template-based approach are compared in Figure 10.7. Although unable to overcome the strong cohesive forces which held together the primary ZnO nanoparticles within the aggregates (as demonstrated in § 10.2), the melt mixing route ensures a good distribution of the filler on micro-scale. On the contrary, the EDS mapping of the compacted sample obtained through the template-based approach reveals an inhomogeneous filler distribution, with ZnO-rich micro-channels intercalated with ZnO-poor regions.

This is in line with what expected: the ZnO suspension can only penetrate the channels of the scaffold, but it cannot permeate their HDPE walls. As a result, micron-sized polymer domains devoid of filler coexist with a continuous network of channels full of nanoparticles. Nonetheless, deriving from isolated ZnO nanoparticles firmly suspended in a the liquid phase, the filler trapped in such a sample is expected to be less aggregated than in the melt mixed one.

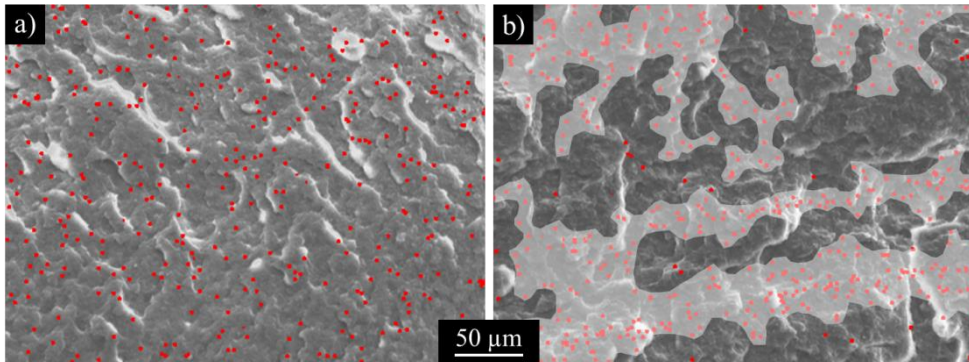


**Figure 10.7** SEM micrographs with the X-ray map of zinc superimposed for nanocomposites obtained by (a) melt mixing and (b) template-based technique.

Again, viscoelastic analyses are used as indirect and yet powerful tool to assess the state of dispersion of the particles. The time evolution of  $G'$  and  $G''$  at low frequency and their frequency dependence are shown in Figure 10.8 for two nanocomposite samples prepared by melt mixing and template-based technique, respectively. Note that the nanocomposites contain both ZnO and O-Clay nanoparticles, the latter remaining trapped in the HDPE during the procedure to prepare the template-based samples and being deliberately added to the melt mixed one for the sake of comparison. Neither the time evolution of  $G'$  at low frequency nor the relaxation spectrum of the melt mixed sample disclose the presence of the filler, confirming the ineffectiveness of such a route in dispersing ZnO nanoparticles within a non-polar matrix such as HDPE. Even possible synergistic effects with a secondary filler such as O-Clay have to be excluded, at least at the investigated filler volume fraction. On the contrary, the filler strongly affects the viscoelasticity of the template-based sample. Specifically, the growth of the low-frequency moduli reflects the structural rearrangements of the nanoparticles, which flocculate in the melt driven by attractive forces. Such a particle mobility has to be ascribed to a finer dispersion of the filler which allows the smaller aggregates to experience the Brownian motions essential for the emergence of the peculiar pseudo solid-like behavior of well dispersed polymer nanocomposites. From the

relaxation spectra collected at the end of the time scan (Figure 10.8b), it can be noticed that the moduli of the template-based sample start to getting flat at low frequency, with a prominent effect on  $G'$ , which increases of more than two order of magnitude with respect to the unfilled matrix despite the low amounts of filler considered. It is worth noting that similar alterations in the viscoelastic behavior cannot be found in the literature for HDPE-based nanocomposites unless performing modifications of the particle surface and/or adding suitable compatibilizers to reduce the chemical incompatibility between the polymer and the filler [Sharif-Pakdaman et al. (2012), Majid et al. (2011), Chae et al. (2006)].

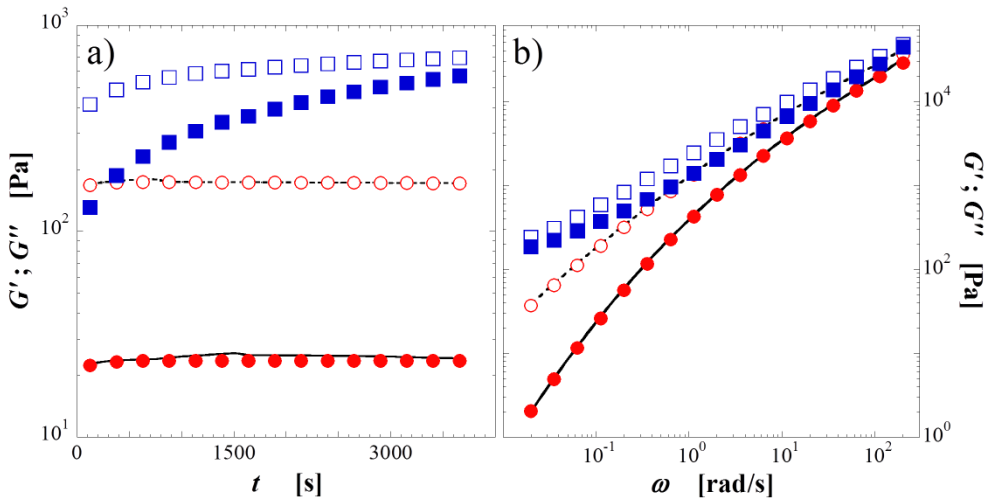


**Figure 10.8** (a) Time evolution and (b) frequency dependence of the elastic (full symbols) and viscous (empty symbols) moduli of the nanocomposites prepared through melt mixing (circles) and template-based method (squares) at  $\Phi_{\text{ZnO}} = 0.0040$  and  $\Phi_{\text{O-Clay}} = 0.0090$ . Solid and dashed lines represent the elastic and viscous moduli of the neat HDPE, respectively.

The viscoelastic behavior has been investigated also in the solid state by means of dynamic mechanical analyses. The elastic,  $E'$ , and viscous,  $E''$ , flexural moduli are shown as a function of temperature in Figure 10.9 for the nanocomposites prepared through the two different approaches and containing the same amounts of ZnO and O-Clay nanoparticles. As in the melt state, the nanoparticles in the template-based sample are much more effective in reinforcing the matrix. Nanoparticles indeed constrain the deformability of the amorphous fraction of HDPE in which they reside, improving the dynamic mechanical moduli. As DSC analyses exclude noticeable alterations of the crystalline structure of the HDPE (Table 10.4), the dynamic-mechanical properties primarily reflect the quality of the filler dispersion.

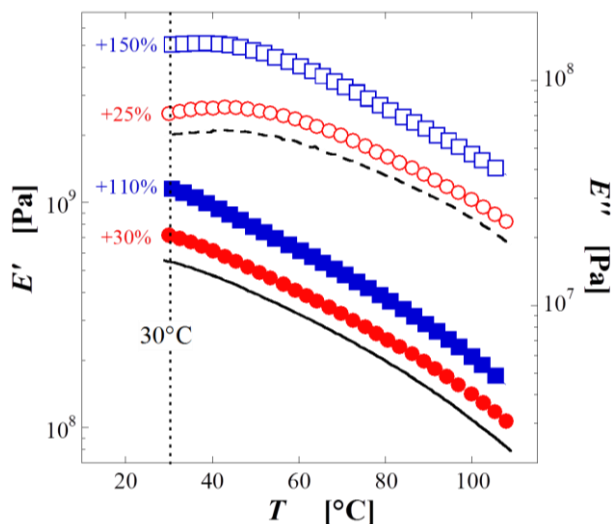


**Figure 10.9** Temperature-dependence of elastic (full symbols) and viscous (empty symbols) flexural moduli of the nanocomposite prepared through melt mixing (circles) and template-based method (squares) at  $\Phi_{\text{ZnO}} = 0.0040$  and  $\Phi_{\text{O-Clay}} = 0.0090$ . Solid and dashed lines are the elastic and viscous flexural moduli of the neat HDPE, respectively.

**Table 10.4** Onset and peak melting temperatures, crystallization temperature and crystallinity of the nanocomposites prepared by melt mixing and template-based method.

Procedure	$T_{\text{m,onset}}$ [°C]	$T_{\text{m,peak}}$ [°C]	$T_{\text{c}}$ [°C]	$\chi_{\text{c}}^a$ [%]
Melt mixing	124.6	128.4	116.3	53.2
Template-based	122.6	128.7	116.1	53.5

<sup>a</sup>  $\chi_{\text{c}}$  values are obtained by dividing the melting enthalpy,  $\Delta H_{\text{f}}$ , of each sample by the  $\Delta H_{\text{f}}$  of a 100% pure crystalline HDPE sample, taken as  $293.1 \text{ J g}^{-1}$  [Wunderlich (1980)].

Finally, the proposed approach is argued to be possibly capitalized to impart specific functionality to the nanocomposite. A similar strategy indeed underpins the double percolation concept, sometimes exploited in case of polymer blends with interfacially-located particles [Sumita et al. (1992)]. The latter condition can be difficult to realize, being dictated by cogent thermodynamic requirements. Differently, the template-based approach in principle could result in low percolation thresholds in monophasic matrices irrespective of wettability considerations.





## Conclusions

Polymer nanocomposites represent a well-established yet still promising class of materials. Actually, new physical properties and novel behaviors that are absent in the unfilled matrix can be provided by the use of nano-sized fillers. In addition, unanticipated improvements and huge dividends are expected in the structural and functional performances if the process could prescribe precise spatial arrangement of the nanoparticles. However, the full exploitation of the exceptional properties arising from the spatial arrangement and ordering of the constituents of polymer nanocomposites is hampered by an inadequate systematic control of the nanoparticles dispersion and material morphology. As thermodynamically out-of-equilibrium materials, indeed, polymer nanocomposites evolve to achieve equilibrium, if provided by sufficient energy. In this process, the nanoparticle rearrange themselves in the melt and typically aggregate, dictating the ultimate microstructure of the material from which its macroscopic performances depend. In this context, the ultimate goal of the research activity reported in the present dissertation is the fundamental study of the physical mechanisms governing the nanoparticle dynamics and connectivity in polymer melts.

In the first part of the dissertation, the study is focused on the restructuring and flocculation processes of nanoparticles in polymer melts. More in detail, the aim of the performed research is to investigate the effect of a reduced or even frustrated mobility of the particles on their dynamics of assembly in polymer melts. To do so, the time evolution of the linear viscoelastic response has been studied for a nanocomposite system based on a biphasic polymer matrix with drop-matrix morphology, in which the filler phase is inclined to gather at the polymer-polymer interface. By anchoring the nanoparticles on the surface of the dispersed polymeric phase, the inherent ability of the nanoparticles to move within the host polymer melt is frustrated, allowing to highlight the key role of the mobility of nanoparticles on their dynamics of assembly. As a result, the evolution of the viscoelastic moduli over time is not affected at all by the presence of the filler, meaning that flocculation phenomena do not take place in the nanocomposite. Nonetheless, above the critical filler content for the saturation of the polymer-polymer interface, the particles are free to rearrange in the host medium. At this threshold, an abrupt jump of the normalized equilibrium elastic modulus is observed, reflecting the “off-to-on” switch of the particle mobility once the filler saturates nearly completely the interface.

The investigation then is directed to the rheological implications of the superstructures formed by the nanoparticles when they are allowed to assemble in the polymer melt. In detail, the study focuses on the space-spanning networks of nanoparticles which build up throughout the host matrix once the filler percolation threshold is exceeded. An evident rheological transition from liquid- to solid-like behavior usually takes place at the percolation threshold and several rheological criteria exists for its identification. However, the performed analyses have proved that recognizing the filler content at which such a transition takes place is not straightforward in the case of nanoparticles characterized by a low bending stiffness. On the other hand, it can be easily accomplished by exploiting a simple two-phase model proposed in the literature for the description of the viscoelasticity of polymer nanocomposites above the percolation threshold. The model typically allows to build a master curve of the elastic modulus for samples at different filler content. The physical constraints invoked when building such master curve are here proved to confer a predictive feature to the model. Indeed, its ability in identifying the elasticity of networks of nanoparticles too weak to be otherwise recognized by conventional viscoelastic measurements is demonstrated. Contextually, the two-phase model is showed to allow to clearly identify the samples whose filler content is below the percolation threshold, which can be thus more accurately estimated. More importantly, the generalization of the model has been proposed and validated, by analyzing the rheological response of different polymer nanocomposite systems. The underlying idea is that the two independent phases envisaged by the model are the neat polymer matrix and the filler network, whose response does not depend on the nature of the nanoparticles. In fact, rather than made of single nanoparticles, the network is composed by bigger structures, namely clusters of nanoparticles, into which the filler reassemble under the effect of Brownian motion and interparticle attraction. The analysis of the linear viscoelastic spectra really demonstrates that the model satisfactorily describes the viscoelasticity of nanocomposite systems differing among them both in the nature of the nanoparticles and in the affinity between the polymer and filler phases. Such a finding confers wide generality to the two-phase model. The latter is thus expected to be useful to describe a wide variety of other kinds of complex fluids in which a superposition of the elasticity of the components is possible. Actually, a further test of the robustness of the approach has been given by verifying the ability of the model to satisfactorily describe the linear viscoelasticity of nanocomposites based on a biphasic polymer matrix having drop-matrix morphology. In such a system, an additional elastic contribution with respect to homogenous fluid media exists, arising from the interfacial relaxation processes. Nonetheless, the two-phase model perfectly works, demonstrating that the overall relaxation dynamics can be still interpreted in terms of only two main populations of dynamical species. Concerning the features of the formed network, however, fractal models have revealed that, with respect to systems based on a homogeneous polymer medium,

the presence of a dispersed polymer phase hinders the free growth of the particle clusters yet providing them additional elasticity.

In the end, the gained fundamental knowledge on the linear viscoelasticity of polymer nanocomposites is exploited for technological purposes. The study has been targeted to the investigation of the effect of material- and process-related factors on the filler state of dispersion in the final system. In detail, two case studies particularly relevant in the field of polymer nanocomposite science have been faced: (i) the difficulties related to the de-agglomeration and dispersion of carbon nanotubes during the mixing with the polymer and (ii) the dispersion of hydrophilic nanoparticles in hydrophobic polymer matrices. For the specific case of carbon nanotubes, rheological measurements have been employed to ascertain the role of filler morphology on its dispersability in polymer melts and the resulting thermal and mechanical properties of the nanocomposite have been assessed. It turns out that the internal structure of the primary aggregates of carbon nanotubes represents a key parameter in ensuring the production of highly dispersed polymer nanocomposites, without the alteration of the integrity of the particles. Concerning the second task, a novel compounding technique has been proposed. The aim is to couple the good filler dispersion typically attained by solution-based methods with the feasibility of conventional melt mixing. Specifically, the procedure envisages the permeation of a well dispersed nanoparticle suspension inside a micro-porous matrix, obtained through selective extraction of a sacrificial phase from a finely interpenetrated co-continuous polymer blend. Linear viscoelastic analyses have been exploited to demonstrate the effectiveness of the proposed approach.





# Methods

*In this section all the experimental details have been collected. The selected raw materials are listed. Then, the processing conditions used for the preparation of the polymer nanocomposites are reported. The exploited characterization methods and the testing conditions are finally specified.*

## Raw materials

Throughout the research activity four different polymeric materials have been used. Specifically, the selected polymers are:

- (i) atactic polystyrene (PS, Edistir<sup>®</sup> 2982 by Polimeri Europa) with glass transition temperature  $T_g = 100^\circ\text{C}$ ;
- (ii) poly(methyl methacrylate) (PMMA, Optix<sup>®</sup> CA-51 by Plaskolite Inc.) with glass transition temperature  $T_g = 110^\circ\text{C}$ ;
- (iii) high density polyethylene (HDPE, code 427985 by Sigma-Aldrich, Italy) with melt flow index  $\text{MFI}_{190^\circ\text{C}/2.16\text{ kg}} = 12\text{ g}\cdot\text{min}^{-1}$ ;
- (iv) poly(ethylene oxide) (PEO, code 181986 by Sigma-Aldrich, Italy) with molecular weight  $M_w = 100\text{ kDa}$ .

Concerning the filler phase of the nanocomposites, various kinds of nanoparticle differing among them in terms of size and shape have been chosen. In detail, the used nanofillers are listed in the following:

- (i) organo-modified montmorillonite (O-Clay, Cloisite<sup>®</sup> 15A by Southern Clay Products, Inc.) having an organic content of  $\sim 43\%$  (dimethyl dihydrogenated tallow quaternary ammonium salt) and a mass density of  $1.66\text{ g}\cdot\text{cm}^{-3}$ ;
- (ii) graphite nanoplatelets (GNPs) obtained from graphite intercalated compounds (GICs, by Faima S.r.l., Italy) and having a mass density of  $2.1\text{ g}\cdot\text{cm}^{-3}$  (the same density of pure graphite has been assumed);
- (iii) unfunctionalized multi-walled carbon nanotubes (MWCNTs), commercial grade (Baytubes<sup>®</sup> C150P by Bayer MaterialScience, Germany) and synthesized ad hoc ones. Both the MWCNTs have a mass density of  $2.1\text{ g}\cdot\text{cm}^{-3}$  (the same density of pure graphite has been assumed);
- (iv) zinc oxide (ZnO) nanoparticles with average dimension of the primary particles of 32 nm and mass density of  $\sim 5\text{ g}\cdot\text{cm}^{-3}$ .

All the previous nanoparticles have been purchased/synthesized and used in the form of dry powders. In addition, two colloidal suspensions of zinc oxide nanoparticles have been purchased from Sigma Aldrich: a water-based dispersion of particles of size <100 nm (50 wt% of ZnO, code 721077) and a dispersion of particle of size <110 nm in butyl acetate (40 wt% of ZnO, code 721093).

For the sake of clarity, each material is related to the corresponding Chapter(s) in Table M.1.

**Table M.1** Selected raw materials, both polymer and filler phases, and corresponding Chapter(s).

	<b>Material</b>	<b>Chapter(s)</b>
POLYMERIC CONSTITUENTS	PS	3, 5-7, 9
	PMMA	3, 7
	HDPE	10
	PEO	10
FILLERS	O-Clay	3, 6, 7, 10
	GNPs	3, 5, 6
	Commercial MWCNTs	9
	Synthesized MWCNTs	6, 9
	ZnO nanoparticles – dry powders	10
	Colloidal suspensions of ZnO nanoparticles	10

Finally, further specifications are need for the procedure followed for the GNPs and the synthesized MWCNTs.

Briefly, to obtain GNPs, GIC flakes have been subjected to thermal shock in a muffle furnace at about 800°C for about 60 s. The resulting expanded graphite (EG) has been dispersed in N,N-dimethylformamide (DMF) (EG/DMF ratio ~0.0013 g/ml) and ultrasonicated (Ultrasonic Processor 750W by Branson) at room temperature for 45 min.

Concerning the MWCNTs, the particles have been synthesized in a large scale (500 g/batch) fluidized bed reactor using a  $\gamma$ -alumina substrate impregnated with iron as catalyst [Mazzocchia et al. (2010)], ethylene as carbon source, hydrogen and nitrogen as fluidizing agents. The reaction has been carried out at T = 600°C and at atmospheric pressure. The reaction has been monitored by an on-line gas-

chromatograph (Double Channel MicroGC 3000 Agilent) to evaluate in real-time the ethylene conversion and the yield of the reaction; the average duration of the synthesis is about 120 min. Then, the pristine MWCNTs have been purified in a three phase slurry bubble vessel through a three-step liquid phase acid treatment: (i) refluxing sulfuric acid solution to dissolve catalyst particles; (ii) water washing to remove the amount of acid; (iii) drying to remove the remaining water.

## Nanocomposite preparation

The nanocomposites samples have been all prepared by melt mixing using a twin-screw micro-compounder (Xplore by DSM). All the extrusion have been performed in nitrogen atmosphere and accurately controlling the residence time by means of a backflow channel. Note that before each extrusion all the constituents have been dried overnight under vacuum.

Specifically, the PS/O-Clay and PS/PMMA/O-Clay nanocomposites have been prepared at  $T = 190^{\circ}\text{C}$  and 150 rpm, roughly corresponding to average shear rates of  $\sim 75\text{ s}^{-1}$  (constituents dried at  $90^{\circ}\text{C}$ ). The PS/GNPs samples have been processed at  $T = 200^{\circ}\text{C}$  and 150 rpm (constituents dried at  $90^{\circ}\text{C}$ ). The PS/MWCNTs nanocomposites (both with commercial and synthesized nanotubes) have been obtained by diluting with neat PS a masterbatch at  $\sim 6\text{ wt.}\%$  of filler (constituents dried at  $90^{\circ}\text{C}$ ). The extrusions for the preparation of the masterbatch and those for the dilutions have been all carried out at  $T = 200^{\circ}\text{C}$  and 200 rpm. Similarly, the HDPE/ZnO samples have been obtained through the dilution at  $150^{\circ}\text{C}$  and 200 rpm of a masterbatch of HDPE at high content of dry ZnO nanoparticles ( $\sim 7\text{ wt.}\%$ ). Note that ZnO-based nanocomposites have been also prepared through a novel compounding method, namely the template-based approach, whose experimental details can be found in Chapter 10. Here it is just specified that the filled blend made of HDPE/PEO/O-Clay which serves in the template-based approach has been prepared by melt mixing at  $150^{\circ}\text{C}$  and 100 rpm (constituents dried at  $50^{\circ}\text{C}$ ).

Further specifications are need for the procedure followed for the PS/GNPs nanocomposite samples. Before the melt mixing step, indeed, the dispersion of GNPs has been mixed with a solution of PS in DMF (PS/DMF ratio  $\sim 0.02\text{ g/ml}$ ) and ultrasonicated again for 45 min. This step is necessary to stabilizes the dispersion owing to the emulsifying action of the polymer chains. Spilling the DMF-based polymer/particle mixture into distilled water (1:15, v/v) under stirring causes the precipitation of polymer and filler, which are then separated through vacuum filtration. The resulting GNP-rich PS powder, dried under vacuum to remove the residual solvent, has been melt mixed with neat PS to adjust the composition.

Finally, the specimens for the subsequent analyses have been produced in the desired shape by compression molding at the same temperature at which the extrusions have been carried out.

## Characterization techniques

The viscoelastic behavior of all the investigated polymer nanocomposite systems have been characterized by time sweep experiment and frequency sweep ones. All the measurements have been performed in the linear viscoelastic regime, which have been identified by strain sweep analyses. Time sweep tests have been carried out at low frequency ( $\omega = 0.1 \text{ rad s}^{-1}$ ) and the tests have been stopped only once the viscoelastic moduli have reached a time-independent value. Frequency sweep tests have been conducted in the frequency range  $\omega = 0.02 \div 200 \text{ rad s}^{-1}$ . In Table M.2 is reported the temperature at which the measurements have been carried out.

**Table M.2** Temperatures of the rheological analyses.

System	<i>T</i> - time sweeps	<i>T</i> - frequency sweeps
PS/O-Clay; PS/PMMA/O-Clay	190°C	190°C
PS/GNPs	200°C	180°C
PS/MWCNTs (both kinds)	220°C	200°C
HDPE/ZnO (both methods)	180°C	180°C

Thermogravimetric analyses have been performed on all nanocomposite samples to accurately estimate the filler content using a Q5000 TGA apparatus (TA Instruments). The samples have been heated up to 700°C at 10°C·min<sup>-1</sup> in nitrogen atmosphere. For each sample, the actual content of filler in the nanocomposite is estimated as the residual weight at  $T = 600^\circ\text{C}$ .

In the following the details of the analyses other than rheological measurements are reported for each nanocomposite system investigated.

### PS/O-Clay and PS/PMMA/O-Clay nanocomposites

Wide angle X-ray diffractometry (WAXD) has been performed on the pristine O-Clay and representative nanocomposites using a Siemens D-500 diffractometer with Cu K $\alpha$  radiation ( $\lambda = 0.154 \text{ nm}$ ). Scans have been taken in the range  $2\theta = 2 \div 10^\circ$  with a step size of  $0.02^\circ$ .

The morphology of the PS/O-Clay and PS/PMMA/O-Clay samples at the nanoscale has been inspected through transmission electron microscopy (TEM, Tecnai G2 Spirit Twin T-12 by FEI). The specimens are slices with thickness  $\sim 100 \text{ nm}$ , cut at room temperature using a Leica EM UC7 ultra-microtome equipped with a diamond knife.

### **PS/GNPs nanocomposites**

Wide angle X-ray diffractometry (WAXD) has been performed on GIC, EG, and GNP powders using a Siemens D-500 diffractometer with Cu K $\alpha$  radiation ( $\lambda = 0.154$  nm). Scans have been taken in the range  $2\theta = 2 \div 40^\circ$  with a step size of  $0.02^\circ$ .

Both scanning (SEM, FEI Quanta 200) and transmission (TEM, Philips EM208) electron microscopy have been performed. The PS/GNPs nanocomposites for SEM analyses are cryo-fractured using liquid nitrogen and the surfaces have been sputter coated with gold before observations. Micrographs have been also taken on GIC and EG bare particles. The samples for TEM analyses are  $\sim 150$  nm-thick slices cut at room temperature using a diamond knife.

The DC volume conductivity has been estimated at room temperature using a FUG HCN35-6500 high voltage generator and a Keithley 6514 pico-ammeter.

### **PS/MWCNTs nanocomposites (both commercial and synthesized particles)**

Transmission electron microscopy (TEM, Tecnai G2 Spirit Twin T-12 by FEI) has been carried out on the pristine powders to evaluate the diameter and length of the single MWCNTs. Scanning electron microscopy (SEM, ZEISS EVO 50 EP apparatus) has been performed on the dry powders to investigate the morphology of the primary aggregates. A CILAS 1180 L particle size analyzer has been used to assess the dimensions of the primary aggregates. TEM analyses on the nanocomposite has been performed through a Philips EM208 apparatus on  $\sim 150$  nm-thick slices cut at room temperature using a diamond knife.

Dielectric spectroscopy has been carried out at room temperature on the disks recovered at the end of rheological tests. Measurements has been performed using a rotational rheometer (ARES, Rheometrics Scientific) equipped with a dielectric thermal analysis tool, constituted by a couple of stainless steel parallel plates ( $d = 25$  mm) connected with a LCR Meter (E4980A, Agilent). Five independent measurements have been performed for each sample.

Dynamic mechanical analyses have been carried out using a Tritec 2000 DMA apparatus (Triton Technology Ltd., Grantham). The measurements have been carried out in single-cantilever bending mode at a frequency of 1 Hz and with a total displacement of 0.02 mm, which is small enough to be in the linear regime. The heating rate has been set to  $2^\circ\text{C min}^{-1}$ . Three independent measurements have been performed for each sample.

### **HDPE/ZnO nanocomposites (both melt mixed and template-based samples)**

Differential scanning calorimetry has been performed under nitrogen flow using a Q20 DSC apparatus (TA Instruments). The samples are first heated from room

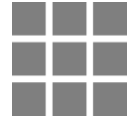
temperature up to 170°C, then cooled down to 25°C, and finally heated again. Each step has been performed at a rate of 10°C min<sup>-1</sup>.

The tensile properties have been estimated at room temperature and humidity using an Instron machine according to ASTM test method D882. The samples, stored at room temperature and humidity, have been tested at 25 mm·min<sup>-1</sup> up to a strain of 2%, then the speed has been increased up to 50 mm·min<sup>-1</sup> until break. Eight independent measurements have been performed for each sample.

The permeability to oxygen (P<sub>O<sub>2</sub></sub>) and carbon dioxide (P<sub>CO<sub>2</sub></sub>) have been measured at 30°C and atmospheric pressure using a constant volume-variable pressure apparatus.

The microstructure of the neat and filled HDPE/PEO blends has been investigated through scanning electron microscopy (FE-SEM, Ultraplus by Zeiss). The samples have been cracked in liquid nitrogen and the fracture surfaces have been observed. Energy dispersive spectroscopy (EDS, Aztec by Oxford Instruments) has been used to infer the presence of the ZnO nanoparticles in the samples obtained by the template-based approach and to investigate the distribution of the filler on micro-scale. The static contact angle of water and butyl acetate on HDPE films surface has been estimated with an automatic video-based measurement of contact angle performed at room temperature and humidity by using a Theta contact angle T200-Auto (KSV/Attension, Helsinki). Five µL of liquid have been placed over the HDPE surface and the Young/Laplace method is used to calculate the static contact angle. Five independent measurements have been performed for each liquid.

Dynamic mechanical analyses have been carried out using a Tritec 2000 DMA apparatus (Triton Technology Ltd., Grantham). The measurements have been carried out in single-cantilever bending mode at a frequency of 1 Hz and with a total displacement of 0.02 mm, which is small enough to be in the linear regime. The heating rate has been set to 2°C min<sup>-1</sup>. Three independent measurements have been performed for each sample.



# Appendices

*In this section additional data and plots are provided. Aiming at preserving the fluency, the data which are not strictly necessary to the discussion of the results presented throughout the dissertation have been collected separately. In detail, each paragraph here is dedicated to a Chapter in order to shown, when needed, further experimental data.*

## Appendix to Chapter 6

### Amplifying factor and shift factor used to build the master curves

The amplifying factors,  $B(\Phi)$ , and the  $G''(\omega)$  curves of the pure matrices on which the shift factors ( $a_\Phi$ ;  $b_\Phi$ ) lie are shown in Figure A6.1 and A6.2, for the master curves of Figure 6.4 and 6.7, respectively. The corresponding numerical values are given in Table A6.1 and A6.2.

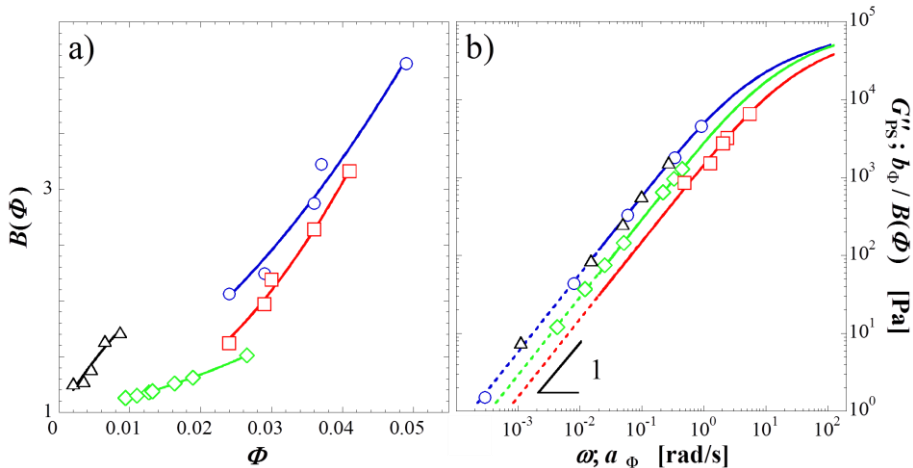


**Figure A6.1** (a) Amplification factors as a function of filler content and (b) shift factors used to scale the  $G'$  curves of the PS/GNPs (circles), PS/O-Clay (diamonds), PS/MWCNTs (triangles) and PS/SiO<sub>2</sub> (squares) samples. Solid lines are (a) guides for the eye and (b) viscous moduli of the unfilled PS at  $T = 180^\circ\text{C}$  (blue),  $190^\circ\text{C}$  (green) and  $200^\circ\text{C}$  (red).

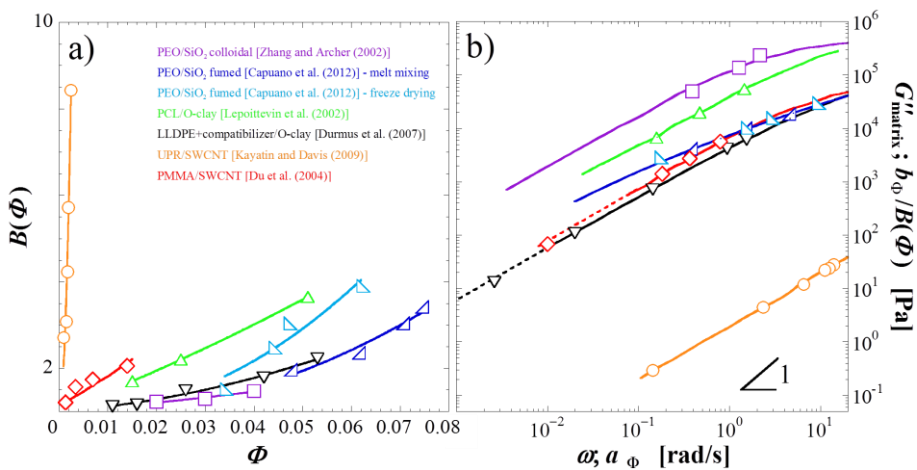


**Figure A6.2** (a) Amplification factors as a function of filler volume fraction and (b) shift factors used to scale the  $G'$  curves. In part (a), solid lines are guides for the eye. In part (b), solid lines represent the viscous modulus of the unfilled matrices of the nanocomposites.

**Table A6.1** Amplification factors ( $B(\Phi)$ ) and shift factors ( $a_\phi, b_\phi$ ) of each scaled  $G'$  curve.

System	$\Phi$ of the scaled $G'$ curves	$B(\Phi)$	$a_\phi$ [rad/s]	$b_\phi$ [Pa]
PS+GNPs	0.049	4.13	0.91	18699.9
	0.037	3.22	0.34	5780.1
	0.036	2.87	0.059	937.6
	0.029	2.24	0.0080	97.3
	0.024	2.06	0.00029	3.1
PS+O-clay	0.0265	1.51	0.45	1942.2
	0.0189	1.31	0.33	1256.3
	0.0163	1.26	0.22	812.7
	0.0132	1.19	0.051	171.5
	0.0127	1.18	0.025	88.3
	0.0110	1.15	0.012	42.7
	0.0094	1.13	0.0043	13.6
PS+MWCNTs	0.0086	1.72	0.27	2682.7
	0.0065	1.64	0.098	939.7
	0.0045	1.39	0.049	352.6
	0.0035	1.28	0.015	110.4
	0.0020	1.26	0.0011	7.6

**Table A6.2** Amplification factors ( $B(\Phi)$ ) and shift factor pairs ( $a_\Phi, b_\Phi$ ) of each scaled  $G'$  curve.\*\*

System	$\Phi$ of the scaled $G'$ curves	$B(\Phi)$	$a_\Phi$ [rad/s]	$b_\Phi$ [Pa]
PEO+SiO <sub>2</sub> colloidal [Zhang and Archer (2002)]	0.04	1.47	2.16	288494
	0.03	1.29	1.27	177830
	0.02	1.23	0.39	72239
PEO+SiO <sub>2</sub> fumed (melt mixed samples) [Capuano et al. (2012)]	0.075	3.42	57.58	230264.9
	0.071	3.04	4.80	56712.9
	0.062	2.36	1.59	23551.7
	0.048	1.97	0.40	8258.5
PEO+SiO <sub>2</sub> fumed (freeze dried samples) [Capuano et al. (2012)]	0.062	3.91	9.11	116135.3
	0.047	3.04	2.85	47665.7
	0.044	2.48	1.50	25519.1
	0.034	1.52	0.17	4343.8
PCL+O-clay [Lepoittevin et al. (2002)]	0.051	3.65	1.45	198654
	0.025	2.20	0.47	43499
	0.015	1.70	0.16	11349
LLDPE+compatibilizer +O-clay [Durmus et al. (2007)]	0.053	2.23	1.53	13698.3
	0.042	1.79	0.93	7441.0
	0.026	1.49	0.14	1074.1
	0.016	1.16	0.021	125.7
	0.011	1.12	0.0026	15.6
UPR+SWCNTs [Kayatin and Davis (2009)]	0.0025	8.43	14.1	235.6
	0.0020	5.72	12.4	136.6
	0.0018	4.23	11.2	93.3
	0.0015	3.08	6.53	36.6
PMMA+SWCNTs [Du et al. (2004)]	0.0010	2.71	2.35	12.1
	0.0140	2.06	0.792	11787.7
	0.0069	1.74	0.367	4812.1
	0.0034	1.57	0.183	2217.5
	0.0014	1.21	0.012	94.9

\*\* Slight differences with the values reported in Filippone and Salzano de Luna (2012) are due to approximations in the cut off of the decimals.

## Appendix to Chapter 7

### Amplifying factor and shift factor used to build the master curves

The analytical expression of the elastic and viscous moduli of the neat PS and PMMA have been estimated by fitting the experimental data to the generalized Maxwell model for a series of  $n$  terms. By exploiting the software RSI Orchestrator by Rheometric Scientific, the best fitting has been obtained for a series of 7 elements. The resulting parameters are reported for in Table A7.1.

**Table A7.1** Parameters obtained fitting the experimental data of the viscoelastic moduli of the neat PS and PMMA to the generalized Maxwell model.

Material	$J_i$ [Pa]	$U_i$ [rad/s]	$L_i$ [Pa]	$Y_i$ [rad/s]
PS	61954.1	0.00167	107740	0.00167
	44990.2	0.00775	35546.7	0.00775
	24879	0.03596	27521	0.03596
	6844.18	0.16686	6395.66	0.16686
	549.356	0.7742	631.842	0.7742
	9.179	3.59212	1.9084	3.59212
	0.19539	16.6667	1.56755	16.6667
PMMA	162820	0.0025	231120	0.0025
	106730	0.01159	91054	0.01159
	79652.2	0.0538	86747.7	0.0538
	37434.4	0.24978	37441.1	0.24978
	9103.93	1.15972	9724.06	1.15972
	618.912	5.38452	760.938	5.38452
	8.40048	25	71.9841	25

### Amplifying factor and shift factor used to build the master curves

The amplifying factors,  $B(\Phi)$ , and the  $G''(\omega)$  curves of the pure matrices on which the shift factors ( $a_\Phi$ ;  $b_\Phi$ ) used to build the master curves of Figure 7.7 lie are shown in Figure A7.1 and the corresponding numerical values are given in Table A7.2.

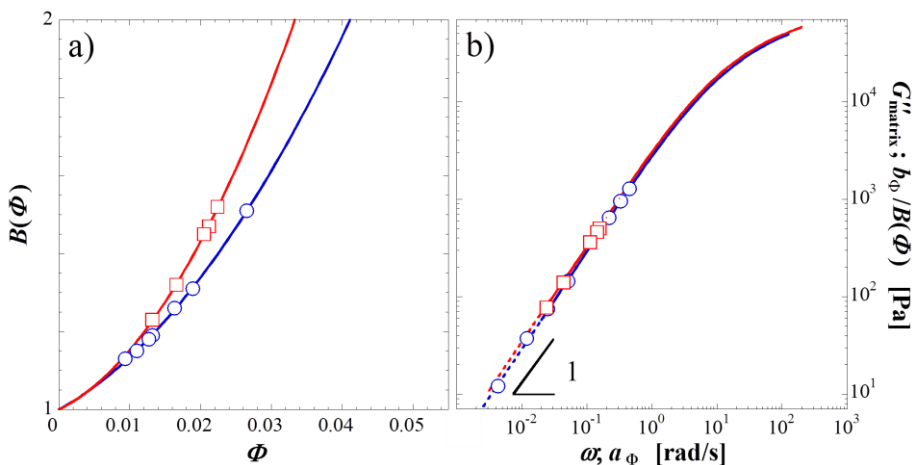


**Figure A7.1** (a) Amplification factors as a function of filler volume fraction and (b) shift factors used to scale the  $G'$  curves of the PS/O-Clay (circles) and PS/PMMA/O-Clay (squares) nanocomposites. In part (a), solid lines are guides for the eye. In part (b), lines represent the viscous modulus of the unfilled PS (blue) and PS/PMMA (red). Dashed lines are the extrapolations according to terminal Maxwellian behavior.

**Table A7.2** Amplification factors ( $B(\Phi)$ ) and shift factor pairs ( $a_\phi$ ,  $b_\phi$ ) of each scaled  $G'$  curve.

System	$\Phi$ of the scaled $G'$ curves	$B(\Phi)$	$a_\phi$ [rad/s]	$b_\phi$ [Pa]
PS/O-clay	0.0265	1.51	0.45	1942.2
	0.0189	1.31	0.33	1256.3
	0.0163	1.26	0.22	812.7
	0.0132	1.19	0.051	171.5
	0.0127	1.18	0.025	88.3
	0.0110	1.15	0.012	42.7
	0.0094	1.13	0.0043	13.6
PS/PMMA/O-Clay	0.0224	1.52	0.157	763.3
	0.0212	1.47	0.143	674.3
	0.0205	1.45	0.113	525.7
	0.0166	1.32	0.044	185.0
	0.0132	1.23	0.024	94.8

## Image analysis and estimation of the box-counting fractal dimension

Concerning the image analysis carried out to estimate the box-counting fractal dimension, the adopted procedure is the following:

(i) the images have been adjusted and equalized to their basic tones and the position of the dark pixels has been obtained through the indices of the low tone image (Figure A7.2);

(ii) the clusters of particles have been identified by assuming that two clay tactoids belong to the same floc if their minimum distance is smaller than 100 nm, i.e. about one tenth of the average lateral dimension of the tactoids (Figure A7.3);

(iii) each identified cluster has been isolated, extracted from the image and subjected to fractal analysis.

The two-dimensional box counting fractal dimension  $D_f$  has been estimated through the counting boxes algorithm. Briefly, the algorithm divides the image into equal-sized square blocks, and then it tests each block to check if it meets a selected criterion: the presence in the box of a fraction of black pixels higher than 25% is considered a positive correspondence. This procedure is repeated for all possible image tessellation, collecting the total number of positive correspondences, hereafter named “counts”.

The result of the box counting algorithm is shown in Figure A7.4 for two representative (a) PS/O-Clay and (b) PS/PMMA/O-Clay samples.

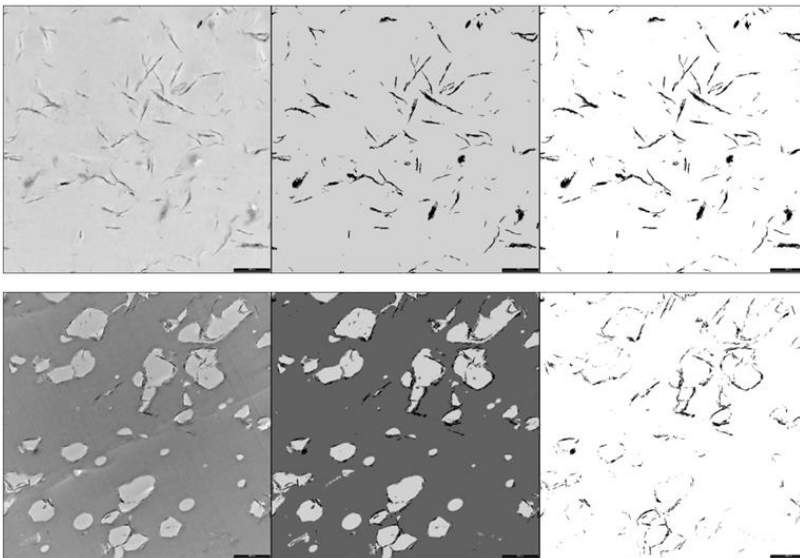


**Figure A7.2** Example of the preprocessing step for two representative PS/O-Clay (top-row) and PS/PMMA/O-Clay (bottom-row) samples at  $\Phi = 0.0132$ .

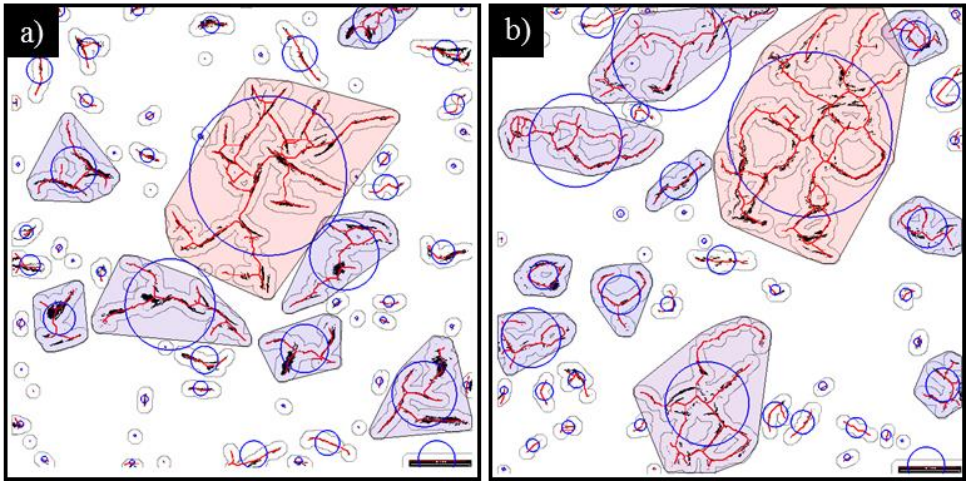


**Figure A7.3** Identification of the particle clusters and image segmentation for two representative (a) PS/O-Clay and (b) PS/PMMA/O-Clay samples at  $\Phi = 0.0132$ . The shaded areas display the identified flocs. Small objects have not been considered in the analyses.

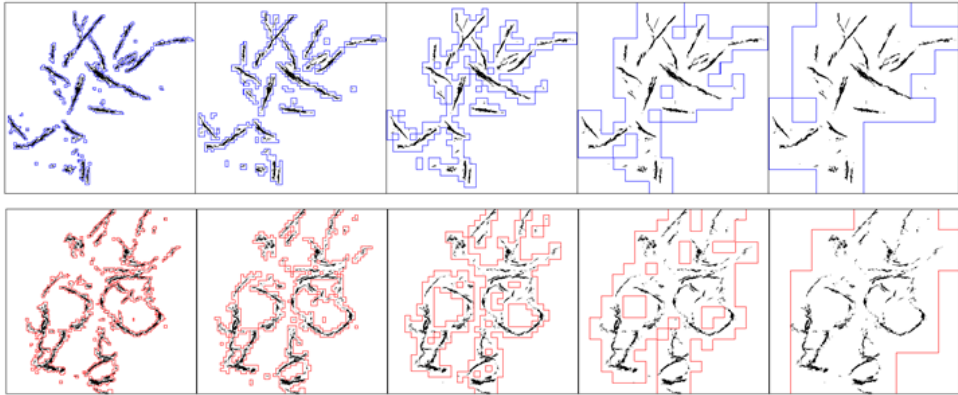


**Figure A7.4** Counting box snapshots at several box lengths (from left to right: 8, 16, 32, 64, and 128 pixels) for two representative PS/O-Clay (top-row) and PS/PMMA/O-Clay (bottom-row) samples at  $\Phi = 0.0132$ .

## Appendix to Chapter 9

### Characteristics of the multi-walled carbon nanotubes

The characteristics of the used nanotubes are summarized in the Table A9.1.

**Table A9.1** Main features of the synthesized and commercial MWCNTs.

Property	Synthesized MWCNTs	Commercial MWCNTs
Carbon purity	> 99% <sup>a</sup>	≥ 95% <sup>b</sup>
Outer mean diameter	~ 10 nm <sup>c</sup>	~ 10.5 nm <sup>d</sup>
Mean length	~ 720 nm <sup>e</sup>	~ 770 nm <sup>d</sup>
$I_D/I_G$ ratio <sup>f</sup>	1.21 ± 0.15	1.22 ± 0.04
Aggregate average size	103 ± 63 μm <sup>g</sup>	382 ± 122 μm <sup>g</sup>
Bulk density	90 – 120 Kg/m <sup>3</sup> <sup>h</sup>	130 – 150 Kg/m <sup>3</sup> <sup>h</sup>

<sup>a</sup> From thermal gravimetric analyses. <sup>b</sup> Taken from [Product Information Baytubes® C150P]. <sup>c</sup> From image analyses of transmission electron micrographs. <sup>d</sup> Taken from [Castillo et al. (2011)]. <sup>e</sup> From the analyses of TEM images following the same procedure of Krause et al. (2011b) (see also Figure A9.1). <sup>f</sup> Ratio between the intensity of the *D* (1280-1350 cm<sup>-1</sup>) and *G* (1580-1600 cm<sup>-1</sup>) bands as deduced through Raman spectroscopy. <sup>g</sup> From particle size analyses. <sup>h</sup> According to EN ISO 60 norm.

The number distribution of lengths estimated on about 100 nanotubes according to the procedure proposed by Krause et al. (2011b) is shown in Figure A9.1 together with the characteristic values  $x_{10}$ ,  $x_{50}$  and  $x_{90}$ .

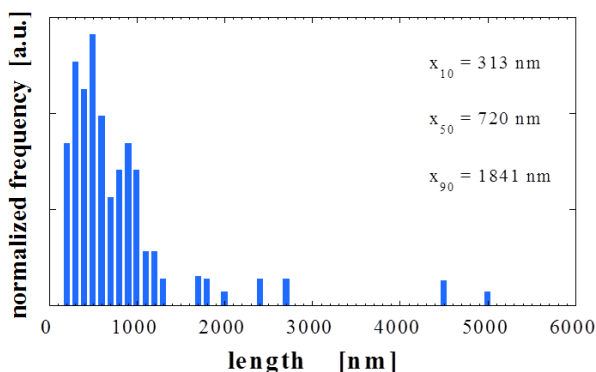


**Figure A9.1** Length distribution of the synthesized nanotubes.

### Amplifying factor and shift factor used to build the master curves

The amplifying factors,  $B(\Phi)$ , and the  $G''(\omega)$  curves of the pure matrices on which the shift factors ( $a_\Phi$ ;  $b_\Phi$ ) used to build the master curves of Figure 9.4 lie are shown in Figure A9.2 and the numerical values are given in Table A9.2.

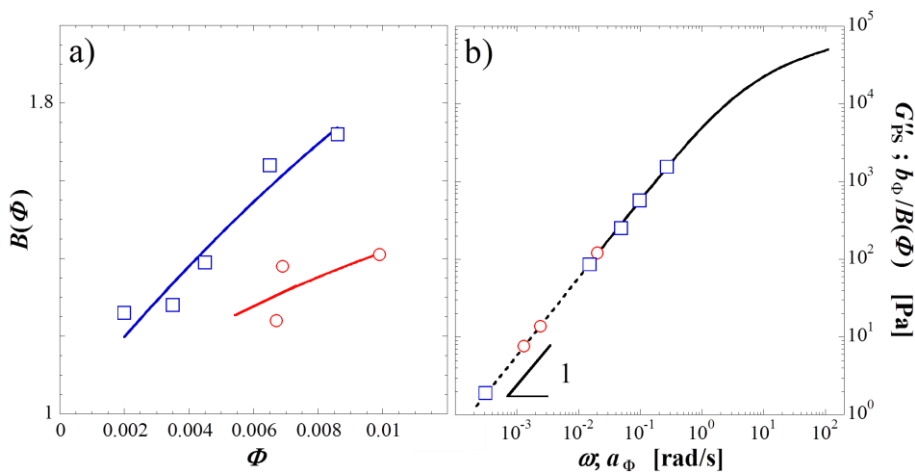


**Figure A9.2** (a) Amplification factors as a function of filler volume fraction and (b) shift factors used to scale the  $G'$  curves of the PS/synthesized MWCNTs (circles) and PS/commercial MWCNTs (squares) nanocomposites. In part (a), lines are guides for the eye. In part (b), the line is the viscous modulus of the unfilled PS as a function of frequency.

**Table A9.2** Amplification factors ( $B(\Phi)$ ) and shift factor pairs ( $a_\Phi$ ,  $b_\Phi$ ) of each scaled  $G'$  curve.

System	$\Phi$ of the scaled $G'$ curves	$B(\Phi)$	$a_\Phi$ [rad/s]	$b_\Phi$ [Pa]
PS+synthesized MWCNTs	0.0086	1.72	0.27	2682.7
	0.0065	1.64	0.098	939.7
	0.0045	1.39	0.049	352.6
	0.0035	1.28	0.015	110.4
	0.0020	1.26	0.0011	7.6
PS+commercial MWCNTs	0.0099	1.41	0.020	170.6
	0.0069	1.38	0.0024	19.12
	0.0067	1.23	0.0013	9.4





## *References*

- Acierno D, Filippone G, Romeo G, Russo P, “Dynamics of stress bearing particle networks in poly (propylene)/alumina nanohybrids”, *Macromol Mater Eng* 292, 347-353 (2007a).
- Acierno D, Filippone G, Romeo G, Russo P, “Rheological aspects of PP-TiO<sub>2</sub> micro and nanocomposites: a preliminary investigation”, *Macromol Symp* 247, 59-66 (2007b).
- Agrawal M, Gupta S, Zafeiropoulos NE, Oertel U, Häßler R, Stamm M, “Nano-level mixing of ZnO into poly(methyl methacrylate)”, *Macromol Chem Phys* 211, 1925-1932 (2010).
- Akcora P, Kumar SK, Moll J, Lewis S, Schadler LS, Li Y, Benicewicz BC, Sandy A, Narayanan S, Ilavsky J, Thiyagarajan P, Colby RH, Douglas JF, “Gel-like mechanical reinforcement in polymer nanocomposite melts”, *Macromolecules* 43, 1003-1010 (2010).
- Alig I, Pötschke P, Lellinger D, Skipa T, Pegel S, Kasaliwal GR, Villmow T, “Establishment, morphology and properties of carbon nanotube networks in polymer melts”, *Polymer* 53, 4-28 (2012).
- Alig I, Skipa T, Lellinger D, Pötschke P, “Destruction and formation of a carbon nanotube network in polymer melts: Rheology and conductivity spectroscopy”, *Polymer* 49, 3524-3532 (2008).
- Althues H, Henle J, Kaskel S, “Functional inorganic nanofillers for transparent polymers”, *Chem Soc Rev* 36, 1454-1465 (2007).
- Anderson PW, “More is different”, *Science* 177, 393-396 (1972).
- Arbabi S and Sahimi M, “Mechanics of disordered solids. I. Percolation on elastic networks with central forces”, *Phys Rev B* 47, 695-702 (1993).
- Baekeland LH, “Bakelite, a new composition of matter: Its synthesis, constitution, and uses”, *Sci Am* 68, 322 (1909).
- Bai JB and Allaoui A, “Effect of the length and the aggregate size of MWNTs on the improvement efficiency of the mechanical and electrical properties of

- nanocomposites - experimental investigation”, *Compos Part A* 34, 689-694 (2003).
- Bailly M, Kontopoulou M, El Mabrouk, K, “Effect of polymer/filler interactions on the structure and rheological properties of ethylene-octene copolymer/nanosilica composites”, *Polymer* 51, 5506-5515 (2010).
- Baird DG and Collias DI, “Polymer Processing Principles and Design”, Butterworth-Heinemann, Newton, MA (1995).
- Balazs AC, Emrick T, Russell TP, “Nanoparticle polymer composites: where two small worlds meet”, *Science* 314, 1107-1110 (2006).
- Bandyopadhyay R, Liang D, Harden JL, Leheny RL, “Slow dynamics, aging, and glassy rheology in soft and living matter”, *Solid State Commun* 139, 589-598 (2006).
- Bauhofer W and Kovacs JZ, “A review and analysis of electrical percolation in carbon nanotube polymer composites” *Compos Sci Technol* 69, 1486-1498 (2009).
- Bonn D, Kellay H, Tanaka H, Wegdam G, Meunier J, “Laponite: What is the difference between a gel and a glass?”, *Langmuir* 15, 7534-7536 (1999).
- Bouchaud JP, Cugliandolo LF, Kurchan J, Mezard M, “Out of equilibrium dynamics in spin-glasses and other glassy systems”, arXiv preprint cond-mat/9702070 (1997).
- Brongniart A, “Notes sur les Coquilles Fossiles qui se trouvent dans les Terrains decrits par M. Studer; sur les Epoque Geognostiques qu'elles indiquent, et sur la Montagne de Diablerets, au N.-E. de Bex”, *Ann Sci Naturelles* 11, 266-280 (1827).
- Brown R, “On the particles contained in the pollen of plants; and on the general existence of active molecules in organic and inorganic bodies”, *Edinb New Philos J* 5, 358-371 (1828).
- Cao J, Wang K, Yang H, Chen F, Zhang Q, Fu Q, “Shear-induced clay dispersion in HDPE/PEgMA/organoclay composites as studied via real-time rheological method”, *J Polym Sci B Polym Phys* 48, 302-312 (2010b).
- Cao Q, Song Y, Tan Y, Zheng Q, “Conductive and viscoelastic behaviors of carbon black filled polystyrene during annealing”, *Carbon* 48, 4268-4275 (2010a).
- Capuano G, Filippone G, Romeo G, Acierno D, “Universal features of the melt elasticity of interacting polymer nanocomposites”, *Langmuir* 28, 5458-5463 (2012).

- Cassagnau P, "Linear viscoelasticity and dynamics of suspensions and molten polymers filled with nanoparticles of different aspect ratios", *Polymer* 54, 4762-4775 (2013).
- Cassagnau P, "Melt rheology of organoclay and fumed silica nanocomposites", *Polymer* 49, 2183-2196 (2008).
- Castillo FY, Socher R, Krause B, Headrick R, Grady BP, Prada-Silvy R, Pötschke P, "Electrical, mechanical, and glass transition behavior of polycarbonate-based nanocomposites with different multi-walled carbon nanotubes", *Polymer* 52, 3835-3845 (2011).
- Chae DW, Kim KJ, Kim BC, "Effects of silicalite-1 nanoparticles on rheological and physical properties of HDPE", *Polymer* 47, 3609-3615 (2006).
- Chandra A, Best A, Meyer WH, Wegner G, "PVT measurements on PMMA: PbTiO<sub>3</sub> polymer-ceramic composites with tunable thermal expansion", *J Appl Polym Sci* 115, 2663-2667 (2010).
- Chatterjee T and Krishnamoorti R, "Rheology of polymer carbon nanotubes composites", *Soft Matter* 9, 9515-9529 (2013).
- Chavarria F and Paul DR, "Comparison of nanocomposites based on nylon 6 and nylon 66", *Polymer* 45, 8501-8515 (2004).
- Chen G, Weng W, Wu D, Wu C, Lu J, Wang P, Chen X, "Preparation and characterization of graphite nanosheets from ultrasonic powdering technique", *Carbon* 42, 753-759 (2004).
- Chen G, Wu C, Weng W, Wu D, Yan W, "Preparation of polystyrene/graphite nanosheet composite", *Polymer* 44, 1781-1784 (2003).
- Chow WS, Leu YY, Mohd Ishak ZA, "Particle size tuning in silver-polyacrylonitrile nanocomposites", *Express Polym Lett* 6, 503-510 (2012).
- Christopoulou C, Petekidis G, Erwin B, Cloitre M, Vlassopoulos D, "Ageing and yield behaviour in model soft colloidal glasses", *Philosop Trans A* 367, 5051-5071 (2009).
- Cipriano BH, Kota AK, Gershon AL, Laskowski CJ, Kashiwagi T, Bruck HA, Raghavan SR, "Conductivity enhancement of carbon nanotube and nanofiber-based polymer nanocomposites by melt annealing", *Polymer* 49, 4846-4851 (2008).
- Cloitre M, Borrega R, Leibler L, "Rheological aging and rejuvenation in microgel pastes", *Phys Rev Lett* 85, 4819-4822 (2000).
- Cole KS and Cole RH, "Dispersion and absorption in dielectrics I. Alternating current characteristics", *J Chem Phys* 9, 341-351 (1941).

- Cugliandolo LF and Kurchan J, "Weak ergodicity breaking in mean-field spin-glass models", *Phil Mag B* 71, 501–514 (1995).
- Demir MM and Wegner G "Challenges in the preparation of optical polymer composites with nanosized pigment particles: a review on recent efforts", *Macromol Mater Eng* 297, 838-863 (2012).
- Domenech T, Zouari R, Vergnes B, Peuvrel-Disdier E, "Formation of fractal-like structure in organoclay-based polypropylene nanocomposites. *Macromolecules*, 47, 3417-3427 (2014).
- Dorigato A, Pegoretti A, Penati A, "Linear low-density polyethylene/silica micro- and nanocomposites: dynamic rheological measurements and modeling" *Express Polym Lett* 4, 115-129 (2010).
- Drosdov AD, Jensen EA, Christiansen JDC, "Non-linear time-dependent response of polypropylene/ nanoclay melts: Experiments and modelling", *Comput Mater Sci* 47, 807-816 (2010).
- Du F, Scogna RC, Zhou W, Brand S, Fischer JE, Winey KI, "Nanotube networks in polymer nanocomposites: rheology and electrical conductivity", *Macromolecules* 37, 9048-9055 (2004).
- Duncan TV, "Applications of nanotechnology in food packaging and food safety: barrier materials, antimicrobials and sensors", *J Colloid Interf Sci* 363, 1-24 (2011).
- Durmus A, Kasgoz A, Macosko CW, "Linear low density polyethylene (LLDPE)/clay nanocomposites. Part I: Structural characterization and quantifying clay dispersion by melt rheology", *Polymer* 48, 4492-4502 (2007).
- Einstein A, "Über die von der molekularkinetischen Theorie der Wärme geforderte Bewegung von in ruhenden Flüssigkeiten suspendierten Teilchen", *Ann Phys* 322, 549-560 (1905).
- Enikolopyan NS, Fridman ML, Stalnova IO, Popov VL, "Filled polymers: mechanical properties and processability" in *Filled Polymers. Science and Technology*, Springer, Berlin, Heidelberg (1990).
- Eslami H, Grmela M, Bousmina M, "Structure build-up at rest in polymer nanocomposites: Flow reversal experiments", *J Polym Sci B Polym Phys* 47, 1728-1741 (2009).
- Fang Z, Xu Y, Tong L, "Effect of clay on the morphology of binary blends of polyamide 6 with high density polyethylene and HDPE-graft-acrylic acid", *Polym Eng Sci* 47, 551-559 (2007).

- Fielding SM, Sollich P, Cates ME, "Aging and rheology in soft materials", *J Rheol* 44, 323-369 (2000).
- Filippone G and Acierno D, "Clustering of coated droplets in clay-filled polymer blends", *Macromol Mater Eng* 297, 923-928 (2012).
- Filippone G and Salzano de Luna M, "A unifying approach for the linear viscoelasticity of polymer nanocomposites", *Macromolecules* 45, 8853-8860 (2012).
- Filippone G, Causa A, Salzano de Luna M, Sanguigno L, Acierno D, "Assembly of plate-like nanoparticles in immiscible polymer blends - Effect of the presence of a preferred liquid-liquid interface", *Soft Matter* 10, 3183-3191 (2014).
- Filippone G, Romeo G, Acierno D, "Role of interface rheology in altering the onset of co-continuity in nanoparticle-filled polymer blends", *Macromol Mater Eng* 296, 658-665 (2011).
- Filippone G, Romeo G, Acierno D, "Viscoelasticity and structure of polystyrene/fumed silica nanocomposites: filler network and hydrodynamic contributions" *Langmuir* 26, 2714-2720 (2010).
- Filippone G, Salzano de Luna M, Acierno D, Russo P, "Elasticity and structure of weak graphite nanoplatelet (GNP) networks in polymer matrices through viscoelastic analyses", *Polymer* 53, 2699-2704 (2012).
- Frey E and Kroy K, "Brownian motion: a paradigm of soft matter and biological physics", *Ann Phys* 14, 20-50 (2005).
- Friedrich C and Braun H, "Generalized Cole-Cole behavior and its rheological relevance", *Rheol acta* 31, 309-322 (1992).
- Galindo-Rosales FJ, Moldenaers P, Vermant J, "Assessment of the dispersion quality in polymer nanocomposites by rheological methods", *Macromol Mater Eng* 296, 331-340 (2011).
- Galindo-Rosales FJ, Moldenaers P, Vermant J, "Assessment of the dispersion quality in polymer nanocomposites by rheological methods", *Macromol Mater Eng* 296, 331-340 (2011).
- Gleissle W and Hochstein B, "Validity of the Cox–Merz rule for concentrated suspensions", *J Rheol* 47, 897-910 (2003).
- Glotzer SC and Solomon MJ, "Anisotropy of building blocks and their assembly into complex structures", *Nature Materials* 6, 557-562. (2007).
- Grady BP, "Recent developments concerning the dispersion of carbon nanotubes in polymers", *Macromol Rapid Commun* 31, 247-257 (2010).

- Graebling D, Muller R, Paliarne JF, "Linear viscoelastic behavior of some incompatible polymer blends in the melt. Interpretation of data with a model of emulsion of viscoelastic liquids", *Macromolecules* 26, 320-329 (1993).
- Guimont A, Beyou E, Martin G, "Viscoelasticity of graphite oxide-based suspensions in PDMS", *Macromolecules* 44, 3893-3900 (2011).
- Gupta S, Zhang Q, Emrick T, Russell TP, "Self-corralling nanorods under an applied electric field", *Nano Letters* 6, 2066-2069 (2006).
- Gusev AA and Lusti HR, "Rational design of nanocomposites for barrier applications", *Adv Mater* 13, 1641-1643 (2001).
- Gusev AA and Rozman MG, "Numerical search for morphologies providing ultra high elastic stiffness in filled rubbers", *Comput Theor Polym S* 9, 335-337 (1999).
- Han CD and Kim JK, "On the use of time-temperature superposition in multicomponent/multiphase polymer systems", *Polymer* 34, 2533-2539 (1993).
- Han Z and Fina A, "Thermal conductivity of carbon nanotubes and their polymer nanocomposites: a review", *Progr Polym Sci* 36, 914-944 (2011).
- Hess S, Demir MM, Yakutkin V, Balushev S, Wegner G, "Investigation of oxygen permeation through composites of PMMA and surface-modified ZnO nanoparticles", *Macromol Rapid Comm* 30, 394-401 (2009).
- Hiemenz P, Rajagopalan R, "Principles of Colloid and Surface Chemistry", Marcel Dekker Inc, New York, USA (1997).
- Huang S, Liu Z, Yin C, Gao Y, Wang Y, Yang M, "Gelation of attractive particles in polymer melt", *Polymer* 53, 4293-4299 (2012).
- Huang S, Liu Z, Yin C, Wang Y, Gao Y, Chen C, Yang M, "Enhancement effect of filler network on isotactic polypropylene/carbon black composite melts", *Colloid Polym Sci* 289, 1673-1681 (2011).
- Huang Y, Ahir S, Terentjev E, "Dispersion rheology of carbon nanotubes in a polymer matrix", *Phys Rev B* 73, 125422 (2006).
- Hule RA and Pochan DJ, "Polymer nanocomposites for biomedical applications", *MRS Bull* 32, 354-358 (2007).
- Inoubli R, Dagr eou S, Lapp A, Billon L, Peyrelasse J, "Nanostructure and mechanical properties of polybutylacrylate filled with grafted silica particles", *Langmuir* 22, 6683-6689 (2006).
- Israelachvili JN, "Intermolecular and surface forces", Academic press (2011).

- Jancar J, Douglas JF, Starr FW, Kumar SK, Cassagnau P, Lesser AJ, Sternstein SS, Buehler MJ, “Current issues in research on structure–property relationships in polymer nanocomposites”, *Polymer* 51, 3321-3343 (2010).
- Jancar J, Douglas JF, Starr FW, Kumar SK, Cassagnau P, Lesser AJ, Sternstein SS, Buehler MJ, “Current issues in research on structure–property relationships in polymer nanocomposites”, *Polymer* 51, 3321-3343 (2010).
- Joshi YM, “Dynamics of colloidal glasses and gels”, *Annu Rev Chem Biomol Eng* 5, 181-202 (2014).
- Jouault N, Dalmas F, Boué F, Jestin J, “Multiscale characterization of filler dispersion and origins of mechanical reinforcement in model nanocomposites”, *Polymer* 53, 761-765 (2012).
- Jouault N, Vallat P, Dalmas F, Said S, Jestin J, Boué F, “Well-dispersed fractal aggregates as filler in polymer-silica nanocomposites: Long-range effects in rheology”, *Macromolecules* 42, 2031-2040 (2009).
- Kamal MR, Calderon JU, Lennox BR, “Surface energy of modified nanoclays and its effect on polymer/clay nanocomposites”, *J Adhes Sci Technol* 23, 663-688 (2009).
- Kaushal M and Joshi Y, “Linear viscoelasticity of soft glassy materials”, *Soft Matter*, 1891-1894 (2014).
- Kayatin MJ and Davis VA, “Viscoelasticity and shear stability of single-walled carbon nanotube/unsaturated polyester resin dispersions”, *Macromolecules* 42, 6624-6632 (2009).
- Ke K, Wang Y, Luo Y, Yang W, Xie B-H, Yang M-B, “Evolution of agglomerate structure of carbon nanotubes in multi-walled carbon nanotubes/polymer composite melt: A rheo-electrical study”, *Compos Part B Eng* 43, 3281-3287 (2012).
- Kim H and Macosko CW, “Processing-property relationships of polycarbonate/graphene composites”, *Polymer* 50, 3797-3809 (2009).
- Kojima Y, Usuki A, Kawasumi M, Okada A, Fukushima Y, Kurauchi T, Kamigaito O, “Mechanical properties of nylon 6-clay hybrid”, *J Mater Res* 8, 1185-1189 (1993).
- Krause B, Boldt R, Pötschke P, “A method for determination of length distributions of multiwalled carbon nanotubes before and after melt processing” *Carbon* 49, 1243-1247 (2011b).

- Krause B, Mende M, Pötschke P, Petzold G, “Dispersability and particle size distribution of CNTs in an aqueous surfactant dispersion as a function of ultrasonic treatment time”, *Carbon* 48, 2746-2754 (2010b).
- Krause B, Petzold G, Pegel S, Pötschke P, “Correlation of carbon nanotube dispersability in aqueous surfactant solutions and polymers” *Carbon* 47, 602-612 (2009).
- Krause B, Ritschel M, Täschner C, Oswald S, Gruner W, Leonhardt A, Pötschke P, “Comparison of nanotubes produced by fixed bed and aerosol-CVD methods and their electrical percolation behaviour in melt mixed polyamide 6.6 composites”, *Compos Sci Technol* 70, 151-160 (2010a).
- Krause B, Villmow T, Boldt R, Mende M, Petzold G, Pötschke P, “Influence of dry grinding in a ball mill on the length of multiwalled carbon nanotubes and their dispersion and percolation behaviour in melt mixed polycarbonate composites”, *Compos Sci Technol* 71, 1145-1153 (2011a).
- Krishnamoorti R and Giannelis EP, “Rheology of end-tethered layered silicate nanocomposites”, *Macromolecules* 30, 4097-4102 (1997).
- Krishnamoorti R and Yurekli K, “Rheology of polymer layered silicate nanocomposites”, *Colloid Interf Sci* 6, 464-470 (2001).
- Krishnamoorti R and Yurekli K, “Rheology of polymer layered silicate nanocomposites”, *Curr Opin Colloid Interf Sci* 6, 464-470 (2001).
- Kuilla T, Bhadra S, Yao D, Kim NH, Bose S, Lee JH, “Recent advances in graphene based polymer composites”, *Progr Polym Sci* 35, 1350-1375 (2010).
- Lacroix C, Bousmina M, Carreau PJ, Favis BD, Michel A, “Properties of PETG/EVA blends: 1. Viscoelastic, morphological and interfacial properties”, *Polymer* 37, 2939-2947 (1996).
- Lan T, Kaviratna PD, Pinnavaia TJ, “Mechanism of clay tactoid exfoliation in epoxy-clay nanocomposites” *Chem Mater* 7, 2144-2150 (1995).
- Lange J and Wyser Y, “Recent innovations in barrier technologies for plastic packaging-a review”, *Packag Technol Sci* 16, 149-158 (2003).
- Langevin P, “Sur la théorie du mouvement brownien”, *CR Acad Sci Paris* 146, 530-533 (1908).
- Larson RG, “The structure and rheology of complex fluids”, Oxford University Press (1999).
- Lee JY, Balazs AC, Thompson RB, Hill RM, “Self-assembly of amphiphilic nanoparticle-coil “Tadpole” macromolecules”, *Macromolecules* 37, 3536-3539 (2004).

- Lee KM and Han CD, "Effect of hydrogen bonding on the rheology of polycarbonate/organoclay nanocomposites", *Polymer* 44, 4573-4588 (2003).
- Lepoittevin B, Devalckenaere M, Pantoustier N, Alexandre M, Kubies D, Calberg C, Jérôme R, Dubois P, "Poly ( $\epsilon$ -caprolactone)/clay nanocomposites prepared by melt intercalation: mechanical, thermal and rheological properties", *Polymer* 43, 4017-4023 (2002).
- Li W, Zhang Y, Yang J, Zhang J, Niu Y, Wang Z, "Thermal annealing induced enhancements of electrical conductivities and mechanism for multiwalled carbon nanotubes filled poly(ethylene-co-hexene) composites", *Appl Mater Interf* 4, 6468-6478 (2012).
- Lim ST, Choi HJ, Jhon MS, "Dispersion quality and rheological property of polymer/clay nanocomposites-ultrasonification effect", *J Ind Eng Chem* 9, 51-57 (2003).
- Lin B, Sundararaj U, Pötschke P, "Melt mixing of polycarbonate with multiwalled carbon nanotubes in miniature mixers", *Macromol Mater Eng* 291, 227-38 (2006).
- Litchfield DW and Baird DG, "The rheology of high aspect ratio nano-particle filled liquids", *Rheology Rev*, 1-60 (2006).
- Logakis E, Pandis C, Pissis P, Pionteck J, Pötschke P, "Highly conducting poly(methyl methacrylate)/carbon nanotubes composites: Investigation on their thermal, dynamic-mechanical, electrical and dielectric properties" *Compos Sci Technol* 71, 854-862 (2011).
- Majid M, Hassan E-D, Davoud A, Saman M, "A study on the effect of nano-ZnO on rheological and dynamic mechanical properties of polypropylene: Experiments and models", *Compos Part B-Eng* 42, 2038-2046 (2011).
- Manias E, "Nanocomposites: Stiffer by design", *Nature Materials* 6, 9-11 (2007).
- Mark JE, "Polymer data handbook (Vol. 27)", New York, Oxford University Press (2009).
- Mazzocchia CV, Bestetti M, Acierno D, Tito AC. European patent, 2213369 (2010).
- Mitchell CA and Krishnamoorti R, "Dispersion of single-walled carbon nanotubes in poly ( $\epsilon$ -caprolactone)", *Macromolecules* 40, 1538-1545 (2007).
- Mitchell CA and Krishnamoorti R, "Rheological properties of diblock copolymer/layered-silicate nanocomposites", *J Polym Sci Part B: Polym Phys* 40, 1434-1443 (2002).

- Mobuchon C, Carreau PJ, Heuzey M-C, "Effect of flow history on the structure of a non-polar polymer/clay nanocomposite model system", *Rheol Acta* 46, 1045-1056 (2007).
- Mobuchon C, Carreau PJ, Heuzey M-C, "Structural analysis of non-aqueous layered silicate suspensions subjected to shear flow", *J Rheol* 53, 1025-1048 (2009).
- Morcom M, Atkinson K, Simon GP, "The effect of carbon nanotube properties on the degree of dispersion and reinforcement of high density polyethylene", *Polymer* 51, 3540-3550 (2010).
- Nazockdast E, Nazockdast H, Goharpey F, "Linear and non-linear melt-state viscoelastic properties of polypropylene/organoclay nanocomposites", *Polym Eng Sci* 48, 1240-1239 (2008).
- Nordström J, Matic A, Sun JZ, Forsyth M, MacFarlane DR, "Aggregation, ageing and transport properties of surface modified fumed silica dispersions", *Soft Matter* 6, 2293-2299 (2010).
- Palierne JF, "Linear rheology of viscoelastic emulsions with interfacial tension", *Rheol Acta* 29, 204-214 (1990).
- Park SD, Han DH, Teng D, Kwon Y, "Rheological properties and dispersion of multi-walled carbon nanotube (MWCNT) in polystyrene matrix", *Curr Appl Phys* 8, 482-485 (2008).
- Pegel S, Pötschke P, Petzold G, Alig I, Dudkin SM, Lellinger D, "Dispersion, agglomeration, and network formation of multiwalled carbon nanotubes in polycarbonate melts", *Polymer* 49, 974-984 (2008).
- Peponi L, Tercjak A, Martin L, Mondragon I, Kenny JM, "Morphology-properties relationship on nanocomposite films based on poly(styrene-block-diene-block-styrene) copolymers and silver nanoparticles", *Express Polym Lett* 5, 104-118 (2011).
- Picard E, Gauthier H, Gérard JF, Espuche E, "Influence of the intercalated cations on the surface energy of montmorillonites: consequences for the morphology and gas barrier properties of polyethylene/montmorillonites nanocomposites", *J Colloid Interf Sci* 307, 364-376 (2007).
- Ploehn HJ and Liu C, "Quantitative analysis of montmorillonite platelet size by atomic force microscopy", *Ind Eng Chem Res* 45, 7025-7034 (2006).
- Pötschke P, Dudkin SM, Alig I, "Dielectric spectroscopy on melt processed polycarbonate-multiwalled carbon nanotube composites" *Polymer* 44, 5023-5030 (2003).

- Pötschke P, Fornes TD, Paul DR, “Rheological behavior of multiwalled carbon nanotube/polycarbonate composites”, *Polymer* 43, 3247-3255 (2002).
- Potts JR, Dreyer DR, Bielawski CW, Ruoff RS, “Graphene-based polymer nanocomposites”, *Polymer* 52, 5-25 (2011).
- Prasad V, Trappe V, Dinsmore AD, Segre PN, Cipelletti L, Weitz DA, “Rideal Lecture Universal features of the fluid to solid transition for attractive colloidal particles”, *Faraday Discuss* 123, 1-12 (2003).
- Product Information Baytubes® C150P, Bayer MaterialScience AG, Edition 2008-03-10.
- Ramasubramaniam R, Chen J, Liu H, “Homogeneous carbon nanotube/polymer composites for electrical applications”, *Appl Phys Lett* 83, 2928-2930 (2003).
- Ray SS and Okamoto M, “Polymer/layered silicate nanocomposites: a review from preparation to processing”, *Prog Polym Sci* 28, 1539-1641 (2003).
- Reichert P, Hoffmann B, Bock T, Thomann R, Mulhaupt R, Friedrich C, “Morphological stability of poly(propylene) nanocomposites”, *Macromol Rapid Commun* 22, 519-523 (2001).
- Ren J, Casanueva BF, Mitchell CA, Krishnamoorti R, “Disorientation kinetics of aligned polymer layered silicate nanocomposites”, *Macromolecules* 36, 4188-4194 (2003).
- Ren J, Silva AS, Krishnamoorti R, “Linear viscoelasticity of disordered polystyrene-polyisoprene block copolymer based layered-silicate nanocomposites”, *Macromolecules* 33, 3739-3746 (2000).
- Rice BP, Chen C, Cloos L, Curliss D, “Carbon fiber composites: organoclay-aerospace epoxy nanocomposites. Part I”, *SAMPE J* 37, 7-9 (2001).
- Romeo G, Filippone G, Fernández-Nieves A, Russo P, Acierno D, “Elasticity and dynamics of particle gels in non-Newtonian melts”, *Rheol Acta* 47, 989-997 (2008).
- Romeo G, Filippone G, Russo P, Acierno D, “Effects of particle dimension and matrix viscosity on the colloidal aggregation in weakly interacting polymer-nanoparticle composites: a linear viscoelastic analysis”, *Polym Bull* 63, 883-895 (2009).
- Romeo G, Filippone G, Russo P, Acierno D, “Effects of particle dimension and matrix viscosity on the colloidal aggregation in weakly interacting polymer-nanoparticle composites: a linear viscoelastic analysis”, *Polym Bull* 63, 883-895 (2009).

- Russel WB, Saville DA, Schowalter WR, "Colloidal dispersions", Cambridge University Press (1992).
- Ryan KM, Mastroianni A, Stancil KA, Liu H, Alivisatos AP, "Electric-field-assisted assembly of perpendicularly oriented nanorod superlattices", *Nano Letters* 6, 1479-1482 (2006).
- Sahimi M and Arbabi S, "Mechanics of disordered solids. II. Percolation on elastic networks with bond-bending forces", *Phys Rev Lett* 1993, 47, 703-712 (1993).
- Sahoo NG, Rana S, Cho JW, Li L, Chan SH, "Polymer nanocomposites based on functionalized carbon nanotubes", *Prog Polym Sci* 35, 837-867 (2010).
- Saint-Michel F, Pignon F, Magnin A, "Fractal behavior and scaling law of hydrophobic silica in polyol", *J Colloid Interf Sci* 267, 314-319 (2003).
- Salzano de Luna M, Galizia M, Wojnarowicz J, Rosa R, Lojkowski W, Leonelli C, Acierno D, Filippone G, "Dispersing hydrophilic nanoparticles in hydrophobic polymers: HDPE/ZnO nanocomposites by a novel template-based approach", *Express Polym Lett* 8, 362-372 (2014).
- Salzano de Luna M, Pellegrino L, Dagheta M, Mazzocchia CV, Acierno D, Filippone G, "A unifying approach for the linear viscoelasticity of polymer nanocomposites", *Compos Sci Technol* 85, 17-22 (2013).
- Sanchez C, Belleville P, Popall M, Nicole L, "Applications of advanced hybrid organic-inorganic nanomaterials: from laboratory to market", *Chem Soc Rev* 40, 696-753 (2011).
- Schaefer DW and Justice, "How nano are nanocomposites?", *Macromolecules* 40, 8501-8517 (2007).
- Sengupta R, Bhattacharya M, Bandyopadhyay S, Bhowmick AK, "A review on the mechanical and electrical properties of graphite and modified graphite reinforced polymer composites", *Progr Polym Sci* 36, 638-670 (2011).
- Sharif-Pakdaman A, Morshedjan J, Jahani Y, "Influence of the silane grafting of polyethylene on the morphology, barrier, thermal, and rheological properties of high-density polyethylene/organoclay nanocomposites", *J Appl Polym Sci* 125, E305-E313 (2012).
- Sheng N, Boyce MC, Parks DM, Rutledge GC, Abes JI, Cohen RE, "Multiscale micromechanical modeling of polymer/clay nanocomposites and the effective clay particle", *Polymer* 45, 487-506 (2004).
- Shih WH, Shih WY, Kim SI, Liu J, Aksay IA, "Scaling behavior of the elastic properties of colloidal gels", *Phys Rev A* 42, 4772-4779 (1990).

- Shokrieh MM and Rafiee R, “Investigation of nanotube length effect on the reinforcement efficiency in carbon nanotube based composites” *Compos Struct* 92, 2415-2420 (2010).
- Sinha Ray S, Okamoto K, Okamoto M, “Structure-property relationship in biodegradable poly (butylene succinate)/layered silicate nanocomposites”, *Macromolecules* 36, 2355-2367 (2003).
- Socher R, Krause B, Boldt R, Hermasch S, Wursche R, Pötschke P, “Melt mixed nano composites of PA12 with MWNTs: Influence of MWNT and matrix properties on macrodispersion and electrical properties”, *Compos Sci Technol* 71, 306-314 (2011).
- Sollich P, Lequeux F, Hébraud P, Cates M, “Rheology of Soft Glassy Materials”, *Phys Rev Lett* 78, 2020–2023 (1997).
- Solomon MJ, Almusallam AS, Seefeldt KF, Somwangthanaroj A, Varadan P, “Rheology of polypropylene/clay hybrid materials”, *Macromolecules*, 34, 1864-1872 (2001).
- Solomon MJ, Almusallam AS, Seefeldt KF, Somwangthanaroj A, Varadan P, “Rheology of polypropylene/clay hybrid materials”, *Macromolecules* 34, 1864-1872 (2001).
- Song Y and Zheng Q, “Application of two phase model to linear dynamic rheology of filled polymer melts”, *Polymer* 52, 6173-6179 (2011).
- Song Y and Zheng Q, “Linear rheology of nanofilled polymers”, *J Rheol* 59, 155-191 (2015).
- Song Y, Cao Q, Zheng Q, “Annealing-induced rheological and electric resistance variations in carbon black-filled polymer melts”, *Colloid Polym Sci* 290, 1837-1842 (2012).
- Song YS and Youn JR, “Influence of dispersion states of carbon nanotubes on physical properties of epoxy nanocomposites”, *Carbon* 43, 1378-1385 (2005).
- Spitalsky Z, Tasis D, Papagelis K, Galiotis C, “Carbon nanotube-polymer composites: Chemistry, processing, mechanical and electrical properties” *Prog Polym Sci* 35, 357-401 (2010).
- Starr FW, Douglas JF, Glotzer SC “Origin of particle clustering in a simulated polymer nanocomposite and its impact on rheology”, *J Chem Phys* 119, 1777-1788 (2003).
- Starr FW, Schröder TB, Glotzer SC, “Effects of a nanoscopic filler on the structure and dynamics of a simulated polymer melt and the relationship to ultrathin films”, *Phys Rev E* 64, 021802 (2001).

- Starr FW, Schröder TB, Glotzer SC, “Molecular dynamics simulation of a polymer melt with a nanoscopic particle”, *Macromolecules* 35, 4481-4492(2002).
- Stauffer D and Aharony A, “Introduction to percolation theory”, Taylor & Francis, 2nd ed., London (1992).
- Steinmann S, Gronski W, Friedrich C, “Influence of selective filling on rheological properties and phase inversion of two-phase polymer blends”, *Polymer* 43, 4467-4477 (2002).
- Struik LCE, “Physical aging in amorphous polymers and other materials”, PhD Thesis, TU Delft, Delft University of Technology (1977).
- Sumita M, Sakata K, Hayakawa Y, Asai S, Miyasaka K, Tanemura M, “Double percolation effect on the electrical conductivity of conductive particles filled polymer blends”, *Colloid Polym Sci* 270, 134-139 (1992).
- Surve M, Pryamitsyn V, Ganesan V, “Universality in structure and elasticity of polymer-nanoparticle gels”, *Phys Rev Lett* 96, 177805-1-177805-4 (2006).
- Tang Y, Yang C, Gao P, Ye L, “Rheological study on high-density polyethylene/organoclay composites”, *Polym Eng Sci* 51, 133-142 (2011).
- Tang Z, Zhang Z, Wang Y, Glotzer SC, Kotov NA, “Self-assembly of CdTe nanocrystals into free-floating sheets”, *Science* 314, 274-278 (2006).
- Theng BKG, “The Chemistry of Clay-Organic Reactions” Wiley, New York (1974).
- Thompson BC and Fréchet JM, “Polymer–fullerene composite solar cells”, *Angew Chem Int Edit* 47, 58-77 (2008).
- Tjong SC, “Structural and mechanical properties of polymer nanocomposites”, *Mat Sci Eng R* 53, 73-197 (2006).
- Trappe V and Weitz DA, “Scaling of the viscoelasticity of weakly attractive particles”, *Phys Rev Lett* 85, 449-452 (2000).
- Trappe V, Prasad V, Cipelletti L, Segre PN, Weitz DA, “Jamming phase diagram for attractive particles”, *Nature* 411, 772-775 (2001).
- Treece MA and Oberhauser JP, “Soft glassy dynamics in polypropylene-clay nanocomposites”, *Macromolecules* 40, 571-582 (2007a).
- Treece MA and Oberhauser JP, “Ubiquity of soft glassy dynamics in polypropylene-clay nanocomposites”, *Polymer* 48, 1083-1095 (2007).
- Treece MA and Oberhauser JP, “Ubiquity of soft glassy dynamics in polypropylene–clay nanocomposites”, *Polymer* 48, 1083-1095 (2007b).

- Tucker CL and Moldenaers P, "Microstructural evolution in polymer blends", *Annu Rev Fluid Mech* 34, 177-210 (2002).
- Tyurin A, De Filpo G, Cupelli D, Nicoletta FP, Mashin A, Chidichimo G, "Particle size tuning in silver-polyacrylonitrile nanocomposites", *Express Polym Lett* 4, 71-78 (2010).
- Usuki A, Kojima M, Okada A, Fukushima Y, Kamigaito O, "Synthesis of nylon 6-clay hybrid", *J Mater Res* 8, 1179-1184 (1993).
- Vaia RA and Maguire JF, "Polymer nanocomposites with prescribe morphology: going beyond nanoparticle-filled polymers", *Chem Mater* 19, 2736-2751 (2007).
- van Gurp M and Palmen J, "Time-temperature superposition for polymeric blends", *Rheol Bull* 67, 5-8 (1998).
- Verge P, Benali S, Bonnaud L, Minoia A, Mainil M, Lazzaroni R, Dubois P, "Unpredictable dispersion states of MWNTs in HDPE: A comparative and comprehensive study", *Eur Polym J* 48, 677-683 (2012).
- Vermant J, Ceccia S, Dolgovskij MK, Maffettone PL, Macosko CW, "Quantifying dispersion of layered nanocomposites via melt rheology", *J Rheol* 51, 429-450 (2007).
- Vermant J, Cioccolo G, Nair KG, Moldenaers P, "Coalescence suppression in model immiscible polymer blends by nano-sized colloidal particles", *Rheol Acta* 43, 529-538 (2004).
- Villmow T, Kretzschmar B, Pötschke P, "Influence of screw configuration, residence time, and specific mechanical energy in twin-screw extrusion of polycaprolactone/multi-walled carbon nanotube composites" *Compos Sci Technol* 70, 2045-2055 (2010).
- Von Smoluchowski M, "Zur kinetischen theorie der brownschen molekularbewegung und der suspensionen", *Ann Phys* 326, 756-780 (1906).
- Wagener R and Reisinger TJG, "A rheological method to compare the degree of exfoliation of nanocomposites", *Polymer* 44, 7513-7518 (2003).
- Wagener R and Reisinger TJG, "A rheological method to compare the degree of exfoliation of nano-composites", *Polymer* 44, 7513-7518 (2003).
- Wang D, Zhang X, Zha JW, Zhao J, Dang ZM, Hu GH, "Dielectric properties of reduced graphene oxide/polypropylene composites with ultralow percolation threshold", *Polymer* 54, 1916-1922 (2013).
- Wang X, Sun P, Xue G, Winter HH, "Late-state ripening dynamics of a polymer/clay nanocomposite", *Macromolecules* 43, 1901-1906 (2010).

- Washburn EW, "The dynamics of capillary flow", *Phys Rev* 17, 273-283 (1921).
- Wolthers W, van den Ende D, Breedveld V, Duits MHG, Potanin AA, Wientjens RHW, Mellema J, "Linear viscoelastic behavior of aggregated colloidal dispersions", *Phys Rev E* 56, 5726-5733 (1997).
- Wu D, Wu L, Zhang M, Zhao Y, "Viscoelasticity and thermal stability of polylactide composites with various functionalized carbon nanotubes", *Polym Degrad Stab* 93, 1577-1584 (2008).
- Wu H and Morbidelli M, "A model relating structure of colloidal gels to their elastic properties", *Langmuir* 17, 1030-1036 (2001).
- Wu S, "Phase structure and adhesion in polymer blends: a criterion for rubber toughening", *Polymer* 26, 1855-1863 (1985).
- Wunderlich B, "Macromolecular Physics Vol. 3", Academic Publishers, New York (1980).
- Yu W, Zhou W, Zhou C, "Linear viscoelasticity of polymer blends with co-continuous morphology", *Polymer* 51, 2091-2098 (2010).
- Zhang Q and Archer LA, "Poly (ethylene oxide)/silica nanocomposites: structure and rheology", *Langmuir* 18, 10435-10442 (2002).
- Zhang Q, Fang F, Zhao X, Li Y, Zhu M, Chen D, "Use of dynamic rheological behavior to estimate the dispersion of carbon nanotubes in carbon nanotube/polymer composites", *J Phys Chem B* 112, 12606-12611 (2008).
- Zhao J, Morgan AB, Harris JD, "Rheological characterization of polystyrene-clay nanocomposites to compare the degree of exfoliation and dispersion", *Polymer* 46, 8641-8660 (2005).
- Zheng X, Forest MG, Vaia R, Arlen M, Zhou R, "A strategy for dimensional percolation in sheared nanorod dispersions", *Adv Mater* 19, 4038-4043 (2007).
- Zhou K, Gu S-Y, Zhang Y-H, Ren J, "Effect of dispersion on rheological and mechanical properties of polypropylene/carbon nanotubes nanocomposites", *Polym Eng Sci* 52, 1485-1494 (2012).
- Zhu Y, Cardinaels R, Mewis J, Moldenaers P, "Rheological properties of PDMS/clay nanocomposites and their sensitivity to microstructure", *Rheol Acta* 48, 1049-1058 (2009).
- Zouari R, Domenech T, Vergnes B, Peuvrel-Disdier E, "Time evolution of the structure of organoclay/polypropylene nanocomposites and application of the time-temperature superposition principle", *J Rheol* 56, 725-742 (2012).